AMERICAN UNIVERSITY OF BEIRUT

AQUEOUS-BASED DYE SENSITIZED SOLAR CELLS: COPPER ELECTROLYTES

by
MEGHRY HAGOP JILAKIAN

A thesis
submitted in partial fulfillment of the requirements
for the degree of Master of Science
to the Department of Chemistry
of the Faculty of Arts and Sciences
at the American University of Beirut

Beirut, Lebanon
June 2020

AMERICAN UNIVERSITY OF BEIRUT

AQUEOUS-BASED DYE SENSITIZED SOLAR CELLS: COPPER ELECTROLYTES

by

MEGHRY HAGOP JILAKIAN

Approved by:

Dr. Tarek Ghaddar, Full Professor — Advisor
Department of Chemistry

Dr. Digambara Patra, Full Professor — Member of Committee
Department of Chemistry

Dr. Pierre Karam, Associate Professor — Member of Committee
Department of Chemistry

Date of thesis/dissertation defense: June 16, 2020

AMERICAN UNIVERSITY OF BEIRUT

THESIS, DISSERTATION, PROJECT RELEASE FORM

Student Name:

Jilakian Meghry

Last First Middle

● Master's Thesis ○ Master's Project ○ Doctoral Dissertation

☐ I authorize the American University of Beirut to: (a) reproduce hard or electronic copies of my thesis, dissertation, or project; (b) include such copies in the archives and digital repositories of the University; and (c) make freely available such copies to third parties for research or educational purposes.

☑ I authorize the American University of Beirut, to: (a) reproduce hard or electronic copies of it; (b) include such copies in the archives and digital repositories of the University; and (c) make freely available such copies to third parties for research or educational purposes
after:

One ---- year from the date of submission of my thesis, dissertation, or project.
Two ---- years from the date of submission of my thesis, dissertation, or project.
Three ☑ years from the date of submission of my thesis, dissertation, or project.

Meghrie June 26, 2020

Signature Date

ACKNOWLEDGEMENTS

First and foremost, I would like to sincerely thank my thesis advisor Prof. Tarek Ghaddar for his patience, motivation, and effort throughout my research work at AUB. Prof. Ghaddar was always available to guide me and answer my questions throughout all my research experience. Thank you for being such a true advisor, a great professor, and an amazing person.

I would also like to thank my committee members; Dr. Digambara Patra and Dr. Pierre Karam, for their encouragement, comments, and questions.

A special thanks to my fellow lab mates for teaching me all that I need for my research work. Thank you my dear AUB friends, for providing me a second family, always supporting me, and making the Graduate Room the most memorable place in the department.

Finally, I would like to thank my parents for their support, unconditional love, and for always believing in me. Making them proud is my duty for everything they have done to me.

Thank you AUB, for providing me a lifetime opportunity and a second home. It has been an experience that I will never forget.

AN ABSTRACT OF THE THESIS OF

Meghry Hagop Jilakian for Master of Science
Major: Chemistry

Title: Aqueous-Based Dye Sensitized Solar Cells: Copper Electrolytes

Nowadays, dye-sensitized solar cells (DSCs) have been a great alternative to the conventional *p-n* junction photovoltaic devices that convert solar energy to electrical current, especially for indoor applications. However, a DSC to be used as the power source in any indoor appliance, it should be an eco-friendly device. One of the most important components of DSCs is the electrolyte, since it plays a crucial role in the regulation of electron transfer kinetics. The most currently used electrolyte systems are the I^-/I_3^- couple and copper or cobalt complexes dissolved in an organic solvent. The solvent is usually a nitrile based organic compound, where some of which are either toxic or of very high volatility.

In this study, we report on the use of eco-friendly aqueous electrolyte systems that contain one of three highly-charged pyridyl-based aqueous copper complexes (anionic or cationic) with hydrophilic groups such as –OHs and their use in DSCs with different commercially available organic and metal complex dyes. Additionally, these complexes bear two groups on the 6, 6' positions for the bipyridine-based or 2, 9 for phenanthroline-based complexes that stabilize the Cu (I) state, achieving DSCs with reduced cost, improved environmental compatibility, and having promising efficiencies.

The Ru-based C106 dye sensitizer showed the best photovoltaic performance with the $Cu(dmdcbpy)_2]^{2+/1+}$ based electrolyte, and was further demonstrated to show a remarkable PCE value at ambient lighting for 100% aqueous-based DSCs. Under illumination from a white LED light (1000 lux) we achieved a PCE value of 6.54%.

CONTENTS

ACKNOWLEDGEMENTS……..…….....v

ABSTRACT…….……vi

LIST OF ILLUSTRATIONS……..……..ix

LIST OF SCHEMES…….xi

LIST OF TABLES…….…..…….xii

Chapter page

1. INTRODUCTION……..……....1

1.1 Sun as a Renewable Energy Source..……..…...…….....1

1.2 Photovoltaic Devices……...…….……...……..4

1.3 Dye-Sensitized Solar Cells...…….……...….5

1.3.1 Device Structure and Working Principle……...……...7

1.3.2 Energetics and Electron Transfer Processes……...……...……...8

1.3.3 Characterization Techniques..……...……15

1.3.4 Components of a DSC…..……...……...16

1.3.4.1 Dye Sensitizers..……..……...16

1.3.4.2 Redox Mediators…….……....20

1.3.4.2.1 Solvents for Liquid Electrolytes.……21

1.3.4.2.2 Redox Couples..…….……..23

1.3.4.2.3 Additive…….……..28

1.3.5 Water in DSCs……..……...……...31

1.3.6 Low Artificial Light…...……..43

1.3.7 Electrochemical Impedance Spectroscopy (EIS)…..…….....44

1.4 Aim of Work……..……...45

2. EXPERIMENTAL METHODS AND INSTRUMENTATION…….……..…..….46

2.1 Materials……..…….46

2.2 Instrumentation……..……...……46

2.3 Solar Cell Fabrication…..……47

2.4 Synthesis of the Copper Complexes……..……...48

2.4.1 Preparation of $[Cu(dmap)_2]^{2+/1+}$ Complex…..……..……...48

2.4.1.1 Synthesis of 1,10-phenanthroline-2,9-dicarbaldehyde…..……..48

2.4.1.2 Synthesis of (1,10-phenanthroline-2,9-diyl)dimethanol (dmap).....49

2.4.1.3 Synthesis of $Cu(I)(dmap)_2Cl$……..…….49

2.4.1.4 Synthesis of $Cu(II)(dmap)_2Cl_2$.....50

2.4.2 Preparation of $[Cu(dmdcbpy)_2]^{2+/1+}$ Complex…….50

2.4.2.1 Synthesis of (1E,5E)-1,6-di(furan-2-yl)hexa-1,5-diene-3,4-dione..50

2.4.2.2 Synthesis of 4,4'-di(furan-2-yl)-6,6'-dimethyl-2,2'-bipyridine..…..50

2.4.2.3 Synthesis of 6,6'-dimethyl-[2,2'-bipyridine]-4,4'-dicarboxylic acid (dmdcbpy)……..…..51

2.4.2.4 Synthesis of $Cu(I)(dmdcbpy)_2Cl$ Complex…..……51

2.4.2.5 Synthesis of $Cu(II)(dmdcbpy)_2Cl_2$ Complex…..…….52

2.4.3 Preparation of $[Cu(tmabpy)_2]^{2+/1+}$ Complex……...…..……52

2.4.3.1 Synthesis of [2,2'-bipyridine]-6,6'-dicarboxylic acid……..……52

2.4.3.2 Synthesis of diethyl [2,2'-bipyridine]-6,6'-dicarboxylate……...53

2.4.3.3 Synthesis of [2,2'-bipyridine]-6,6'-diyldimethanol……..……53

2.4.3.4 Synthesis of 6,6'-bis(bromomethyl)-2,2'-bipyridine……..……..54

2.4.3.5 Synthesis of 1,1'-([2,2'-bipyridine]-6,6'-diyl)bis(N,N,N-trimethylmethanaminium) (tmabpy)…..…….....54

2.4.3.6 Synthesis of Cu(I)(tmabpy)$_2$Cl Complex…..……..……54

2.4.3.7 Synthesis of Cu(II)(tmabpy)$_2$Cl$_2$ Complex……..…….…...55

2.5 Preparation of the Electrolytes…..……..55

2.5.1 Preparation of [Cu(dmdcbpy)$_2$]$^{2+/1+}$ based Electrolyte……..…..…….....55

2.5.2 Preparation of [Cu(tmabpy)$_2$]$^{2+/1+}$ based Electrolyte…….....……...55

3. RESULTS AND DISCUSSION……...…….....57

3.1 Design, Synthesis and Characterization of Water-Soluble Redox Mediators.…57

3.2 Electrochemical Properties……..……64

3.3 Photovoltaic Performance and IPCE Spectra……..……66

3.4 Dye Regeneration……..……..77

3.5 Electrochemical Impedance Spectroscopy……..……79

3.6 Light Intensity Dependence Measurements……..……..82

3.7 Indoor Applications Under Ambient Light……..……...87

4. CONCLUSION…….……....91

5. SUPPORTING INFORMATION……..……...92

REFERENCES……..…100

ILLUSTRATIONS

Figure page

1. Photon flux of AM 0, AM 1.5 G, and AM 1.5 D spectrums (ASTM G173-03)……..3

2. Main electron transfers and transport processes in a DSC device……9

3. The molecular structures of the N3 and N719 dyes possessing –COOH anchoring groups……..18

4. The molecular structures of the D35 dye possessing cyanoacrylate anchor and the NI-6 dye possessing a pyridyl anchor……...20

5. The structures of some ligands used for the synthesis of coordination complexes….28

6. The molecular structure of the TG6 dye sensitizer……..34

7. The molecular structure of the PEDOT cathode catalyst……42

8. A typical Nyquist plot and the equivalent circuit of a DSC device…….44

9. The molecular structures of $[Cu(dmdcbpy)_2]^{2+/1+}$ and $[Cu(tmabpy)_2]^{2+/1+}$ with their corresponding redox potentials vs NHE……..64

10. Cyclic Voltammograms of 5 mM solutions of (a) $Cu(I)(dmdcbpy)_2$ and (b) $Cu(I)(tmabpy)_2$ in 0.1 M KCl/water at a scan rate of 10 mV/s……..65

11. The molecular structures of the organic CO, D35, and DNF-05 dyes and the corresponding $\lambda_{abs,max}$ values…….67

12. Photocurrent-Voltage characteristics of DSCs sensitized with CO, D35, and DNF-05 with the $[Cu(dmdcbpy)_2]^{2+/1+}$ electrolyte and the corresponding dark currents…….68

13. IPCE% spectra of DSCs with the CO, D35, and DNF-05 dyes and the $[Cu(dmdcbpy)_2]^{2+/1+}$ electrolyte…….70

14. The molecular structures of the organic D45 and D51 dyes…….72

15. Photocurrent-Voltage characteristic of DSCs sensitized with the CO dye using the $[Cu(tmabpy)_2]^{2+/1+}$ electrolyte and the corresponding dark current…..…...…….73

16. The molecular structure of the Ru-based metal-organic C106 dye……...74

17. Photocurrent-Voltage characteristic of DSCs sensitized with the C106 dye using the $[Cu(dmdcbpy)_2]^{2+/1+}$ electrolyte and the corresponding dark current……..75

18. IPCE% spectra of a DSC with the C106 dye and the $[Cu(dmdcbpy)_2]^{2+/1+}$ electrolyte……..…76

19. PIA spectra of C106 sensitized TiO_2 with the $[Cu(dmdcbpy)_2]^{2+/1+}$ electrolyte……78

20. PIA spectra of TiO_2 with the $[Cu(dmdcbpy)2]^{2+/1+}$ electrolyte…….78

21. Charge transfer resistance values extracted from EIS measurements of C106 sensitized DSCs…….79

22. Chemical capacitance values extracted from EIS measurements of C106 sensitized DSCs……..80

23. Electron lifetime values extracted from EIS measurements of C106 sensitized DSCs……..80

24. Light intensity dependence of a) I-V characteristic and b) short circuit photocurrent of DSC devices based on the $Cu(dmdcbpy)_2]^{2+/1+}$ electrolyte…….……..83

25. Nyquist plot of a DSC sensitized with C106 dye using the $Cu(dmdcbpy)_2]^{2+/1+}$ electrolyte……..84

26. Photocurrent-Voltage characteristics of DSCs sensitized with C106 using the $[Cu(dmdcbpy)_2]^{2+/1+}$ electrolyte as a result of an applied reverse-bias……..86

27. The spectral output from white LED light source…….87

28. Photocurrent-Voltage characteristics of C106 sensitized small DSCs with the $[Cu(dmdcbpy)_2]^{2+/1+}$ electrolyte under low light intensities of 200 and 1000 lux….88

29. Photocurrent-Voltage characteristic of C106 sensitized DSC with the $[Cu(dmdcbpy)_2]^{2+/1+}$ electrolyte under low ambient light for indoor applications and the corresponding dark current……..90

30S. ^{1}HNMR of 1,10-phenanthroline-2,9-dicarbaldehyde (**2**) in DMSO at 500 MHz…92

31S. ^{1}HNMR of (1,10-phenanthroline-2,9-diyl)dimethanol (dmap) (**3**) in DMSO at 500 MHz…….93

32S. ^{1}HNMR of (1E,5E)-1,6-di(furan-2-yl)hexa-1,5-diene-3,4-dione (**8**) in $CDCl_3$ at 500 MHz……..94

33S. ^{1}HNMR of 4,4'-di(furan-2-yl)-6,6'-dimethyl-2,2'-bipyridine (**10**) in DMSO at 500 MHz…….95

34S. ^{1}HNMR of 6,6'-dimethyl-[2,2'-bipyridine]-4,4'-dicarboxylic acid (dmdcbpy) (**11**) in D_2O at 500 MHz……..96

35S. ^{1}HNMR of Cu(I)(dmdcbpy)$_2$Cl Complex (**12**) in D_2O at 500 MHz……...97

36S. ^{1}HNMR of 6,6'-bis(bromomethyl)-2,2'-bipyridine (**18**) in $CDCl_3$ at 500 MHz…..98

37S. ^{1}HNMR of 1,1'-([2,2'-bipyridine]-6,6'-diyl)bis(N,N,N-trimethylmethanaminium) (tmabpy) (**19**) in D_2O at 500 MHz……...99

SCHEMES

Scheme page

1. Synthetic Scheme of $[Cu(dmap)_2]^{2+/1+}$ Complex……..…59

2. Synthetic Scheme of $[Cu(dmdcbpy)_2]^{2+/1+}$ Complex……...61

3. Synthetic Scheme of $[Cu(tmabpy)_2]^{2+/1+}$ Complex……..63

TABLES

Table page

1. Photovoltaic parameters of CO, D35, and DNF-05 with the $[Cu(dmdcbpy)_2]^{2+/1+}$ electrolyte……..……68

2. Photovoltaic parameters of CO with the $[Cu(tmabpy)_2]^{2+/1+}$ electrolyte……..73

3. Photovoltaic parameters of C106 with the $[Cu(dmdcbpy)_2]^{2+/1+}$ electrolyte……...75

4. Photovoltaic parameters of C106 with the $[Cu(dmdcbpy)_2]^{2+/1+}$ electrolyte at different light intensities (%sun)……84

5. Photovoltaic parameters of C106 with the $[Cu(dmdcbpy)_2]^{2+/1+}$ electrolyte at different low light intensities of 200 and 1000 lux……88

6. Photovoltaic parameters of C106 with the $[Cu(dmdcbpy)_2]^{2+/1+}$ electrolyte under low ambient light (1000 lux) for indoor applications……90

CHAPTER 1

INTRODUCTION

1.1 Sun as a Renewable Energy Source:

The growth in the global population and the economic development that people are witnessing nowadays is leading to an enormous rise in energy demand. The collective consumption of human beings was equivalent to 13.5 TW of power, according to the studies done by professor Nathan Lewis in 2001, and most energy experts have predicted that by 2050 an additional power of almost 30 TW would be needed.[1] Until recent years, most of the energy sources are supplied by carbon-based fossil fuels, which unfortunately emit carbon dioxide (CO_2) into the atmosphere as a primary greenhouse gas. This emission of CO_2 is also subjected to a drastic increase in the coming years, putting our planet in a global risk more than ever witnessed before. The high concentration of CO_2 in the atmosphere is responsible for major and severe environmental consequences including pollution, exploitation of natural resources, and increase in the global mean temperature leading to the rise of sea level caused by melting of ice sheets and glaciers, all projecting the human health to many uncertainties.[2] To avoid the emission of CO_2 while satisfying the energy demand of human life, carbon-based fossil fuels should be replaced by carbon-free, "clean" energy sources that do not harm our environment and keep the human life safe.[3] Alternatives to fossil fuels include hydropower, biomass, solar energy, wind power, and geothermal,

with solar energy being the most important source of renewable energy, the reason which drove scientists to launch major research on it.

Earth's surface receives energy from the sun of about 100,000 TW energy hours, which is more than what humanity's energy needs for a year, thus making the sun a suitable renewable energy source candidate to replace fossil fuels.[4]

The sun emits light with different wavelengths covering the ultraviolet, visible, and infrared regions of the electromagnetic spectrum. While passing through the atmosphere, some atmospheric molecules absorb and scatter the light, changing the shape of the spectrum that reaches the earth's surface. The most elevated solar irradiance is at the visible wavelengths; 300-800 nm because O_2, O_3, and N_2 absorb the ultraviolet wavelengths below 300 nm while CO_2 and water absorb at the infrared region, filtering out some parts of the sun and causing dips in the absorption spectrum at the corresponding wavelengths. Furthermore, the position of the sun influences the nature of the light reaching the earth's surface. When the sun is directly overhead, it has the shortest path length which is called air mass (AM) and strikes the earth with maximum radiation. Therefore, AM quantifies the spectral irradiance and is estimated to be $1/\cos\theta$, where θ is the angle of elevation of the sun from the earth's surface. The solar spectrum outside the atmosphere is referred to as AM 0, while AM 1.5 corresponds to the solar irradiance when θ is equal to 42˚. Moreover, sunlight is distinguished as direct or diffuse light, where the latter is the result of scattered light in the atmosphere and is represented by AM 1.5 Global (AM 1.5 G) while the former by AM 1.5 Direct (AM 1.5 D)[5]. AM 1.5 G being the standard solar spectrum used for

efficiency measurements of photovoltaic devices, and its integrated amount of radiant energy received from the sun per unit area per unit time is 1000 Wm^{-2}. The spectral irradiance of AM 0, AM 1.5 G, and AM 1.5 D are given in Figure 1.

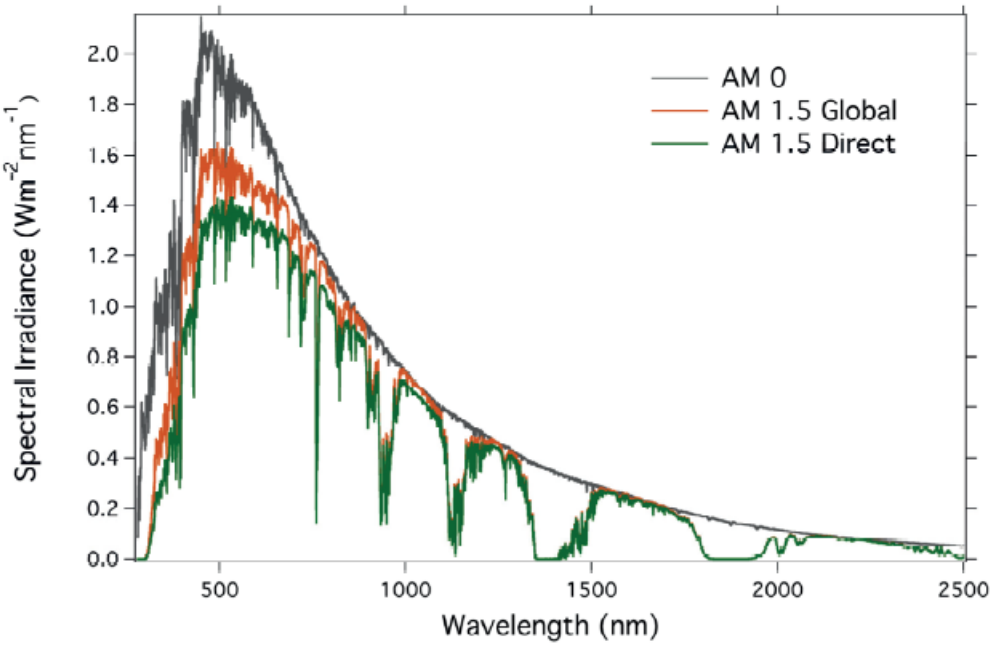

Figure 1: Photon flux of AM 0, AM 1.5 G, and AM 1.5 D spectrums (ASTM G173-03).

Solar photovoltaics (PVs) directly convert sunlight, being the planet's most abundant renewable energy source, to electricity without any environmental emissions and are becoming a very significant source in solving the world's problem of the huge rise in energy demand.[6]

1.2 Photovoltaic Devices:

Theoretically, 0.16% of the earth's land surface should be covered with solar panels of 10% efficiency in turning sunlight to electricity, to obtain 20 TW of power.[7] Satisfyingly, solar panels of 12-18% power conversion efficiencies are manufactured, and the industry has been witnessing a remarkable growth at a rate of 30% per annum of solar photovoltaics production over the past 20 years, targeting to minimize cost and increase efficiency.[8]

In fact, PVs are divided into three generations based on their material abundance, module cost, power conversion efficiencies, and other factors. First-generation (G1) PVs constitute 90% of today's worldwide production capacity[9] and are based on wafer crystalline silicon (c-Si) and gallium arsenide (GaAs).[10] The operation of these cells follows the concept of p-n junction, resulting in efficiencies of 15-21%. Nevertheless, c-Si cells dominate today's global PV market, but their low light absorption and the high cost needed for their manufacturing process, which focuses on purity and a large amount of silicon semiconductor, led scientists to search for cheaper alternatives giving rise to the second generation (G2) PVs. G2 solar cells include cadmium telluride (CdTe), which have the lowest module cost in the PV market, copper indium gallium diselenide (CIGS), and hydrogenated amorphous silicon (a-SiH).[11] These cells are made up of thin-film technology, which minimizes the amount of materials used, aiming to reduce their production cost. The fact that these active materials can be used in small amounts, forming films of few microns, is due to their efficient light absorption, which exceeds that of silicon by 10-100 times. However, the

raw materials utilized in G2 PVs are non-abundant, which increases their cost, and their power conversion efficiencies of 12-15% remain lower than that of c-Si.[9] Finally, the third generation (G3) PVs aim at achieving cheap solar cells by using more simplistic processing methods in addition to abundant and inexpensive materials. These cells consist of novel thin-film technology devices, including organic and quantum dot solar cells, hot carrier collection, thermophotovoltaics, perovskite solar cells[12], and the widely known dye-sensitized solar cells.[13]

1.3 Dye-Sensitized Solar Cells:

The dominance of silicon-based solid-state junction devices, in the field of photovoltaics, is now being challenged by a new generation of devices specially for indoor applications; the dye-sensitized solar cells (DSCs). DSCs are based on nanocrystalline materials and different types of electrolytes, including liquid, gel, or organic solids. These cells offer high conversion efficiencies in addition to the ease and cheapness of their fabrication, together with their flexibility and use in various applications.[13]

Originally, the idea of liquid state devices has been motivated by the pioneering work of Becquerel[14], who applied liquid and not solid-state devices in his photoelectric experiments in 1839. Moreover, the history of DSC technology, which is based on the concept of semiconductor sensitization, goes back to the first photographic images, which were made by Daguerre in 1837, followed by the silver halide process used by Fox Talbot in 1839 and finally the work of Gurney and Mott.[15] Initially, the films used

in photography were insensitive to the mid and red light regions of the spectrum, with negligible absorption of sunlight at wavelengths above 460 nm. This is because the semiconductors used, which were silver halide grains, have a bandgap ranging between 2.7 and 3.2 eV. Furthermore, in 1883, Vogel discovered that sensitizing the silver halide with a dye extends its photosensitivity to longer wavelengths.[16] And after four years, Moser designed photoelectrochemical cells using silver halide electrodes sensitized with erythrosine.[17] In 1964, Namba and Hishiki[18] recognized that the dyes used for photographic processes were also possible to effectively be used for photoelectrochemical sensitization processes. At a certain stage, the idea of sensitization was still under consideration, whether it occurred via the transfer of energy from the dye to the semiconductor or via the transfer of electrons. The studies of Hauffe[19], Tributsch, and Grischer[20] pointed that for both processes, electron transfer is the accepted mechanism.

The semiconductors that can absorb efficiently in the visible region due to their narrow bandgap are prone to photo corrosion, therefore, semiconductors with wide bandgap and thus photostable, typically oxides of metals such as titanium, were used. Nevertheless, TiO_2 semiconductors have been preferred over others due to the work of Fujishima and Honda, which focused on its use in water photolysis.[21] Furthermore, mesoscopic semiconductor materials, forming a closely packed monolayer with high internal surface area, were needed to absorb most of the incident light. These mesoscopic oxide films include TiO_2, ZnO, SnO_2, and Nb_2O_5 and are made up of few nanometres tiny crystals. Accordingly, in 1991, Brian O'Regan and Michael Gratzel[22] demonstrated a DSC using

a trimeric ruthenium complex sensitizer along with a mesoporous TiO_2 film, which enhanced the dye adsorption, resulting in power conversion efficiency values above 7%. This achievement allowed the DSC technology to grab global attention for being a low-cost photovoltaic device with promising efficiencies, and since then, studies are being carried out mainly by focusing on synthesizing new dyes and electrolytes and developing working electrodes that can enhance the stability and efficiency of the DSCs.

1.3.1 *Device Structure and Working Principles:*

The main components of a DSC include a photoanode (working electrode) consisting of a fluorine-doped SnO_2 (FTO) conductive glass, coated by a TiO_2 film which contains a dye sensitizer adsorbed on its surface. On top of the photoanode lies the cathode (counter electrode), in most cases a platinized FTO glass[23], and finally between the two electrodes lies a redox mediator (electrolyte) layer, usually triiodide/iodide couple dissolved in an organic solvent.[24]

When the dye sensitizer (S) in the photoanode is exposed to sunlight, its photoexcitation takes place resulting in the injection of the excited electron to the conduction band of the semiconductor, giving the oxidized form of the sensitizer (S^+). On the other hand, at the cathode, the redox couple donates an electron to the dye, thus regenerating the dye by restoring its ground state. Finally, the electron loss in the electrolyte is compensated by the external migration of the injected electron from the anode to the cathode completing the electrical circuit. In DSCs, the functions of light absorption and charge

carrier transportation are separated, unlike in the conventional silicon-based devices, where both are performed by the semiconductor only.[25]

1.3.2 *Energetics and Electron Transfer Processes:*

The performance of a DSC is governed by the electron transfer and transport kinetics at the oxide/dye/electrolyte interfaces, as well as their energy levels (driving forces). The main electron transfers and transport processes involved in a DSC are illustrated in Figure 2.

The Fermi energy level (E_F) of the TiO_2 in the dark is at the same level as the Nernst redox potential (E_{redox}) of the electrolyte, resulting in 0 open circuit photovoltage (V_{OC}). The V_{OC} of a DSC is defined as the difference between the conduction band energy (E_{CB}) of the TiO_2 and the E_{redox} of the electrolyte. The Nernst redox potential is given by Equation 1, where $E^{\circ\prime}_{redox}$ is the formal redox potential of the electrolyte, R is the gas constant, T is the temperature, n is the number of electrons transferred in the reaction, and C is the concentration of the oxidized and reduced species.

$$E_{redox} = E^{\circ\prime}_{redox} - \frac{RT}{nF} \ln\left(\frac{C_{ox}}{C_{red}}\right) \qquad (1)$$

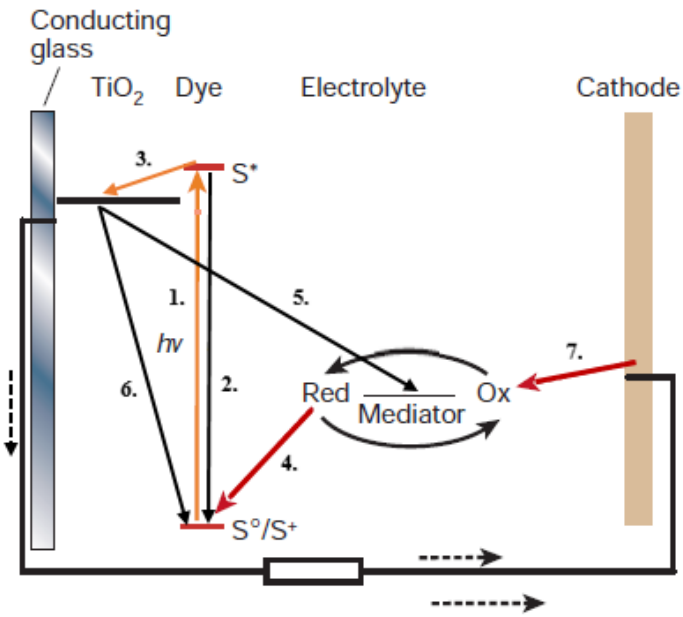

1. $S + h\upsilon \rightarrow S^*$	Dye photoexcitation
2. $S^* \rightarrow S + h\upsilon$	Dye relaxation
3. $S^* \rightarrow S^+ + e^-_{TiO_2}$	TiO_2 charge injection
4. $2S^+ + 3I^- \rightarrow 2S + I_3^-$	Dye regeneration
5. $I_3^- + 2e^-_{TiO_2} \rightarrow 3I^-$	Recombination to electrolyte
6. $S^+ + e^-_{TiO_2} \rightarrow S$	Recombination to dye
7. $I_3^- + 2e^- \rightarrow 3I^-$	Reduction of I^-

Figure 2: Main electron transfers and transport processes in a DSC device.

Upon illumination, an electron in the dye sensitizer (S) excites from the highest occupied molecular orbital (HOMO) level to the lowest unoccupied molecular orbital (LUMO) level, resulting in the photoexcited state of the dye (S^*) (Reaction **1**). The

excited electron is then injected to the Fermi level of the TiO_2 (Reaction **3**), which is said to take place in femto-to-picosecond timescale, giving the oxidized form of the sensitizer (S^+). Opposing to this injection exists the excited state decay of the sensitizer back to its ground state (Reaction **2**), which should be significantly slower with a rate constant of almost 100 times smaller than that of electron injection for a highly efficient device.[26-27] The electron injection efficiency (Φ_{inj}) is defined by Equation 2, where k_{inj} is the rate constant of electron injection and k_1 is the rate constant of decay of the excited dye.

$$\Phi_{inj} = \frac{k_{inj}}{k_{inj} + k_1} \qquad (2)$$

As electrons fill into the TiO_2, the E_F shifts up getting very close to the conduction band[28] (CB) and causes an increase in the V_{OC}. On the other hand, the energy difference between the TiO_2 CB and the excited state of the sensitizer (LUMO) will decrease, minimizing the driving force and the efficiency of electron injection, thus causing a drop in the short-circuit photocurrent density (J_{SC}) of the DSC. Furthermore, the TiO_2 conduction band energy relative to the LUMO of the dye depends on its structure and some additives that may be present in the electrolyte.[29] The replacement of the protons with *tert*-butyl pyridine (TBP^+), raises the TiO_2 E_{CB} leading to a decrease in the electron injection driving force and thus lower J_{SC}. Whereas, keeping the labile protons of the dye molecules or adding Li^+ counter ions will have an exact opposite effect, promoting the electron injection efficiency and J_{SC} while diminishing the V_{OC}, as a result of lowered E_{CB}. Due to the injection of electrons from the LUMO

to the TiO_2 CB, the sensitizer now is in the oxidized form (S^+) and will be regenerated by an electron donor species in the electrolyte (Reaction **4**). Regeneration plays a crucial role in completing the electric circuit by reducing the oxidized dye back to its ground state, and this occurs in the microsecond timescale with the iodide electrolyte.[30] The regeneration time has a lower limit given by the diffusion-limited kinetics of the redox mediator. The higher the diffusion coefficient the faster the diffusion, resulting in faster regeneration thus minimizing the limitation of the photocurrent. For non-viscous electrolytes, this diffusion has a rate constant, k_{diff}, in the range of 10^9-10^{10} $M^{-1}s^{-1}$ for electrolytes having the concentration of their reduced species being more than 0.1 M, resulting in a regeneration time of some nanoseconds.[31] Regeneration also competes with the recombination reaction, which is the reduction of the oxidized dye by an electron from the TiO_2 (Reaction **6**), taking place over a timescale of microseconds to milliseconds.[31] Therefore, the efficiency of regeneration (Φ_{reg}) is defined by the probability of the dye sensitizer going back to its ground state by regeneration rather than recombination, and is given by Equation 3, where k_{reg} is the rate constant of dye regeneration and k_{rec} is the rate constant of dye recombination.

$$\Phi_{reg} = \frac{k_{reg}}{k_{reg} + k_{rec}} \qquad (3)$$

In addition to the limitations by diffusion, Φ_{reg} is also affected by the reorganization energy of the redox couple while changing from geometry to another. In most cases, iodide has been the choice of the electron donor species and very high Φ_{reg} are obtained

while using it with different types of dye sensitizers. Moreover, the kinetics of regeneration also depends on several parameters, including the redox potential of the electrolyte and the oxidation potential of the dye which affects the driving force, ΔG°, of regeneration i.e., the difference between the HOMO level and E_{redox}. The triiodide/iodide electrolyte has a redox potential of about +0.35 V vs NHE when dissolved in an organic solvent, resulting in an efficient driving force for the regeneration of almost all sensitizers. Studies show that Ru complex sensitizers with oxidation energies more positive than the I_3^-/I^- redox potential by 0.5 V, are enough to obtain efficient regenerations.[32] Furthermore, the presence of the cations of the iodine salt in the electrolyte influences the regeneration kinetics. Rapid regenerations have been observed with Li^+ and Mg^{2+} cations, because they adsorb on the TiO_2 surface and increase the local iodide concentration near the semiconductor, resulting in high Φ_{reg}, while much slower regenerations are observed when tetra butyl ammonium (TBA^+) cations are used, since they do not adsorb efficiently on the semiconductor surface.[33] Additionally, the structure of the dye molecule can have a negative effect on the kinetics of regeneration. Dyes that have bulky alkyl groups increase the steric hindrance around the central metal and form a nonpolar shield repelling away the electrolyte and thus resulting in low regeneration efficiencies.[34]

After the injection of the excited electron to the conduction band of the TiO_2 and the regeneration of the dye by the electron donating species in the electrolyte, electrons should migrate externally from the photoanode to the conductive cathode inducing an external circuit photocurrent in the DSC device. There, two electrons will reduce

triiodide back to iodide (reaction **7**).[35]A high catalytic activity for the counter electrode is needed to obtain a fast reduction of the electrolyte, and Pt has been the choice of catalyst in most cases.[36] A series resistance is obtained in the DSC due to the reduction of triiodide and is known as the charge transfer resistance, R_{CT}, which is defined by Equation 4, where J is the current density at which an overpotential, η, is needed to ensure the regeneration of the electrolyte.

$$R_{CT} = \eta / J \qquad (4)$$

Therefore, higher current density values at the electrolyte/counter electrode interface leads to lower R_{CT} values implying higher DSC efficiencies. For an ideal DSC, R_{CT} should be $\leq 1\ \Omega cm^{-2}$ in order to avoid significant losses. A counter electrode with low catalytic activity will lower the fill factor (FF) of the DSC, affecting negatively on the current-voltage (J-V) curve characteristics.

Undesirable reactions that are disadvantageous to the DSC could also occur, leading to a low electrical current which reduces the efficiency of the cell. These reactions, known as electron recombination reactions, occur when the injected electrons in the TiO_2 semiconductor are captured by either the oxidized redox mediator or the oxidized dye sensitizer (S^+) (reactions **5** and **6**, respectively).[37] The reason behind these reactions is the slow transportation of the injected electrons through the mesoporous TiO_2 film, being at a distance of few nanometres away from the semiconductor/electrolyte interface. Hence, recombination is always a possibility.[38] Additionally, recombination kinetics depends on the electron concentration in the TiO_2 and the electron lifetime.[39] As the electron concentration increases the recombination

kinetics increases, while on the contrary, when electron lifetime increases the recombination decreases. Two ways are suggested for the recombination of electrons with the electrolyte. The first is at the interface between the oxide and the electrolyte, which is diminished in the cells where dyes with bulky alkyl groups are used forming somehow a nonpolar compact layer, blocking the movement of the electrolyte towards the oxide and reducing recombination reactions. Moreover, a proposal by O'Regan[40] showed that most organic dyes create a binding site for iodine near the TiO_2 surface resulting in short electron lifetimes and high recombination rates. The other suggested way of recombination is at the areas of contact between the photoanode and the electrolyte, which can be suppressed by using a blocking layer of metal oxide[41] and this type of recombination is usually observed while using one electron redox systems, including cobalt and copper complexes. Moreover, recombination with the electrolyte can also be suppressed by some additives, including TBP which shifts the TiO_2 conduction band towards negative potentials, increasing electron lifetime and thus reducing recombination.[42] Also, using smaller TiO_2 nanoparticles provide a larger surface area, increasing the concentration of the electrons and thus accelerating electron recombination.[43] Another factor that increases recombination rates is the increase in the concentration of the oxidized species of the redox couple, for the purpose of increasing the diffusion rate for dye regeneration and minimizing the possibilities of obtaining diffusion limited currents.[44] Therefore, the charge collection efficiency[45] (Φ_{CC}) is defined by the electron recombination and the electron transport in the TiO_2 and is given by Equation 5, where τ_e is the electron lifetime defined by the time for

recombination with the electrolyte and τ_{tr} is the time interval for electron transportation through the TiO_2 film, referred to as electron transport time.

$$\Phi_{CC} = \frac{1}{1 + \frac{\tau_e}{\tau_{tr}}} \quad (5)$$

1.3.3 *Characterization Techniques*:

The overall solar cell efficiency (η) can be given by the ratio of the maximum power output (P_{max}) obtained to the total input power (P_{in}) of the irradiated light as in Equation 6, where P_{max} is also defined by the product of the maximum photovoltage (V_{max}) and the maximum photocurrent density (J_{max}), given in Equation 7.

$$\eta = \frac{P_{max}}{P_{in}} \quad (6)$$

$$P_{max} = V_{max} J_{max} \quad (7)$$

The open circuit photovoltage (V_{OC}), which is the difference between E_{CB} and E_{redox}, is defined as the potential at which the collected current is zero i.e., at the J=0 intercept of the J-V curve, while the short circuit photocurrent density (J_{SC}) is defined as the current when the voltage is zero. Furthermore, the fill factor (FF) of a DSC device describes the non-ideality of the J-V curve, it adopts values between 0 and 1, and includes the effects of some loss mechanisms. It is described as the ratio of P_{max} to the multiplication of J_{SC} and V_{OC} as given in Equation 8.

$$FF = \frac{P_{max}}{V_{OC} J_{SC}} \quad (8)$$

Therefore, the efficiency of a DSC device can be given by Equation 9.

$$\eta = \frac{J_{SC} V_{OC} FF}{P_{in}} \quad (9)$$

The Incident Photon-to-current Conversion Efficiency (IPCE) is defined by the efficiency of the cell in converting the flux that hits the photoanode to short circuit current under monochromatic illuminations, and is given by Equation 10, where e is the elementary charge and Φ(λ) is the photon flux as a function of wavelength (λ).

$$IPCE = \frac{J_{SC}(\lambda)}{e\Phi(\lambda)} = 1240 \frac{J_{SC}(\lambda)[Acm^{-2}]}{\lambda P_{in}(\lambda)[Wcm^{-2}]} \quad (10)$$

IPCE can also be expressed as in Equation 11, where LHE is the Light Harvesting Efficiency and is given in Equation 12 (A is the absorbance of the film), Φ_{inj} is the quantum yield of electron injection, Φ_{reg} is the dye regeneration efficiency and Φ_{coll} is the photo-generated charge collection efficiency.

$$IPCE = LHE\Phi_{inj}\Phi_{reg}\Phi_{coll} \quad (11)$$

$$LHE = 1 - 10^{-A} \quad (12)$$

1.3.4 *Components of a DSC:*

1.3.4.1 Dye Sensitizers:

Since the dye sensitizer is one of the main components of the DSC, due to its role in harvesting sunlight and converting it to electrons at the semiconductor, therefore it should fulfil some important characteristics to improve the performance of the cell. Most importantly, the dye should absorb efficiently in the visible and near infrared (NIR) regions of the spectrum, possessing high molar extinction coefficients that allows the use of thin TiO_2 films. Also, it should contain anchoring groups including

carboxylic acid (–COOH), phosphonic acid ($–H_2PO_3$), sulfonic acid ($–SO_3H$), etc., to adsorb strongly on the TiO_2 surface.[46] Concerning the energy levels, the excited state of the dye must be at a higher energy level than the CB of the semiconductor to obtain an efficient electron injection[47], while the oxidized state should be at a lower level than the redox potential of the electrolyte so that a good dye regeneration process takes place.[48] Furthermore, to avoid dye aggregation on the TiO_2 surface, the molecular structure of the dye should be optimized or co-adsorbers must be used.[49] Moreover, the dye must possess photo stability in addition to some thermal and electrochemical stability.[50] By applying all these characteristics, many different dye sensitizers have been synthesized including metal complexes, porphyrins, phtalocyanines, metal free organic dyes, and others.

Due to their broad absorption spectra and favourable photovoltaic properties, metals complexes have gained a lot of interest in the application of DSCs. Metal complexes are made up of a central metal ion with ligands containing at least one anchoring group. Light absorption in this type of sensitizers is due to a metal to ligand charge transfer (MLCT) process, making the central metal an important part of the overall properties of the complexes. In most cases, ruthenium has been the choice of the central ion resulting in DSCs of high efficiencies, reaching more than 10% under standard measurement condition.[51] In 1993, many mononuclear Ru complexes were synthesized by Gratzel and co-workers[52], including the N3 dye that showed an outstanding property with a 10% power conversion efficiency (PCE). Later, Nazeeruddin *et al*.[53] improved the PCE of the N3 dye by its doubly deprotonated N719

dye, after their investigation about the effect of the proton content on the performance of the DSC. Thus, the N3 and N719 dyes, which possess –COOH anchoring groups, have been used as references to design new Ru photosensitizers and their structures are shown in Figure 3. Other central metals have also been used including Os, Fe, Pt, and Cu, but none have exceeded the efficiency of the Ru complexes.

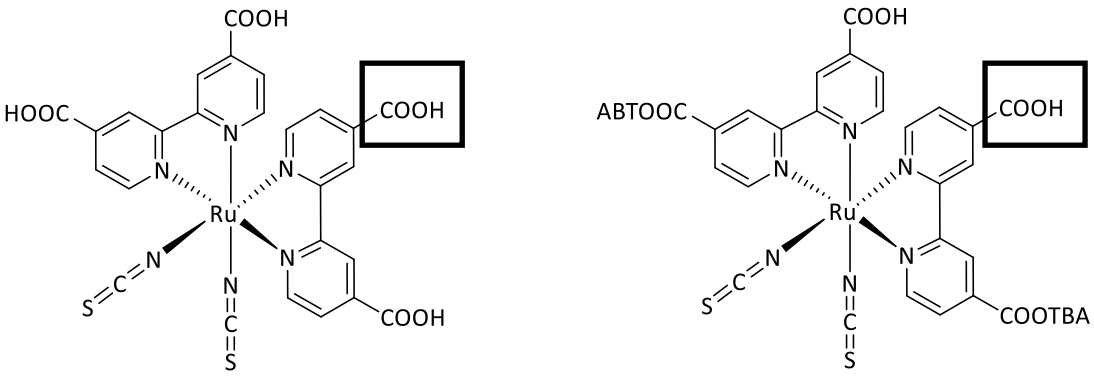

Figure 3: The molecular structures of the N3 and N719 dyes possessing –COOH anchoring groups.

Due to the limited absorption of Ru complexes in the NIR region, porphyrins[54-55] and phthalocyanines[56-57] have been good candidates for DSC applications. These dyes possess good photochemical and thermal stability with intense spectral response bands in the NIR. Metal free organic dyes have also been synthesized and used as alternatives for Ru complexes, since they exhibit many advantages.[58] Organic dyes can be easily synthesized due to their molecular structures which are in diverse forms. Furthermore, they have higher molar extinction coefficients than that of Ru complexes, in addition to

their reduced cost and low impact on the environment. In general, organic dyes have a donor-πbridge-acceptor (D-π-A) structure, making it easy to design new structures with extended absorption spectra and to adjust the HOMO and LUMO energy levels. Metal complexes mainly contain a carboxylic acid anchoring group, while organic dyes have mostly cyanoacrylic acid anchoring group[59] (ex: D35).[60] Until now, many metal free organic dyes have been synthesized and used in DSCs including coumarin dyes[61-62], indoline dyes[63], carbazole dyes[64] and many others. Carbazole organic dyes[65] are known for having pyridine as the anchoring group (ex: NI-6).[66] Approaches have been developed in co-sensitizing the semiconductor with different types of dyes, aiming at increasing the spectral response and elevating the performance of the cell. Dyes with different absorption spectra can be used together for co-sensitization, resulting in higher incident-to-current power conversion efficiencies (IPCEs) and overall efficiencies.[67-69] Additionally, studies show that the binding sites of the carboxylate anchor is different than that for the pyridyl anchor, making it possible to incorporate a –COOH based dye with a pyridine based dye and improve the PCE of a DSC[70-71]. The molecular structures of D35 and NI-6 are shown in Figure 4.

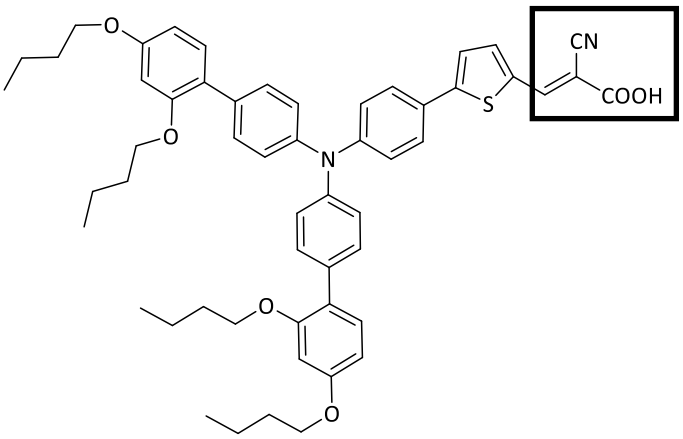

D35

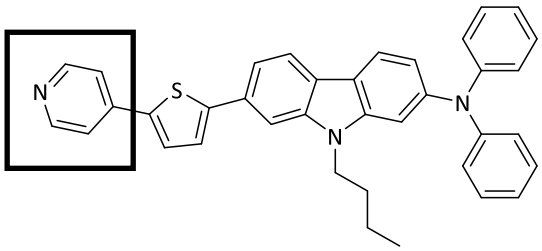

NI-6

Figure 4: The molecular structures of the D35 dye possessing a cyanoacrylate anchor and the NI-6 dye possessing a pyridyl anchor.

1.3.4.2 Redox Mediators:

As one of the major components of the DSC, due to its crucial role in transferring electrons from the counter electrode to the oxidized dye and completing the electrical circuit, the properties of the redox mediator influence the efficiency and the stability of the solar cells.[72] Electrolytes for DSCs are classified into three different categories: liquid electrolyte, quasi-solid electrolyte, and solid-state hole conductor[73], with liquid electrolyte being the center of our interest.

Fast dye regeneration, slow electron recombination, and fast reduction with a very low overpotential at the counter electrode are key features that should be taken into consideration while choosing an effective electrolyte. The mentioned kinetic processes are influenced by the presence of the cations Li^+, Mg^{2+} (alkaline metal ions) and TBA^+ (organic cations) in addition to some other additives in the electrolyte. Moreover, the J_{SC} is directly affected by the driving force for dye regeneration. Therefore, the liquid electrolyte should have a redox potential as positive as possible i.e., very close to the HOMO of the dye, but at the same time having a sufficient driving force for dye regeneration,[74] in addition to the good interfacial wetting property with the anode.[75] Consequently, the properties of the electrolyte directly influence the V_{OC}, J_{SC}, and FF values of a DSC device. Other requirements include the negligible absorbance in the visible region compared to the absorbance of the dye molecules.[24] Based on the mentioned requirements, triiodide/iodide and cobalt liquid electrolytes have become the most known redox shuttles among the few that have been synthesized and used for DSC applications in addition to several solvents.

1.3.4.2.1 Solvents for Liquid Electrolytes:

Requirements for the electrolyte solvent includes a good solubility of the redox couple and the additives without any significant dissolution of the dye sensitizer or the semiconductor. For metal complexes, reactive protic solvents and water have not been the choice of the solvent since many of these dyes are known for being sensitive towards hydrolysis. Furthermore, low viscosity and high ionic mobility are required to

satisfy a continuous electron transfer processes without any limitations by the mass transport problems. Additionally, the electrolyte solvent should be inert to a suitable sealing material that is used to prevent evaporation or leakage. Two major types of solvents that have fulfilled the mentioned requirements include the fairly polar organic solvents and ionic liquids.[31]

The first choice of electrolyte solvent has been organic carbonates and mixtures of organic carbonates[76], followed by mixtures of nitriles having higher boiling points, aiming at further minimizing losses by evaporation.[77] One of the most common electrolyte solvent used nowadays is the 3-methoxypropionitrile (MPN) and acetonitrile (ACN), that have resulted in good DSC performances with high efficiencies.[78] Other organic solvents that have been investigated by Anakawa and others while using LiI/I_2 electrolyte, include tetrahydrofuran (THF), dimethylformamide (DMF), dimethyl sulfoxide (DMSO), various nitriles, alcohols, etc.[79] Due to the difficulty of finding all the mentioned requirements in a single solvent, scientists sometimes used a mixture of solvents in order to achieve a good cell performance. In the 1991 famous paper of Gratzel and O'Regan[22], the electrolyte used was an 80:20 mixture by volume between ethylene carbonate and ACN. The latter was the choice of the second solvent since it possesses high solubilizing ability and chemical stability, in addition to its low viscosity.

The second choice of electrolyte solvent is ionic liquids, which were initially demonstrated by Gratzel and co-workers as a new non-volatile solvent. The most

commonly used ionic liquid in electrochemical and DSC applications is the imidazolium family, showing good photoelectrochemical performance and stability.[80]

1.3.4.2.2 Redox Couples:

In the history of DSCs, triiodide/iodide redox couple has been the conventional electrolyte due to the high efficiencies that have been observed while using it with different types of dye sensitizers, which have exceeded the efficiencies of other redox mediators. The I_3^-/I^- electrolyte has been the most commonly used redox mediator due to its desirable kinetic properties, which provide DSCs with high photovoltages and currents, in addition to its excellent stability and solubility in several solvents. This electrolyte exhibits high diffusion rates and fast forward electron donation, resulting in efficient dye regeneration. Moreover, it has shown supressed electron recombination rates at the photoanode, leading to high charge collection efficiencies. By now, the best PCE value that has been reported for cells based on I_3^-/I^- is 11.7%.[81]

Despite its remarkable performance in DSCs, scientists tend to find suitable alternatives because of several reasons. Firstly, the I_3^-/I^- redox couple lowers the J_{SC} and thus the overall efficiency of the DSC device, due to its absorbance in the visible region and specifically the blue part of the electromagnetic spectrum, minimizing the light harvesting efficiency of the photoanode.[82] Furthermore, the reduction of the I_3^- to I^- at the cathode, which involves several coupled steps, is a two electron process, causing large internal losses in the cells.[83] Another drawback of this redox mediator is its corrosiveness when it comes in contact with several metals, affecting its long term

durability.[72] Additionally, as previously mentioned, the difference between the HOMO of most dyes and E_{redox} is about +0.5 V or more, which is considered to be more than the amount needed for an efficient driving force for dye regeneration while using one electron transfer systems, thus causing losses in the V_{OC} of the device.

The first 1 electron redox couple that has been demonstrated is the cobalt polypyridyl complexes, aiming at solving the problem of the overpotential and increasing the device V_{OC}.[84]

The ease of ligand modification of these cobalt complexes makes it possible to control their redox potentials, electron transfer kinetics, and stability, in addition to the tuning of their chemical and physical properties.[85] The redox potentials of these complexes can be made as positive as possible, resulting in improved photovoltages and thus higher power conversion efficiencies compared to those obtained by the I_3^-/I^-electrolyte. So far, the highest efficiency value obtained with cobalt redox mediator $[Co(bpy)_3]^{3+/2+}$ (bpy = bipyridyl) is 14%.[67] However, the positive increase of the redox potential causes a decrease in the dye regeneration rates and an increase in the recombination kinetics.[86] Furthermore, the dye regeneration is limited by the large internal reorganization energy of the complex, which is required between the high spin (d^7) and low spin (d^6) states, while being oxidized from Co(II) to Co(III).[87] In addition, the recombination rate of the injected electrons to the redox mediator increases, limiting the photovoltage and photocurrent of the device and thus suppressing its overall performance.[88] The problem of increased recombination rates can be solved by using sterically insulating ligands on the Co metal, but these ligands will form bulky

complexes and create mass transport limitation problems.[89] Additionally, Co metals possess a high coordination number (CN=6) which increases the size of the complex and causes the slower diffusion of Co^{3+} compared to I_3^-. Hence, the diffusion of Co^{3+}(4,4'-di-tert-butyl-2,2'-bipyridine) was studied by Nelson *et al*.[90] and it turned out to be an order of magnitude slower than that of I_3^-.

Another 1 electron redox couple that has been demonstrated is a family of copper complexes. Cu being a first row transition metal, its ions can form coordination complexes with different geometries. Cu(I) being a d^{10} system favors a tetrahedral geometry forming a four coordinate complex[91], while Cu(II) being a d^9 system can exhibit different geometries including distorted octahedral (six-coordinate tetragonal), square pyramidal or triganol bipyramidal (five-coordinate complex).[92] Therefore, significant reorganizational energies are expected by the electron transfer reactions in Cu(II/I) complexes, as a result of internal changes in bond lengths and angles. However, the addition of sterically hindered ligands can alter the change in coordination number and geometry, thus modifying the energy barrier for electron transfer reactions.[93]

The first time copper complexes were used as DSC electrolytes was in the pioneering work of Yanagida and coworkers[94], where they employed [(-)-sparteine-N,N'](maleonitriledithiolato-S,S') copper ([Cu(SP)(mmt)]), a blue copper complex that has a similar redox and spectral behaviour as the naturally found blue copper proteins involved in photosynthesis. A good dye regeneration was obtained with this redox mediator since it possessed a distorted tetragonal geometry thus minimizing the difference in the geometries of Cu(I) and Cu(II) species. Furthermore, they compared

the [Cu(SP)(mmt)] to another newly synthesized bis(2,9-dimethyl-1,10-phenanthroline copper complex ($[Cu(dmp)_2](CF_3SO_3)_2$), which also possessed a distorted tetragonal geometry due to the methyl substitutions at the phen 2,9 positions, and the $[Cu(phen)_2]$ complex. Results showed a minimal change in the structure between Cu(I) and Cu(II) for the $[Cu(dmp)_2]^{2+/1+}$ redox mediator. Additionally, cells that were fabricated with the N719 dye and the three mentioned electrolytes, showed that with $[Cu(dmp)_2]$ the highest V_{OC} and highest PCE value of 1.4% were obtained.

Bignozzi and co-workers[95] demonstrated new copper complexes ($[Cu(bpy\text{-}(COOEt)_2)_2]^{2+/1+}$, $[Cu(bpy\text{-}(COOnbut)_2)_2]^{2+/1+}$, $[Cu(bpy\text{-}(COOTbut)_2)_2]^{2+/1+}$, $[Cu(PQ)_2]^{2+/1+}$, $[Cu(MeTBPQ)_2]^{2+/1+}$, $[Cu(BQ)_2]^{2+/1+}$). These electrolytes, which have high reorganization energies, were used in DSCs with the Z907 dye in order to minimize recombination rates but slow dye regeneration processes were observed. The use of these copper complexes showed that substituents at the 4,4' positions were not able to diminish electron recombination reactions in addition to the slow electron transfer kinetics which affected negatively the dye regeneration and the electrochemical response of the DSC device.

The $[Cu(dmp)_2]^{2+/1+}$ redox mediator was re-studied by Wang and co-workers[96] with the C218 dye with different counter electrode materials including carbon black, conductive oxides, and noble metals but low fill factors were obtained with low electron transfer rates and PCEs. Also, Freitag *et al*.[97] studied this complex with an organic dye (Y123) using a poly(3,4-ethylenedioxythiophene) (PEDOT) counter electrode, and a remarkably high V_{OC} was obtained of above 1.0 V, resulting in a higher PCE value.

Compared to the Co based electrolytes, the copper complexes showed less mass transport limitations due to their higher diffusion coefficients resulting mainly from their lower coordination number. A drawback that was observed by using $[Cu(dmp)_2]^{2+/1+}$ redox electrolyte with the organic LEG4 dye was the excited state decay of the dye, which competes with the electron injection resulting in low photocurrents.

In the work of the development of a copper complex using the 1,8-bis(2'-pyridyl)-3,6-dithiaoctane (PDTO) and TBP additive in ACN by Hoffeditz *et al.*[98], the replacement of PDTO with TBP was observed upon oxidation. By this observation, a mixture of Cu(I) and Cu(II) complexes of different ligands was obtained. Concerning the performance of DSCs fabricated with this electrolyte, it is highly dependent on the concentration of TBP which directly affects the V_{OC}, J_{SC}, and FF values.

Saygili *et al.*[99] introduced two new copper complexes using dimethyl bipyridyl ligand ($[Cu(dmby)_2]^{2+/1+}$) with the methyl substituents at the 6,6' positions and tetramethyl bipyridyl ligand ($[Cu(tmby)_2]^{2+/1+}$) with the methyl substituents at the 4,4' and 6,6' positions. The efficiencies of these electrolytes were studied in DSCs with the organic Y123 dye and compared to the efficiency of the $[Cu(dmp)_2]^{2+/1+}$ redox mediator. Results showed high V_{OC} values of above 1.0 V with PCEs reaching 10.0% or more. Some of the ligands used for coordination complexes are given in Figure 5.

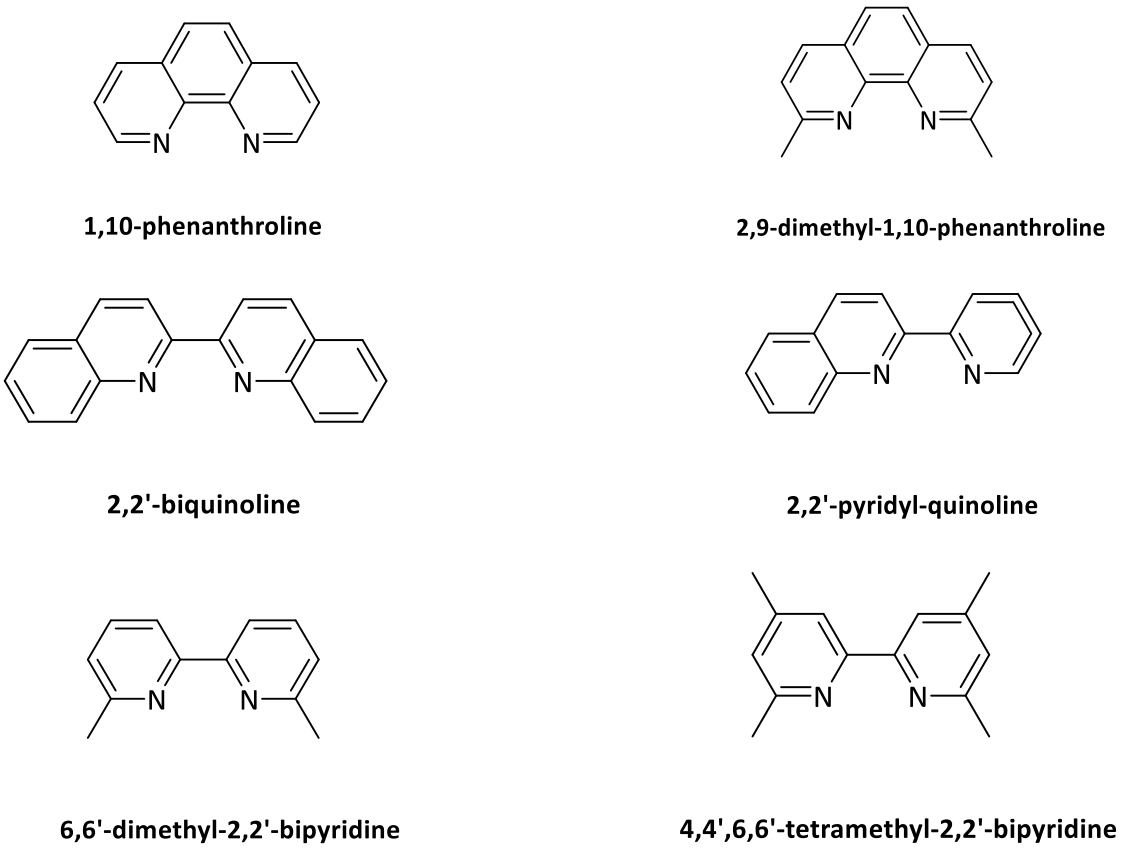

Figure 5: The structures of some ligands used for the synthesis of coordination complexes.

1.3.4.2.3 Additives:

The presence of additives often results in modifications of redox mediator potential and band edge shifts of the semiconductor, in addition to their effects of dye organization and surface blocking, thus affecting directly the photoelectrochemical performance of the DSC devices.

In the pioneering work of Gratzel and co-workers in 1993[52], TBP was added to the LiI-based electrolyte and resulted in a remarkable increase in V_{OC}. This result was explained by the negative shift of the TiO_2 conduction band caused by the adsorption of

TBP, which contains an electron donating nitrogen heterocycle, on its surface. Following this work, Haque *et al*.[39] studied the contribution of TBP and Li^+ on the TiO_2 CB and the recombination kinetics, showing a direct relation between the two.

Other additives that have been used in DSCs include several pyridine derivatives[100] such as 4-ethoxy-2-methylpyridine[101], ammonia, and other N-heterocycles, all showing generally the same results as TBP. The use of these additives has minimized recombination reaction rates causing an increase in V_{OC}. This increase in V_{OC} was explained by Boschloo *et al*.[42] as a combination between the negative shift of the TiO_2 CB and the increase in electron lifetimes. Additionally, the same effects were observed for other nitrogen containing derivatives such as pyrimidines, aminotriazoles, and quinolines, which were investigated by Kusama, Arakawa, and co-workers.[102] A suggested explanation for the observed results is that these additives cause the blocking of the contact sites between TiO_2 and I_3^- after their adsorption on the semiconductor surface, thus suppressing recombination reactions by preventing the approach of I_3^- ions to the oxide layer. The reduction of recombination rates was studied by Huang *et al*. and it turned out to be lower by 1-2 orders in magnitude.[100]

Specific cations have also been frequently used as additives in DSCs. This class of additives contains lithium[103] and guanidinium $[C(NH_2)_3^+]$ (abbreviated as G^+) ions that also improves the performance of the cells, however, with a mechanism different from that of TBP.[104-105] The adsorption of these ions on the semiconductor surface causes a positive shift of the TiO_2 CB edge, thus increasing the driving force of electron injection by increasing the difference between the LUMO energy level and E_{CB}. Hence,

these ions enhance the photocurrents of the DSC devices. And this characteristic was observed in the work of Zhang *et al*.,[106] where G^+ ions were used as additives in the electrolyte. A recorded efficiency of 11% was observed when G^+ ions along with the N3 dye were adsorbed on the TiO_2 surface forming a compact dye monolayer, blocking the direct contact of the electrolyte with the semiconductor material and thus reducing recombination rates and enhancing photovoltage. Kopidakis *et al*.[107] indicated an improvement in the V_{oc} of about 20 mV caused by the TiO_2 CB positive shift, in addition to the slower electron recombination rates by a factor of 20 in the cells when G^+ ions were added.

The two different classes of additives i.e., the nitrogen containing heterocycles and the specific cations, which have opposite effects on the TiO_2 conduction band edge, are often used simultaneously in DSCs. The Durrant group reported the highest device performance, where Li^+ ions and TBP were added to the electrolyte, giving a better result than the electrolytes where each additive was used individually. This achievement was explained by the collective effect of each type of additive, causing suppressed electron recombination rates by blocking the semiconductor surface and the upward shift of the TiO_2 band edge.[108]

Therefore, the performance of the redox mediator is highly affected by the properties of its constituents, including the solvent and the additives used, and its interaction with the dye sensitizer.

1.3.5 *Water in DSCs:*

The motivation of introducing water-based electrolyte into DSCs is its minimized cost, reduced volatility, non-flammability, and improved environmental compatibility. Conventional DSCs are made up of organic solvent-based electrolytes, which have low boiling points and harmful environmental effects. Unfortunately, the long term stability and the performance of aprotic devices are highly affected by the contamination of the cells with water, a problem that still remains unsolved even if barrier materials are used.[109] In fact, the amount of water has been calculated in the electrolyte of cells with 1 year of outdoor usage, and it turned out to be more than 10%. These traces of water can be introduced into the electrolyte solution and the pores of the semiconductor during the fabrication of the solar cells,[110] and this phenomenon is observed more frequently in flexible DSCs which are rapidly permeated by water, even in the presence of barriers.[111-112] Therefore, most scientists and researchers have believed that the presence of water of about 10% is poisonous and can have deadly effects on the DSC devices. Thus, many studies have been reported in the aim of understanding the influence of the water traces on the performance of the DSCs.

Harmful effects have been observed as a result of the permeation of the water molecules, except for DSCs assembled in N_2 or Ar filled glove box. Hence, water molecules can either adsorb on the TiO_2 semiconductor, permeate the materials used for sealing the device, or get into the solvents and the solutions of the dye sensitizer and the liquid electrolyte. The first study on the stability of cis-X_2bis(2,2'-bipyridyl-4,4'-dicarboxylate) ruthenium (II) (X= Cl^-, Br^-, I^-, CN^-, and SCN^-) sensitizer was done by

Gratzel *et al.*,[113] after the invention of the DSCs by few years. As a result of water contamination, a 20-30% decay in the J_{SC} was observed. However, this decay was then suppressed in the cells where water-tight sealants were used.

Initially, in 1998, Lindquist *et al.*[44] investigated the contamination of water using an electrolytic solution (LiI 0.10 M and I_2 10 mM in MAN) containing 2.2 M of water, which resulted in a decrease in J_{SC} and an increase in V_{OC}. The increase in V_{OC} was proportional to the amount of water added, and these results were explained by the strong adsorption of the water molecules on the TiO_2 surface, blocking the recombination reaction with I_3^- in the electrolyte and causing the upward shift of the TiO_2 CB. However, the increase in the V_{OC} did not enhance the device performance due to the huge reduction of J_{SC} and resulted in a depression in the overall efficiency from 6.4% to 5.2%. Several hypotheses were argued by Lindquist and co-workers including the detachment of the N3 dye from the TiO_2 surface, the change in the absorption properties of the dye due to the increase in the polarity of the solvent, and the substitution of the –NCS ligand of the dye which is induced by photon absorption.

In another study, electrodes were immersed in an electrolytic solution (LiI 0.50 M and I_2 50 mM in MPN) containing 5% by volume water. The FTIR spectrum showed a decreased intensity and broadening at the absorption band of the –NSC ligand (2100 cm^{-1}). Additionally, a small absorption peak was observed at 1575 cm^{-1} by Hagfeld and co-workers,[114] which contributed to the symmetric bending of H_2O molecules. Furthermore, a blue shifted absorption maxima was observed by the UV-Vis spectra and

it was suggested that these shifts are due to the replacement of the –NCS ligands with water or OH^- ions in the water permeated devices.

The work of Tributsch *et al.*[115] showed an increase in the internal resistance of the water contaminated cells, which was explained by the absence of the reduction reaction of I_3^- at the cathode. The absence of the reduction was suggested to be due to the bleaching of the electrolyte by the conversion of I_3^- ions to iodate (IO_3^-) in the electrolyte. However, the FTIR spectrum showed the absence of the absorption of IO_3^- at 800 cm^{-1} in addition to increased water concentration in the acetonitrile solvent, which was explained by the absorption peak in the region of OH-stretching, and after 84 days this signal became the main signal of the spectrum. Thus, it was proposed that the iodate ions were adsorbed on the TiO_2 surface and their formation was due to the water which acts as a weak base similar to TBP, causing the instability of I_3^- and the formation of IO_3^- at basic pH in addition to the enhancement of V_{OC}.

The final challenge of the twenty-first century is the full replacement of the conventional organic-based electrolyte with a 100% water-based redox mediator. Therefore, scientists have launched again a deep investigation on the effects of water on the performance of the DSC devices. In 2010, O'Regan and co-workers[116] published a seminal paper in which they prepared different electrolytes with varying the relative fraction of MPN and water. The electrolytes contained PMII 2.0 M, I_2 50 mM, GuSCN 0.10 M and TBP 0.5 M (PMII= 1-propyl-3-methylimidazolium iodide) with 0, 20, 40, 60, 80, and 100% volume water with respect to MPN. Additionally, a hydrophobic dye sensitizer (TG6) was used to avoid the dye desorption from the TiO_2 surface into water,

1% Triton X-100 was added to prevent phase separation in the water-based electrolyte, and a high concentration of PMII was selected to act as an iodide source and a surfactant. The molecular structure of the TG6 dye is shown in Figure 6.

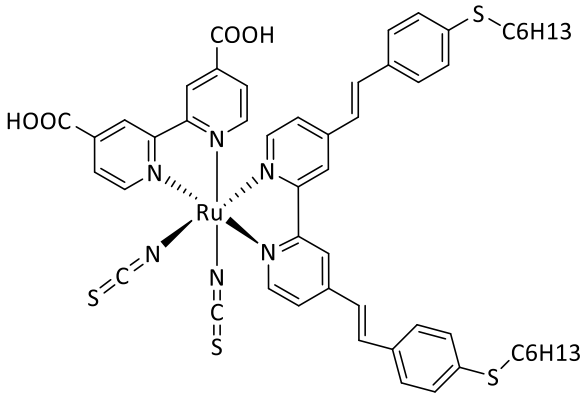

TG6

Figure 6: The molecular structure of the TG6 dye sensitizer.

The results obtained by this work showed no influence on the performance of the cells up to 40% vol of H_2O and the introduction of 80% vol water into the cell caused only 7-8% of losses in the J_{sc} and V_{oc} after 1000 h exposure to sunlight. Furthermore, by checking the efficiencies of the cells at different light intensities, it was observed that all the electron transfers and transport processes of the cells were performing well, even at high concentrations of water, since the data obtained showed no decrease in the performance of the cells at 0.4 suns and below. However, the saturation of the photocurrents was observed at light intensities of 0.5 suns and higher, and this was explained by the mass transport problems due to the slow diffusion of triiodide ions in the electrolyte. Moreover, as the water content increased the variation between identical cells also increased. Dye detachment was not observed in the cells,

but a reduction in the dye excited-state lifetime was observed due to the change of the solvent from MPN to water, which causes an increase in the dielectric constant.[117] All the cells showed the positive shift of the redox potential of the redox mediator, which decreases the driving force of dye regeneration which in return increases the recombination rates with the oxidized dye. Nevertheless, the electron lifetime was calculated for all the cells and it was decreased by a factor of two among all water contents. All the obtained results were explained by O'Regan *et al*. as follows: phase segregation takes place inside the pores of the semiconductor due to the different pore sizes and the heterogeneity of dye coverage, resulting in two types of pores in the TiO_2. Some pores will contain high iodine/TBP phases and other high iodide/water phases, with iodide being more soluble in water. This causes the reduced diffusion of the iodine giving saturated photocurrents, and the dyes which are in contact with pores poor in iodide concentration will undergo recombination rather than regeneration. These explanations have also clarified the variation between identical DSCs at high water content.

Weng and co-workers[118] reported that a specific amount of water in the electrolyte can enhance the photovoltaic performance of the DSC devices with the N3 dye. Their studies showed an increase in the V_{OC} and FF values in the presence of 2.2 M of water, in addition to a continuous decrease in the J_{SC}. Hence, causing an increase in the overall efficiency of the cells from 3.8% to 4.5% with 1.7 M of H_2O in the electrolyte (LiI 0.5 M and I_2 50 mM in MPN/H_2O). The reasons behind the increased V_{OC} were explained using the following hypotheses: the electron injection efficiency has

increased while the electron density has decreased in the presence of water, in addition to the reduction of the dye excited state decay rate and the recombination rates.

Frank and co-workers[119] compared the efficiencies of the ACN:VAN-based DSCs to MPN-based DSCs and the former cells gave higher V_{OC}, FF, and η values, however, the latter gave higher J_{SC}. They further investigated mixtures of water and organic solvents using Z907 dye, where the addition of water to the liquid electrolyte (PMII 1.0 M, I_2 0.15 M, GuSCN 0.10 M and NBBI 0.50 M; NBBI= N-butylbenzimidazole) increased both V_{OC} and J_{SC} but lowered FF values. The improvements in the J_{SC} values were explained by the positive shift of the TiO_2 CB which increases the driving force for electron injection, in addition to the enhanced charge collection efficiencies shown by the transport and recombination measurements. These investigations were carried out by means of Electrochemical Impedance Spectroscopy (EIS). The downward shift of the TiO_2 CB was attributed to the minimized potential difference between E_{CB} and E_{redox} by about 28 mV. This behaviour was explained to be the result of increased proton concentration at the semiconductor surface.[120] Moreover, as a result of the positive shift of the TiO_2 CB, a decrease in V_{OC} was expected, however, the photovoltage had increased by 15-19 mV and this was justified by a supressed recombination rate in the presence of water by a factor of 4-5. Concerning the stability of the cells, the J-V characteristic of electrolytes with the addition of water showed the same ageing behaviour as the ones without water, after 1000 h of continuous exposure to sunlight.

Miyasaka and co-workers[121] proposed the reuse of the of water-ethanol mixtures, which are produced as effluents from industrial processes[122], in aqueous DSCs. Pristine photoanodes, which were used in their studies, were hydrophobic enough to repel the water molecules from the TiO_2 pores. However, the use of ethanol activated the TiO_2/electrolyte (KI 0.50 M and I_2 0.25 M) interface, improving the wettability and thus increasing the J_{SC} of the cells.

All these scientific reports have evidenced that water is not a poison to DSCs and can be introduced in the cells in larger amounts. However, each and every component of the cell must be deeply investigated and studied to provide aqueous devices with the highest possible efficiency.

As previously mentioned, the introduction of some specific additives to the electrolyte solution can enhance the performance of the DSC device, by improving either the V_{OC} or J_{SC} or both. TBP has also been introduced in some water-based electrolytes, but it possessed low solubility in water. Therefore, alternative additives have been demonstrated or surfactants have been used to ensure their solubility in water. N-alkylbenzimidazole[123] derivatives have been introduced as another class of organic derivatives, having a similar behaviour to TBP. Yang and co-workers observed the increase in V_{OC} and FF of the water-based cells after adding bis-benzimidazole additives containing ethylene glycol repeating unit ($BBEG_n$) to the electrolyte (DMPII 0.50 M, LiI 0.10 M, I_2 50 mM and TBP/$BBEG_n$ 0.50 M in ACN/H_2O).[124] The enhancement in V_{OC} was attributed to the blocked recombination reaction between I_3^- ions and the injected electron due to the adsorption of water molecules on the TiO_2

surface, in addition to the downward shift of the redox potential of the redox mediator as stated previously by O'Regan *et al*. However, the N719 dye that was used in this study was detached from the semiconductor surface, thus limiting the flux of the injected electrons and minimizing J_{SC} values. Nevertheless, the introduction of $BBEG_n$ did not improve the overall efficiency of the DSC devices when compared to TBP, but enhanced the stability of the cells.

Surfactants, which have been used as another class of additives, are considered as key ingredients for water-based DSCs due to their ability in lowering the interfacial tension between two liquids or between a liquid and a solid.[125] These additives have been introduced specifically to homogenise a mixture of water and organic solvents used in an electrolyte, or to ensure the solubility of all the electrolytic components added in a 100% aqueous-based electrolyte. Kim and co-workers proposed the use of Triton X-100[125], a non-ionic surfactant having a hydrophilic polyethylene oxide chain and a lipophilic or hydrophobic aromatic hydrocarbon group of the formula $C_{14}H_{22}O(C_2H_4O)_n$. The addition of 0.02 M Triton X-100 into an aqueous electrolyte (LiI 0.10 M, I_2 50 mM, HDMII 0.60 M and TBP 0.50 M in MPN/H_2O; HDMII=1-hexyl-2,3-dimethylimidazolium iodide) resulted in an increase in the V_{OC} and FF values, with the increased amount of water (0.0-4.4 M), and a decreased J_{SC}. A maximum efficiency of 5.9% was obtained with 2.2 M of water. Several hypotheses were made to justify the increase in the V_{OC} values, including the downward shift of the redox potential of the electrolyte, the reduction in the recombination reaction rates and the upward shift of the TiO_2 CB. The reason behind the reduced recombination was explained by the fact that

I_3^- ions are more soluble in the hydrophilic Triton X-100 phase than at the photoanode interface, while the negative shift of the TiO_2 CB was attributed to the removal of some of the protons that are transferred from the sensitizer (containing –COOH groups) to the semiconductor by Triton X-100/H_2O phase. Concerning the decrease in the J_{SC} values, it was attributed to the decreased driving force for electron injection caused by the upward shift of the TiO_2 conduction band.[126] However, despite the decrease in J_{SC}, an increase in the limiting current was observed due to the enhanced diffusion of I^- ions in the presence of Triton X-100, which also caused, on its turn, a decrease in the charge transfer resistance at the cathode.

Based on the reported studies, the photovoltaic performance of 100% aqueous-based DSCs remains low compared to the organic based devices, and one of the main reasons is the incomplete wetting of the dye-adsorbed TiO_2 interface by the aqueous liquid electrolyte, which can be minimized by the addition of a surfactant.

By the introduction of water as an electrolyte solvent, new redox mediators have been demonstrated. In 2008, Teoh and co-workers proposed the use of a cerium-based electrolyte ($Ce(NO_3)_3$ 0.10 M and $Ce(NO_3)_4$ 50 M in a 35:65 EtOH:H_2O) with several commercial and natural dyes.[127] Additionally, a Schottky barrier composed of Au NPs was deposited on the photoanode which resulted in the passing of the excited electrons through the Au layer by tunnelling the TiO_2 CB, thus preventing electron recombination reactions and improving the performance of the cells.

The use of ferrocyanide/ferricyanide redox couple was also introduced by Spiccia *et al*. in 2012[128], to overcome the problems of light absorption, corrosiveness,

and iodate formation of the conventional electrolyte. In their work, a hydrophobic carbazole dye (MK-2) was used with a 100% aqueous-based electrolyte ($K_4Fe(CN)_6$ 0.40 M, $K_3Fe(CN)_6$ 40 mM, KCl 0.10 M and 0.1% by volume Tween 20) at pH 8. The redox potential of $Fe(CN)_6^{4-/3-}$ is similar to that of I_3^-/I^-, and the cells resulted in an overall efficiency of 4.1% showing only a decrease in J_{SC} values, when compared to the conventional I_3^-/I^- based DSCs, and faster recombination rates of 3 orders of magnitude. Furthermore, there was no difference in the V_{OC} values due to the upward shift of the TiO_2 CB by 150 mV. However, due to the photocatalytic decomposition of this new redox mediator, a decay in the performance was observed when measured under unfiltered white light illumination.

Despite the low water solubility of sulphur-based systems, Sun and co-workers demonstrated an aqueous based thiolate/disulphide redox couple, as a non-corrosive alternative to the photosensitive ferrocene based electrolyte.[129] The novel redox couple consisted of 1-ethyl-3-methylimidazolium-4-methyl-1,2,4-triazole-3-thiolate (TT^-EMI^+) and 3,3'-dithiobis[4-methyl-1,2,4-triazole (DTT). In their work, a hydrophobic organic dye (D45) was used with a 100% water-based electrolyte (TT^-EMI^+ 0.20 M, DTT 0.20 M, TBP 0.50 M and Triton X-100 1% by volume) and resulted in an overall efficiency of 2.6%. Moreover, the diffusion coefficient was minimized when compared to the conventional I_3^-/I^- based DSCs, and the regeneration of the dye was slowed down by a factor of 4. Additionally, a higher efficiency of 3.5% was observed when a D51 dye, having a higher molar extinction coefficient and broader absorption spectra, was used. Furthermore, in the work of Ghaddar *et al*., a new water soluble and stable redox

electrolyte system based on a thiolate/disulphide system was synthesized and used with a novel tetrazolate based dye, the T169 dye, that exists in the zwitterionic form at pH 5.0. Results showed a very high current and IPCE% due to the sufficient wetting of the dye by the aqueous electrolyte, promising a new site to explore aqueous-based DSCs with high efficiencies and photovoltaic performances.

Recently, as previously stated, the iodide based organic electrolytes have been replaced by cobalt complexes, which have recorded high photovoltaic performances. The use of cobalt complexes in aqueous DSCs has been also possible due to their high water solubility, being transition metal ion complexes. Spiccia *et al*. introduced a truly water-based electrolyte ($[Co(bpy)_3]^{2+}$ 0.20 M, $[Co(bpy)_3]^{3+}$ 40 mM and NMBI 0.70 M), where NMBI was used as an additive to increase V_{OC}.[130] Additionally, different amounts of polyethylene glycol (PEG 300) was added to minimize phase separation while using the hydrophobic MK-2 dye. The maximum conversion efficiency of 4.2% was obtained with the addition of 1% by weight of PEG. Interestingly, by the addition of PEG, the lowest diffusion resistance and the highest recombination resistance were obtained. Furthermore, only a 10% decrease in the efficiency of the DSCs was observed after keeping them more than three months in the dark.

For many years, platinum has been the choice of the catalyst at the cathode due to its high catalytic activity and excellent conductivity. However, its high cost and scarcity, in addition to the introduction of 100% aqueous-based electrolytes have motivated scientists to find alternative catalysts, aiming at obtaining low cost and more water compatible cathodes. Transition metal compounds (carbides, nitrides) have been

suggested as alternatives because they have high catalytic activity, specially towards sulphur and cobalt-based electrolytes.[131-132] Organic polymers have also grabbed attention, specifically poly(3,4-ethylenedioxythiophene) (PEDOT),[133] which has been used by Sun and co-workers in order to improve the FF of the DSCs based on thiolate/disulphide redox mediator.[129] Surprisingly, the PEDOT was detached from the conductive glass showing poor stability in the aqueous medium, while the opposite was observed in the work of Boschloo and co-workers, where V35 dye was used with a truly water-based I_3^-/I^- electrolyte.[134] In the work of Boschloo *et al*., PEDOT improved the efficiencies of the cells by increasing the V_{OC} and J_{SC} values, compared to the Pt counter electrode, and this was explained by the structure of the PEDOT which increased the surface area at the cathode, thus enhancing its catalytic activity. The structure of the PEDOT is given in Figure 7.

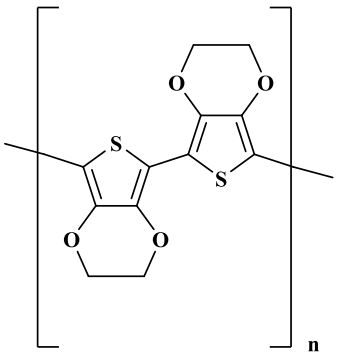

PEDOT

Figure 7: The molecular structure of the PEDOT cathode catalyst.

1.3.6 *Low Artificial Light*:

In recent years, DSCs have also been tested under low light reaching efficiencies of up to ca. 30%.[135] De Rossi *et al*. observed the increase in the PCE of a flexible DSC from 2.3% to 6.6% using indoor light.[136] Most of the reported studies of low light DSCs use Ru complex sensitizers and iodide-base redox mediator, however, Fukuzumi introduced a copper-based electrolyte which also worked well under reduced light intensities.[94] Wang and co-workers, who used an organic dye and Cu electrolyte, further supported these results by showing an increase in PCE from 7.0% to 8.3% when reducing the light intensity.[96] Furthermore, Gratzel and co-workers used the $[Cu(tmby)_2]^{2+/1+}$ redox shuttle with the D35 and XY1 dye sensitizers and reported a 28.9% efficiency under ambient room lighting.[137]

1.3.7 *Electrochemical Impedance Spectroscopy (EIS):*

EIS is an important technique for DSCs since it provides an information about the electron processes taking place in a device. EIS data are given in the form of Nyquist plots, shown in Figure 8. The first semicircle indicates the resistance at the electrolyte/counter electrode interface (R_{Pt}). The second semicircle in the middle region represents the charge recombination resistance (R_{CT}) and the last circle is associated to the diffusion of the oxidized species in the electrolyte (Z_d). A high charge transfer resistance of the electron recombination is expected, which indicates a decrease in the recombination processes of a DSC, while the remaining resistances must be low to obtain a fast diffusion of the electrolyte in addition to a fast reduction of the oxidized species at the counter electrode. R_S is the transport resistance of the FTO and C_μ is the chemical capacitance at the TiO_2 interface.

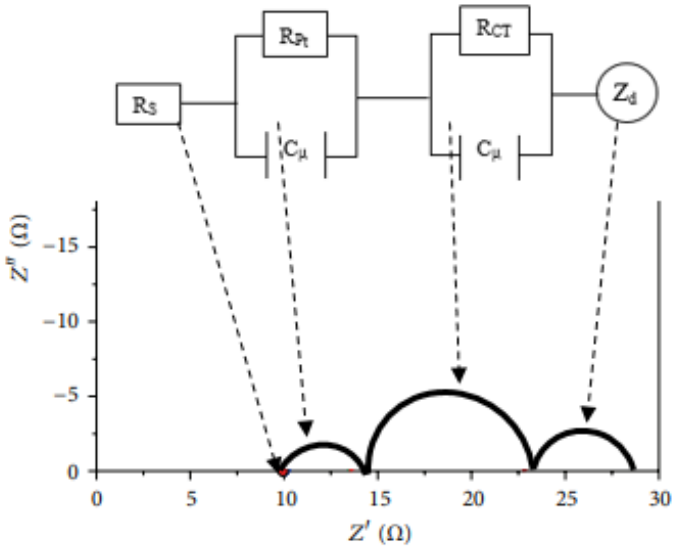

Figure 8: A typical Nyquist plot and the equivalent circuit of a DSC device.

1.4 Aim of Work:

Motivated by the work of O'Regan *et al*. concerning aqueous-based DSCs despite the thought that water has some deadly effects on their performance, and in addition to the inspiring facts that make copper complexes great candidates for 1 electron redox couples, we designed and synthesized three different pyridyl-based copper complexes, $[Cu(dmap)_2]^{2+/1+}$, $[Cu(dmdcbpy)_2]^{2+/1+}$, and $[Cu(tmabpy)_2]^{2+/1+}$. The reorganization energy between Cu(I) and Cu(II) species was minimized by the addition of substituents at the 6,6' positions of the bipyridine or the 2,9 positions of the phenanthroline groups to stabilize the Cu(I) geometry. Furthermore, hydrophilic groups such as –OHs were added to assure their dissolution in water and their use in 100% aqueous-based DSCs. Finally, the photovoltaic performances of fully assembled solar cells were investigated under 1 sun for outdoor applications, and under low ambient light for indoor applications with several commercially available organic and metal complex dye sensitizers.

CHAPTER 2

EXPERIMENTAL METHODS AND INSTRUMENTATION

2.1 Materials:

Chemicals were purchased from Sigma-Aldrich and used as supplied. TiO_2 colloids 30NR-D and WER2-O were purchased from Dyesol (Australia). Commercial dyes were purchased from Dyenamo (Sweden). Fluorine-doped tin oxide (FTO) transparent conducting glasses "Tec 8" and "Tec 15" were purchased from Pilkington (USA).

2.2 Instrumentation:

The NMR spectra (^1H) were measured on a Bruker AM 500 MHz spectrometer. Cyclic Voltammetry was done using an electrochemical setup consisted of a three-electrode cell, with a gold or platinum rod as the working electrode, a platinum wire ~ 1 mm diameter as the counter electrode, and Ag/Ag^+ (10 mM $AgNO_3$) as the reference electrode.

Electrochemical impedance spectra of the DSCs were performed with CH instrument 760B (USA). The obtained impedance spectra were fitted with the Z-view software (v2.8b, Scribner Associates Inc.). The spectra were performed in the frequency range 0.1 Hz-105 Hz with oscillation potential amplitudes of 10 mV at RT under open circuit conditions at different light levels.

IPCE% spectra were recorded using a Newport 74000 Cornerstone™ monochromator. Photocurrent vs. Voltage (J-V) characteristics were measured with a Keithley 2400 source meter. For outdoor applications, a solar simulator illuminated by a Xenon arc lamp (Oriel) through an AM 1.5 simulation filter (ScienceTech) was used, and the irradiated area of the cell was 0.5 x 0.5 cm^2 with a 0.6 x 0.6 cm^2 black mask. For indoor applications, a White light LED of 13 W (KONNICE, BL13W) was used.

The photoinduced absorption spectra of the cells were acquired using photo-induced absorption spectroscopy system from Dyenamo (Sweden). The spectra were recorded over a wavelength range of 450-1000 nm following an (on/off) photo-modulation from a royal blue LED (455 nm). White probe light from a quartz tungsten-halogen lamp (10 W) was used as an illumination source. The light was focused into a monochromator (Cornerstone 130) and detected using a Si, connected to a lock-in amplifier (Stanford Research Systems model SR830).

The spectrum and power of the white light was measured with a spectrometer (Stellar). A neutral density filter was used for the light intensity dependence measurements.

2.3 Solar Cell Fabrication:

Dye sensitized solar cells were fabricated using standard procedures. Compact TiO_2 blocking layers were deposited by spray pyrolysis using hand-held atomizer, following the method developed by Kavan and Gratzel. A solution of 0.2 M titanium di-isopropoxide bis(acetylacetonate) in 2-propanol was sprayed in very short pulses of 1 s duration onto a clean fluorine-doped conductive glass Tec15 placed on a hotplate at 450

˚C. This was followed by a pre-treatment process with 40 mM $TiCl_4$ aqueous solution at 70 ˚C for 1 hour. After that, a 6 μm mesoporous layer of TiO_2 was printed on the glass by the doctor-blading method from a titania paste (TiO_2 Dyesol 30NR-D), followed by a 6 μm Dyesol WER2-O TiO_2 paste scattering layer. Then, the electrodes were sintered at 500 ˚C for 60 min, followed by a post-treatment process with 40 mM $TiCl_4$ aqueous solution at 70 ˚C for 30 min. An additional heating of the films at 500 ˚C for 1 hour is required before sensitizing them with the corresponding dye solutions overnight. The PEDOT counter electrodes were prepared by electro-polymerization of the EDOT (3,4-ethylenedioxythiophene) monomer by a periodic reversal potential technique onto clean conductive glasses Tec8. The electrodeposition bath contained an aqueous solution of 0.01 M EDOT and 0.1 M $LiClO_4$ with a 24 s pulse at a potential of 1.2 V and 12 s of -0.6 V vs. Ag/AgCl. Solar cell assembly was done by sealing the counter electrode to the TiO_2 working electrode using a 60 μm Surlyn (Dupont) spacer at ~ 100 ˚C for 3 min.

2.4 Synthesis of the Copper Complexes:

2.4.1 *Preparation of $[Cu(dmap)_2]^{2+/1+}$ Complex:*

2.4.1.1 Synthesis of 1,10-phenanthroline-2,9-dicarbaldehyde:

A mixture of 2,9-dimethyl-1,10-phenanthroline (2.90 g, 13.9 mmol) and selenium dioxide (7.25 g, 65.3 mmol) in dioxan containing 4% water (200 mL) was heated under reflux for 2 hours and then filtered over celite while hot. The filtrate was then cooled and the dialdehyde was separated from it as yellow crystals (2.00 g, 61%).

^{1}H NMR (500 MHz, DMSO) δ 10.37 (d, *J* = 5 Hz, 1H), 8.82 (d, *J* = 10, 1H), 8.33 (d, *J* = 10 Hz, 1H), 8.31 (s, 1H).

2.4.1.2 Synthesis of (1,10-phenanthroline-2,9-diyl)dimethanol (dmap):

A solution of 1,10-phenanthroline-2,9-dicarbaldehyde (1.00 g, 4.2 mmol) and sodium borohydride (0.30 g, 7.9 mmol) in ethanol (100 mL) was heated under reflux for 2 hours. The mixture was then concentrated and the residue recrystallized from water to give the dialcohol as yellow crystals (0.65 g, 64%).

^{1}H NMR (500 MHz, DMSO) δ 8.48 (d, *J* = 10 Hz, 1H), 7.93 (s, 1H), 7.88 (d, *J* = 5 Hz, 1H), 5.69 (s, 1H), 4.88 (s, 2H).

2.4.1.3 Synthesis of Cu(I)(dmap)$_2$Cl:

(1,10-phenanthroline-2,9-diyl)dimethanol (0.20 g, 0.80 mmol) was dissolved in water (1 mL) and CuCl (0.04 g, 0.40 mmol) was added and the mixture was stirred over 2 hours. The resulting complex was slightly soluble in water.

And

To a solution of (1,10-phenanthroline-2,9-diyl)dimethanol (0.25 g, 1.04 mmol) in ethanol $CuCl_2.2H_2O$ (0.09 g, 0.52 mmol) and water were added sequentially and left stirring for 2 hours. The mixture was then concentrated and ascorbic acid (0.14 g, 0.78 mmol) was dissolved in water and added to the reaction mixture which was then cooled to 0˚C, filtered and washed with water giving the complex as red precipitate (0.20 g, 59%). The resulting complex was slightly soluble in water.

2.4.1.4 Synthesis of $Cu(II)(dmap)_2Cl_2$:

(1,10-phenanthroline-2,9-diyl)dimethanol (0.04 g, 0.16 mmol) was dissolved in water (2 mL) and $CuCl_2.2H_2O$ (0.013 g, 0.08 mmol) was added and the mixture was stirred over 2 hours.

2.4.2 ***Preparation of*** $[Cu(dmdcbpy)_2]^{2+/1+}$ ***Complex*****:**

2.4.2.1 Synthesis of (1E,5E)-1,6-di(furan-2-yl)hexa-1,5-diene-3,4-dione:

To a solution of furfural (15.4 mL, 185 mmol) and 2,3-butanedione (4.08 mL, 46 mmol) in MeOH (40 mL), piperidine (0.92 mL, 9 mmol) and glacial acetic acid (0.54 mL, 9 mmol) were added sequentially. The mixture was set to reflux for 6.5 h. When cooled to room temperature and then to 0˚C, the mixture was filtered and washed with cold MeOH and then dried giving the desired product as brownish yellow solid (5.06 g, 45%).

^{1}H NMR (500 MHz, Chloroform-*d*) δ 7.54 (d, *J* = 15.9 Hz, 1H), 7.50 (d, *J* = 1.8 Hz, 1H), 7.25 (d, *J* = 15.8 Hz, 1H), 6.74 (d, *J* = 3.5 Hz, 1H), 6.47 (dd, *J* = 3.5, 1.8 Hz, 1H).

2.4.2.2 Synthesis of 4,4'-di(furan-2-yl)-6,6'-dimethyl-2,2'-bipyridine:

To a solution of (1E,5E)-1,6-di(furan-2-yl)hexa-1,5-diene-3,4-dione (5.06 g, 20.88 mmol) in MeOH (160 mL), N-Acetonylpyridinium chloride (7.17 g, 45.49 mmol) and ammonium acetate (10.13 g, 131.42 mmol) were added and the mixture was set to

reflux for 12h. When cooled to room temperature and then to 0˚C, the mixture was filtered and washed with cold MeOH and then dried giving the desired product as brown solid (3.51 g, 53%).

^{1}H NMR (500 MHz, Chloroform-*d*) δ 8.91 (s, 1H), 7.56 (dd, *J* = 1.7, 0.7 Hz, 1H), 7.53 (d, *J* = 1.5 Hz, 1H), 7.35 (s, 1H), 6.55 (dd, *J* = 3.5, 1.8 Hz, 1H), 2.82 (s, 3H).

2.4.2.3 Synthesis of 6,6'-dimethyl-[2,2'-bipyridine]-4,4'-dicarboxylic acid (dmdcbpy):

To a solution of 4,4'-di(furan-2-yl)-6,6'-dimethyl-2,2'-bipyridine (4.30 g, 15.77 mmol) in t-BuOH (300 mL) and water (60 mL), $KMnO_4$ (27 g, 170.89 mmol) and 1 palette of KOH were added and the mixture was set to reflux overnight. Later, another 4 equivalences of KMnO4 and 1 palette of KOH was added and set to reflux for 2 hrs. Then the mixture was filtered hot over Celite to get rid of MnO_2. (water was added to the MnO_2 and 1 palette of KOH and let to heat until it boils and then filtered over the filtrate). The volume of the filtrate was decreased to around 50 mL (rotavap 50˚C) and HCl (2M) was added to lower the pH to 2, as a result white precipitate was formed which was then filtered and dried giving the desired product (2.36 g , 55%).

^{1}H NMR (500 MHz, Deuterium Oxide) δ 7.98 (dd, *J* = 1.4, 0.7 Hz, 1H), 7.69 – 7.58 (m, 1H), 2.64 (s, 3H).

2.4.2.4 Synthesis of Cu(I)(dmdcbpy)$_2$Cl Complex:

The solution of 6,6'-dimethyl-[2,2'-bipyridine]-4,4'-dicarboxylic acid (0.60 g, 2.20 mmol) in water (13 mL) was heated to 70˚C. Then KOH (1M) was added until complete

dissolution of the compound. $CuSO_4.5H_2O$ (0.18 g, 0.72 mmol) was dissolved in water (13 mL) and added to the solution followed by the addition of 50 drops of KOH (1M). Then ascorbic acid (0.30 g, 1.70 mmol) was dissolved in water (13.5 mL) and added to the reaction mixture followed by the addition of HCl (1M) until the pH was adjusted to 2. The mixture was filtered and washed with water and then dried giving the desired product as red solid (0.75 g, 96%).

^{1}H NMR (500 MHz, Deuterium Oxide) δ 8.46 (s, 1H), 7.78 (s, 1H), 2.28 (s, 3H).

2.4.2.5 Synthesis of $Cu(II)(dmdcbpy)_2Cl_2$ Complex:

$Cu(I)(dmdcbpy)_2Cl$ (0.32 g, 0.49 mmol) and concentrated KOH were added to water, followed by 15 drops of H_2O_2 reaching a total volume of 5 mL and left stirring until a green solution is obtained giving the desired product (0.09 M).

2.4.3 *Preparation of $[Cu(tmabpy)_2]^{2+/1+}$ Complex*:

2.4.3.1 Synthesis of [2,2'-bipyridine]-6,6'-dicarboxylic acid**:**

6,6'-dimethyl-2,2'-bipyridine (10.00 g, 54.27 mmol) was added slowly, with stirring, to concentrated sulphuric acid (200 mL). The resulting solution was cooled by an ice-bath and chromium (VI) oxide (32.60 g, 326 mmol) was added in small portions keeping the temperature below 40˚C. After the addition was complete, the reaction mixture turned dark green. It was left to stir overnight at room temperature and then poured onto crushed ice. The white precipitate that was formed was filtered and washed thoroughly

with cold water and dried under vacuum overnight giving the desired product (11.40 g, 86%).

2.4.3.2 Synthesis of diethyl [2,2'-bipyridine]-6,6'-dicarboxylate:

To a solution of [2,2'-bipyridine]-6,6'-dicarboxylic acid (5.74 g, 23.50 mmol) in ethanol (500 mL) concentrated sulphuric acid (5 mL) was added dropwise. The mixture was stirred for 30 minutes at room temperature and then refluxed overnight. Afterwards, the ethanol was evaporated and the mixture was cooled to 5˚C by an ice-bath and saturated $NaHCO_3$ solution (300 mL) was added slowly to neutralize (pH=8). The mixture was extracted with chloroform (3x50 mL). the combined organic layers were dried over Na_2SO_4, filtered and the solvent was removed to give the desired product as white solid (6.06 g, 86%).

2.4.3.3 Synthesis of [2,2'-bipyridine]-6,6'-diyldimethanol:

To a suspension of diethyl [2,2'-bipyridine]-6,6'-dicarboxylate (6.00 g, 19.98 mmol) in ethanol (350 mL) sodium borohydride (18.00 g, 343.64 mmol) was added in small portions and the reaction mixture was refluxed overnight. After cooling, saturated aqueous ammonium chloride (75 mL) was added and ethanol was evaporated. Water was added until all the white solids were dissolved and the aqueous layer was extracted with ethyl acetate (4x250 mL) and the combined organic layers were dried over anhydrous Na_2SO_4, filtered and the solvent was removed to give the desired product as white solid (4.00 g, 90%).

2.4.3.4 Synthesis of 6,6'-bis(bromomethyl)-2,2'-bipyridine:

To a solution of [2,2'-bipyridine]-6,6'-diyldimethanol (1.00 g, 4.62 mmol), 40% hydrobromic acid (30 mL) and sodium bromide (6.50 g, 63.17mmol) concentrated sulphuric acid (7 mL) was added dropwise. The reaction mixture was refluxed overnight and then cooled to 0˚C by an ice-bath, followed by the addition of ice water (60mL). The pH was adjusted to 8-9 with saturated aqueous solution of potassium hydroxide and extracted with chloroform (3x50 mL), the combined organic layers were dried over anhydrous Na_2SO_4, filtered and the solvent was removed to give the desired product as grey solid (0.92 g, 58%).

2.4.3.5 Synthesis of 1,1'-([2,2'-bipyridine]-6,6'-diyl)bis(N,N,N-trimethylmethanaminium) (tmabpy):

To a solution of 6,6'-bis(bromomethyl)-2,2'-bipyridine (1.50 g, 4.38 mmol) in chloroform (100 mL), trimethyl amine (50% aqueous solution, 20 mL) was added and was stirred at room temperature overnight. The solvent was then evaporated completely to give the desired product (1.80 g, 89%).

2.4.3.6 Synthesis of $Cu(I)(tmabpy)_2Cl$ Complex:

To a stirring solution of 1,1'-([2,2'-bipyridine]-6,6'-diyl)bis(N,N,N-trimethylmethanaminium) (1.00 g, 2.17 mmol) in H_2O (5 mL), $CuCl_2.2H_2O$ (0.12 g, 0.71 mmol) was added followed by the addition of ascorbic acid (0.16 g, 0.91 mmol)

resulting in a red solution. Ethanol (125 mL) was added and the reaction mixture was left at 0˚C overnight resulting in the formation of precipitate which was filtered giving the desired product as red solids (0.50 g. 64%).

2.4.3.7 Synthesis of $Cu(II)(tmabpy)_2Cl_2$ Complex:

To a stirring solution of 1,1'-([2,2'-bipyridine]-6,6'-diyl)bis(N,N,N-trimethylmethanaminium (1.00 g, 2.17 mmol) in H_2O (5 mL), $CuCl_2.2H_2O$ (0.12 g, 0.71 mmol) was added resulting in a green solution. Followed by the addition of ethanol (75 mL) resulting in the formation of precipitate. The mixture was left at 0˚C overnight and filtered giving the desired product as green solids (0.35 g, 45%).

2.5 Preparation of the Electrolytes:

2.5.1 *Preparation of $[Cu(dmdcbpy)_2]^{2+/1+}$ based Electrolyte*:

To a solution of $Cu(II)(dmdcbpy)_2Cl_2$ (1.11 mL) $Cu(I)(dmdcbpy)_2Cl$ (0.13 g, 0.39 mmol) and KOH were added until the total dissolution of the compound. Then the pH was adjusted to 5.8 with the addition of HCl reaching a total volume of 2 mL, giving the Cu(I) (0.1 M)/Cu(II) (0.05 M) electrolyte. 0.1 M KCl, 0.1 M $LiClO_4$, 0.5% Triton X-100, 0.02% FS-35, and 1% by weight PEG (6000) were added to the electrolyte solution.

2.5.2 *Preparation of $[Cu(tmabpy)_2]^{2+/1+}$ based Electrolyte*:

To a stirring solution of $Cu(I)(tmabpy)_2Cl$ (0.20 g, 0.2 mmol) in water (2 mL), $Cu(II)(tmabpy)_2Cl_2$ (0.11 g, 0.1 mmol) was added giving the Cu(I) (0.1 M)/Cu(II) (0.05 M) electrolyte. 0.1 M KCl, 0.5% Triton X-100, and 0.02% FS-35 were added to the electrolyte solution.

CHAPTER 3

RESULTS AND DISCUSSION

3.1 Design, Synthesis and Characterization of Water-Soluble Redox Mediators:

To start with, three different copper (I/II) complexes were designed in a way to show some solubility in water. These complexes were synthesized for the purpose of using them as 100% aqueous-based redox mediators for dye-sensitized solar cells. The approach that we adopted in the design was the synthesis of highly-charged pyridyl-based copper complexes (anionic or cationic) with hydrophilic groups such as –OHs, in addition to bearing two groups on the 6 and 6' positions for the bipyridine-based or 2 and 9 for phenanthroline-based complexes that stabilize the copper in the (I) state. Three different copper complexes that possessed the above criteria were synthesized using the procedures shown in the synthetic Schemes 1, 2, and 3, and the water solubility was evaluated. The synthesis of the $[Cu(dmap)_2]^{2+/1+}$ complex started with the oxidation of 2,9-dimethyl-1,10-phenanthroline using selenium dioxide giving the di-aldehyde, which was reduced in the presence of sodium borohydride forming the desired di-alcohol product. The complexation with copper (II) was attained using $CuCl_2.2H_2O$ giving $Cu(II)(dmap)_2Cl_2$ which was further reduced to $Cu(I)(dmap)_2Cl$ by ascorbic acid. The resulting Cu(I) complex was slightly soluble in water even with the presence of four hydroxyl groups, and therefore was not further investigated. As an alternative the $[Cu(dmdcbpy)_2]^{2+/1+}$ complex was synthesized, which bears four carboxyl

groups that exist in the anionic forms at pH's around 6. The synthesis of the second complex started with the aldol condensation of furfural and 2,3-butanedione, the resulted product was further condensed in the presence of *N*-acetonylpyridinium and ammonium acetate giving the di-furyl functionalized bipyridine, which was later oxidized using $KMnO_4$ resulting in the desired dicarboxylic acid. The copper (II) complexation was performed with $CuSO_4.5H_2O$ in the presence of KOH giving $Cu(II)(dmdcbpy)_2Cl_2$ which was further reduced to $Cu(I)(dmdcbpy)_2Cl$ using ascorbic acid. The attained product had a good solubility in water for the copper (I) and copper (II) complexes (up to 0.2 M Cu(I) in water). Finally, for the third complex first step of the synthesis involved the oxidation of 6,6'-dimethyl-2,2'-bipyridine using CrO_3, followed by esterification reaction and reduction in the presence of $NaBH_4$ yielding the di-alcohol product. By an acid-catalysed S_N2 reaction the di-alcohol was transformed to the dibromo derivative which was followed by another substitution reaction with trimethyl amine giving the desired product bis-quaternary ammonium salt. The complexation reaction with copper (II) was similar to that of the first complex. The attained complexes had very high solubility in water (of more than 0.2 M in water). The structures of the compounds were confirmed by ^1H NMR when applicable.

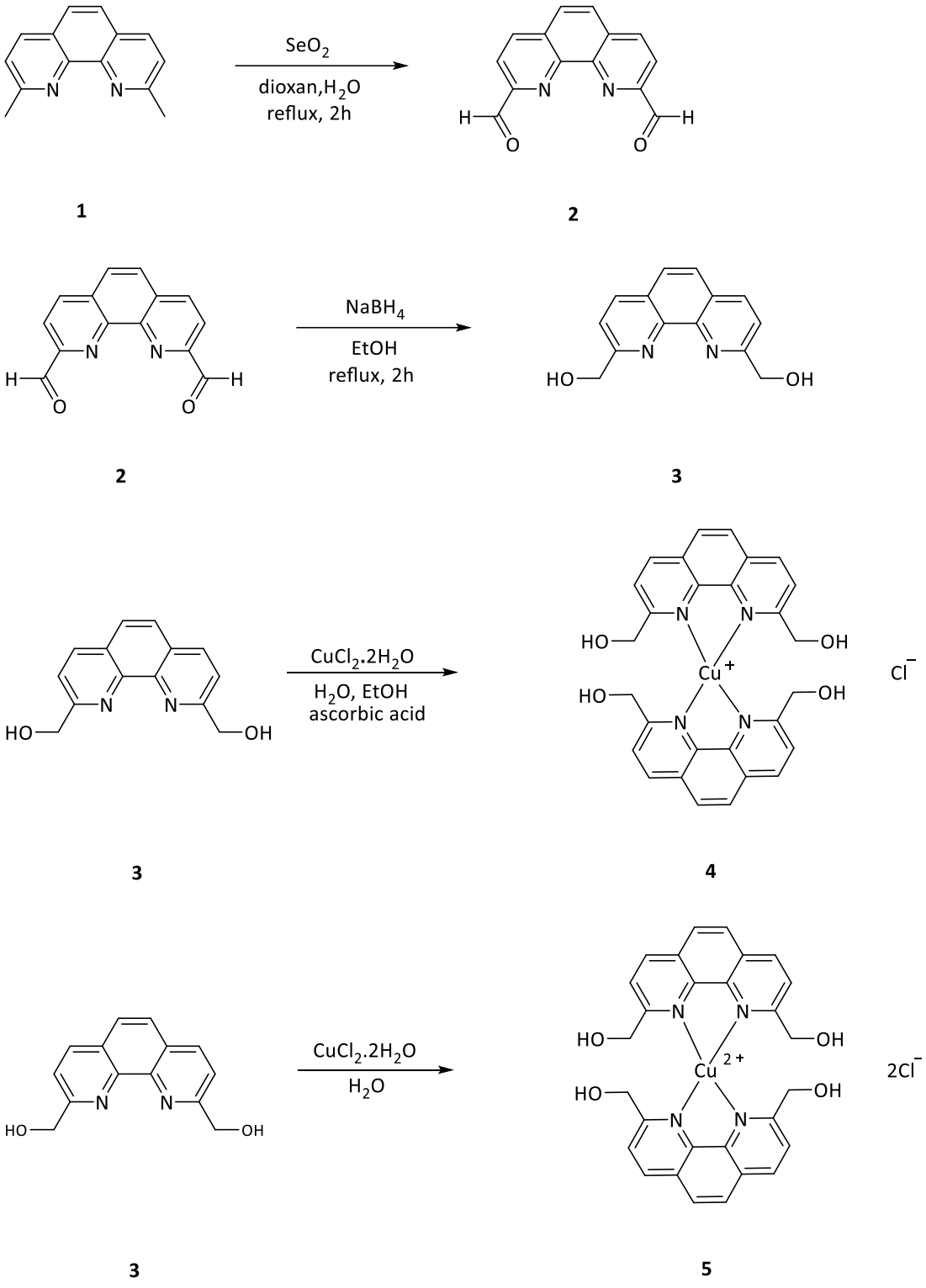

Scheme 1: Synthetic Scheme of $[Cu(dmap)_2]^{2+/1+}$ Complex.

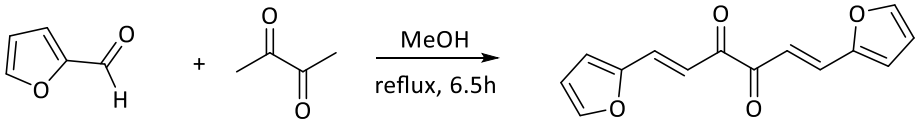

6 **7** **8**

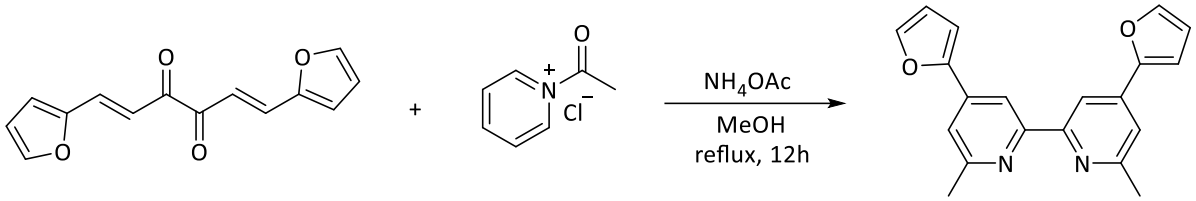

8 **9** **10**

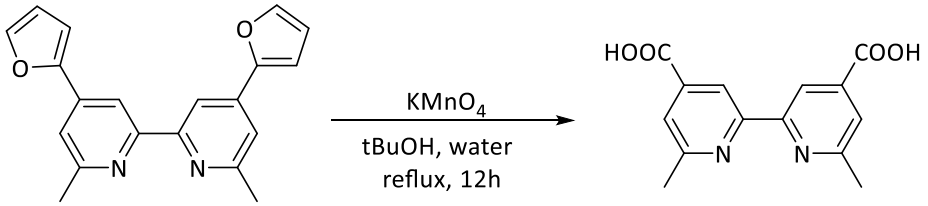

10 **11**

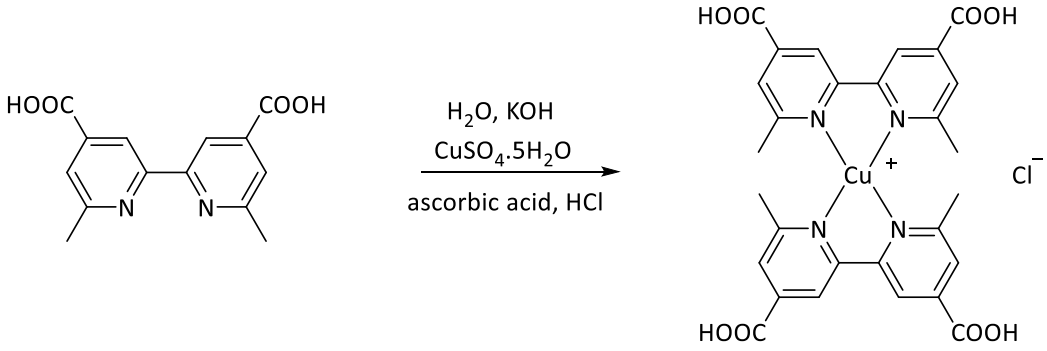

11 **12**

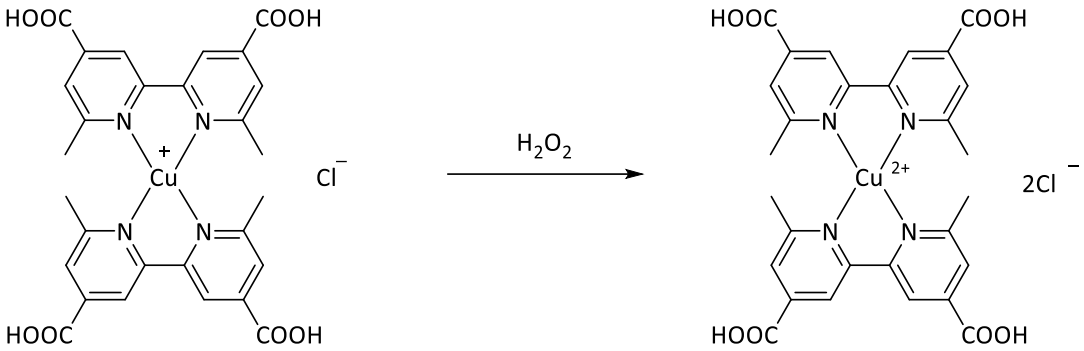

12 **13**

Scheme 2: Synthetic Scheme of $[Cu(dmdcbpy)_2]^{2+/1+}$ Complex.

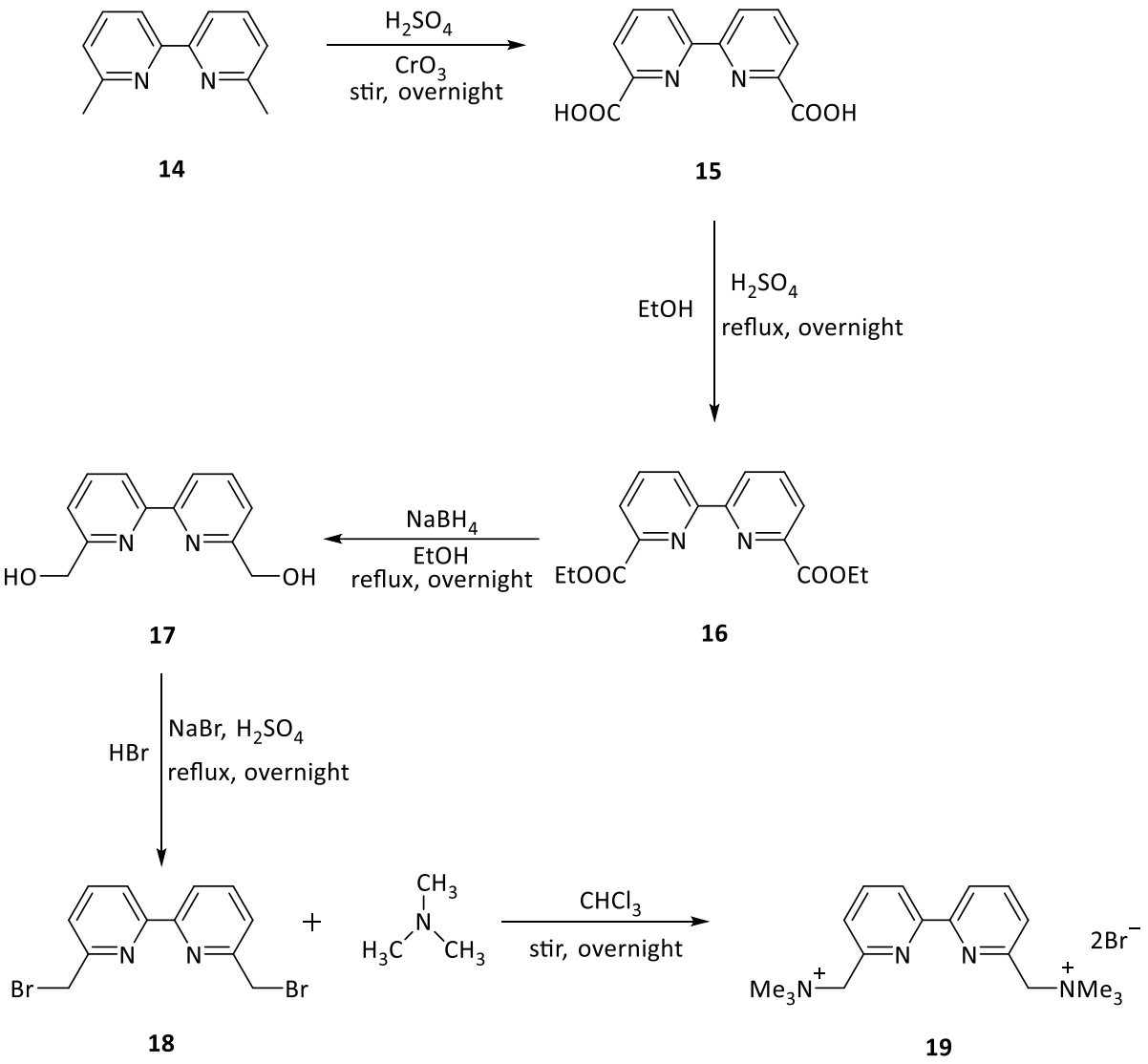
H2SO4
CrO3
stir, overnight
HOOC
COOH
14
15
EtOH
H2SO4
reflux, overnight
NaBH4
EtOH
reflux, overnight
HO
OH
EtOOC
COOEt
17
16
HBr
NaBr, H2SO4
reflux, overnight
Br
Br
CHCl3
stir, overnight
Me3N
NMe3
2Br−
18
19

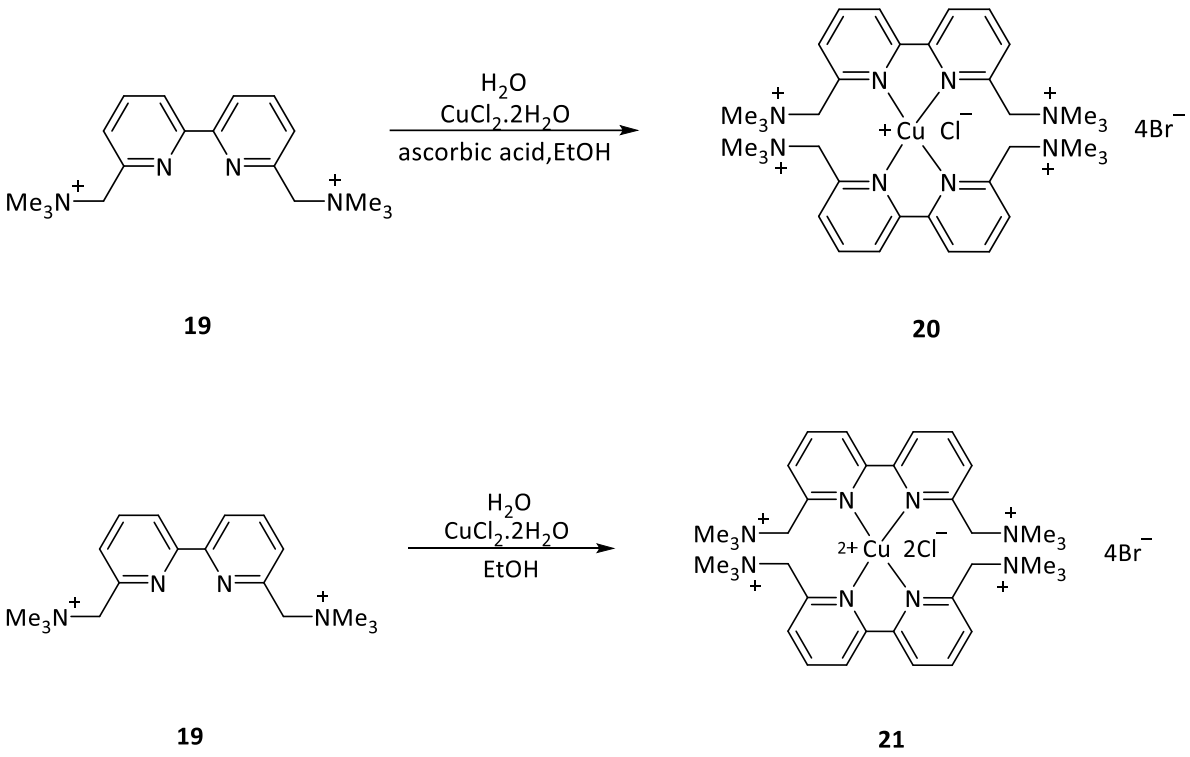

Scheme 3: Synthetic Scheme of $[Cu(tmabpy)_2]^{2+/1+}$ Complex.

3.2 Electrochemical Properties:

The formal redox potentials of the $[Cu(dmdcbpy)_2]^{2+/1+}$ and $[Cu(tmabpy)_2]^{2+/1+}$ complexes are determined by cyclic voltammetry using three electrodes setup with a gold working electrode and Ag/AgCl reference electrode. From the obtained voltammograms; which is semi-reversible for $[Cu(dmdcbpy)_2]^{2+/1+}$ (distinguished by the difference in the anodic and cathodic peak currents) and reversible for $[Cu(tmabpy)_2]^{2+/1+}$ (distinguished by the equal anodic and cathodic peak currents) of Cu(I) species, the formal redox potentials for $[Cu(dmdcbpy)_2]^{2+/1+}$ and $[Cu(tmabpy)_2]^{2+/1+}$ were determined. The redox potentials were measured to be 0.47 V and 0.19 V vs Ag/AgCl for $[Cu(dmdcbpy)_2]^{2+/1+}$ and $[Cu(tmabpy)_2]^{2+/1+}$, respectively. The redox potentials were referenced to NHE by the addition of 0.15 V with respect to the formal potential of the reference ferricyanide/ferrocyanide redox couple being 0.25 V vs Ag/AgCl and having a theoretical potential of 0.40 V vs NHE, see Figure 10.

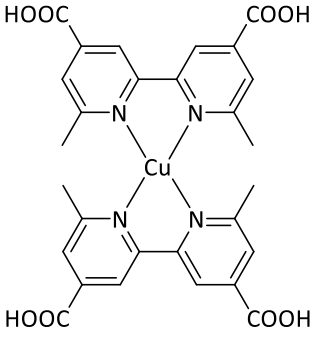

$[Cu(dmdcbpy)_2]^{2+/1+}$
$E_{1/2}$= 0.62 V

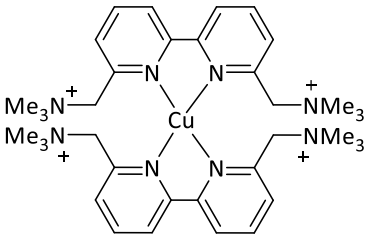

$[Cu(tmabpy)_2]^{2+/1+}$
$E_{1/2}$= 0.34 V

Figure 9: The molecular structures of $[Cu(dmdcbpy)_2]^{2+/1+}$ and $[Cu(tmabpy)_2]^{2+/1+}$ with their corresponding redox potentials vs NHE.

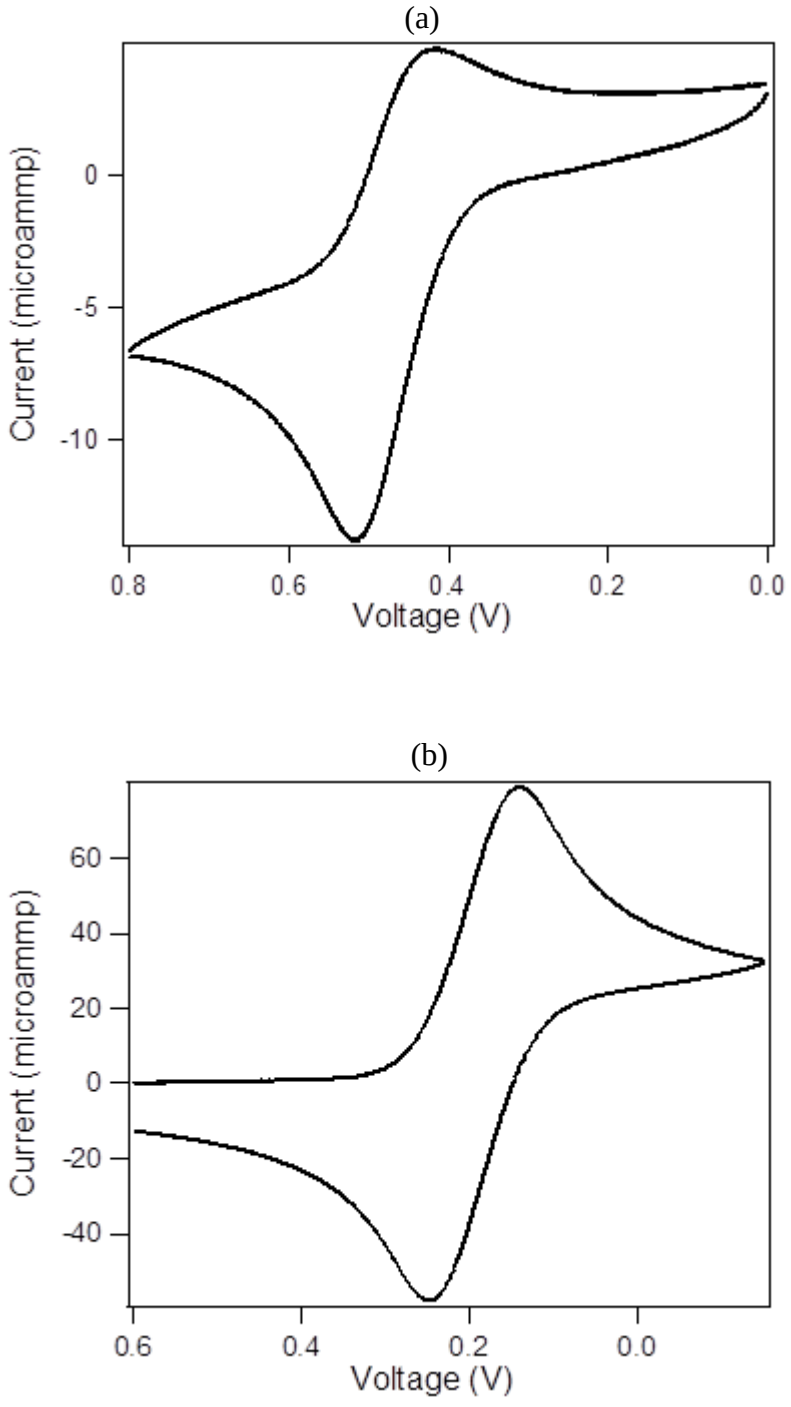

Figure 10: Cyclic Voltammograms of 5 mM solutions of (a) $Cu(I)(dmdcbpy)_2$ and (b) $Cu(I)(tmabpy)_2$ in 0.1 M KCl/water at a scan rate of 10 mV/s.

3.3 Photovoltaic Performance and IPCE Spectra:

The performance of the two redox couples was assessed by fabricating 100% aqueous-based liquid DSCs with several commercial organic dye sensitizers. For the preliminary studies, the electrolyte solution of the two redox couples contained 0.1 M of the Cu(I) species and 0.05 M of the Cu(II) species. The solvent used for the preparation of the electrolytes was 100% water, the pH was adjusted to 5.6-6.0 using either KOH or HCl, 0.1 M KCl or $LiClO_4$ was added and lastly 0.02% FS-35 and 0.5% Triton X-100 were added as surfactants to lower the interfacial surface tension between the water-based electrolytes and the hydrophobic dyes/TiO_2 interface. Initially, the $[Cu(dmdcbpy)_2]^{2+/1+}$ redox mediator was studied with three organic dyes, including the Cloudberry Orange (CO), the D35 and the DNF-05 dyes (their molecular structures with their corresponding $\lambda_{abs,max}$ are shown in Figure 11). These dyes were used as hydrophobic sensitizers to avoid their desorption upon introducing the water-based electrolyte system. The corresponding I-V curves measured under standard AM 1.5 conditions are shown in Figure 12, and the photovoltaic parameters are summarized in Table 1. The DSC based on the CO dye showed the highest photovoltaic performance with a $J_{SC} = 1.6\ mA.cm^{-2}$, a $V_{OC} = 604\ mV$, a $FF = 0.40$, and an overall efficiency η (PCE%) of 0.39%. An overall PCE% value of 0.21% ($J_{SC} = 0.8\ mA.cm^{-2}$, $V_{OC} = 568\ mV$, $FF = 0.46$) was obtained for the DNF-05 based DSC. The D35 dye gave the poorest photovoltaic performance of 0.5 $mA.cm^{-2}$ for short-circuit photocurrent, 604 mV for open-circuit voltage, a 0.56 FF, and an efficiency of 0.17%.

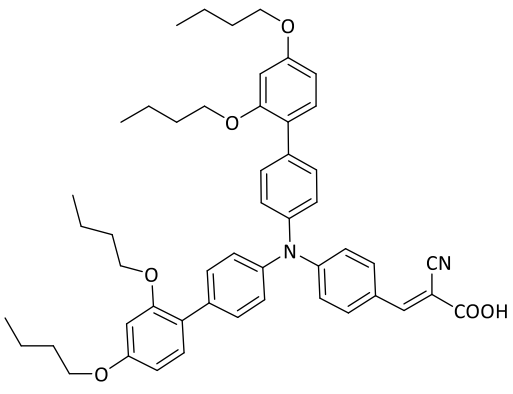

CO

$\lambda_{abs,max} = 451$ nm

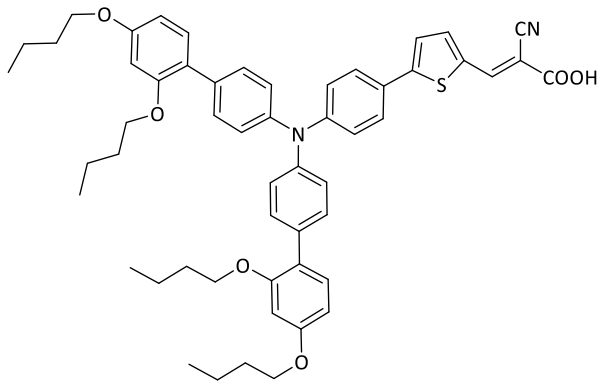

D35

$\lambda_{abs,max} = 500$ nm

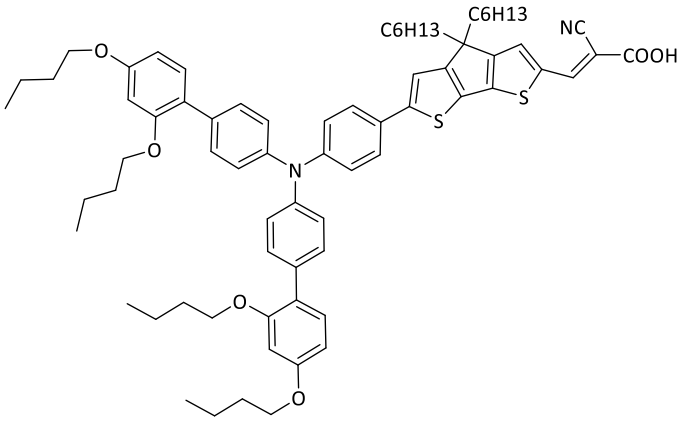

DNF-05

$\lambda_{abs,max} = 541$ nm

Figure 11: The molecular structures of the organic CO, D35, and DNF-05 dyes and the corresponding $\lambda_{abs,max}$ values.

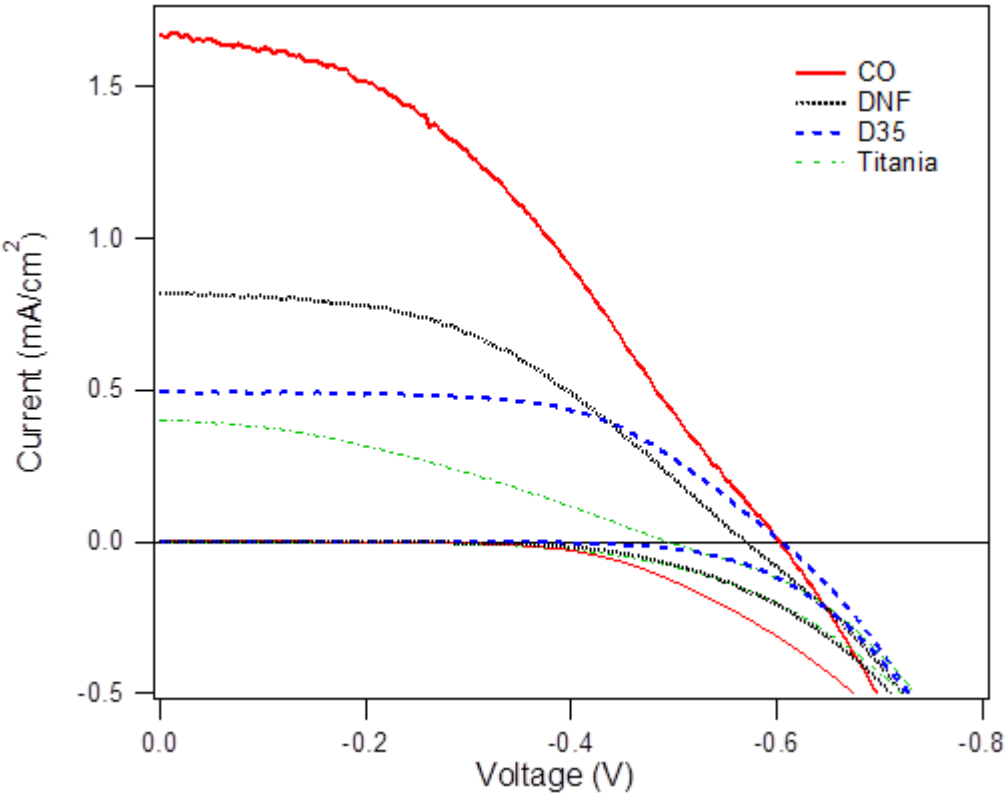

Figure 12: Photocurrent-Voltage characteristics of DSCs sensitized with CO, D35, and DNF-05 with the $[Cu(dmdcbpy)_2]^{2+/1+}$ electrolyte and the corresponding dark currents.

Table 1: Photovoltaic parameters of CO, D35, and DNF-05 with the $[Cu(dmdcbpy)_2]^{2+/1+}$ electrolyte.

Dye	J_{sc} (mA.cm^{-2})	V_{oc} (mV)	FF	PCE (%)[a]
CO	1.6 ± 0.1	604 ± 2	0.40	0.39
D35	0.5 ± 0.1	604 ± 2	0.56	0.17
DNF-05	0.8 ± 0.1	568 ± 2	0.46	0.21

[a]Measured under 100 mW.cm^{-2} simulated AM 1.5 G spectrum with an active area 0.5 x 0.5 cm^2 and a black mask (0.6 x 0.6 cm^2).

The spectra of monochromatic incident photon-to-current conversion efficiency (IPCE%) for DSCs sensitized with the three commercial organic dyes and using the $[Cu(dmdcbpy)_2]^{2+/1+}$-based electrolyte system is shown in Figure 13. The onset wavelength of the IPCE% spectrum of the DSC based on the CO dye was 610 nm, whereby an IPCE% value of around 31% was recorded at around 430 nm. D35 demonstrated a 3% IPCE% at 580 nm, with a starting wavelength of 430 nm. With a starting wavelength of 420 nm, a maximum IPCE% of around 5% at 607 nm was observed for DNF-05 based solar cells. The IPCE bands in the case of D35 and DNF-05 around 600 nm are anomalous and we could not assign them to neither the two dyes nor to the copper electrolyte. One hypothesis could be an electron injection from an aggregated form of the dye speciality that the band of the DNF-05 dye is at a lower energy when compared to that of the D35 dye. This is consistent with the band gap energies of both dyes.

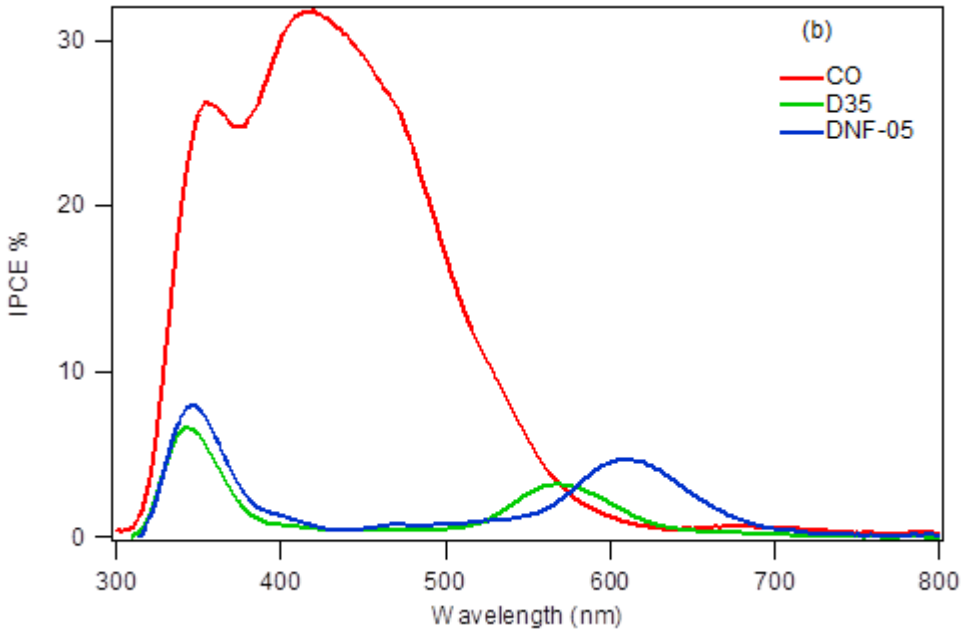

Figure 13: IPCE% spectra of DSCs with the CO, D35, and DNF-05 dyes and the $[Cu(dmdcbpy)_2]^{2+/1+}$ electrolyte.

The main possible problem of using 100% aqueous-based electrolyte with hydrophobic organic dyes is the incomplete wetting of the photoanode by the electrolyte, due to phase separation, even in the presence of specific surfactants. This causes a depression in the dye regeneration, thus supressing the electron flow in the device and diminishing the short circuit photocurrent. The previously used three dyes possess high hydrophobicity due to the butoxy groups found in their molecular structure which limits the wetting of the sensitized TiO_2 nanoparticles and thus lowers the J_{sc}. Therefore, alternative dyes were used, including the commercial D45 and D51 organic dyes. D45 and D51 have similar structures to D35 and DNF-05, respectively, shown in Figure 14, but the butoxy groups are substituted with methoxy groups which possess less hydrophobicity aiming at further minimizing phase separation and increasing the

wetting of the photoanode and thus increasing the photocurrent. However, there was no significant improvement in the performances of the D45 and D51 based cells compared to the D35 and DNF-05 based DSCs, their overall efficiencies remained lower than that for the CO based devices, thus selecting CO as the dye with the best photovoltaic performance, when used with $[Cu(dmdcbpy)_2]^{2+/1+}$ electrolyte. Since the replacement of the butoxy groups with less hydrophobic methoxy groups did not improve the short circuit current of the cells, the obtained results were explained by the nature of the structures of the organic dyes and their $\lambda_{abs,max}$ and not by wetting problems. The CO dye has the smallest structure and the lowest $\lambda_{abs,max}$, thus having the highest energy gap between the HOMO and the LUMO energy levels. This allows the dye to have the lowest HOMO, which increases the driving force of dye regeneration by the redox mediator, and the highest LUMO which increases the driving force of electron injection from the dye to the TiO_2 surface, thus enhancing the electron flow inside the DSC and improving its overall efficiency.

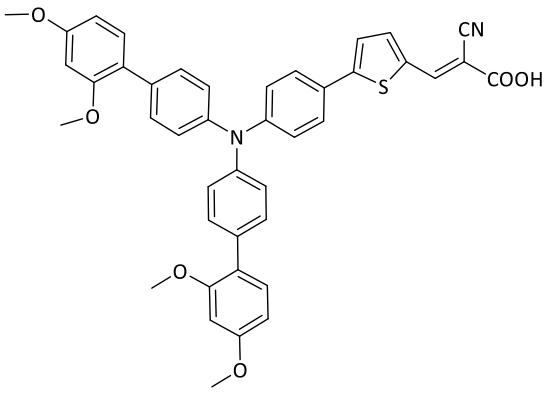

D45

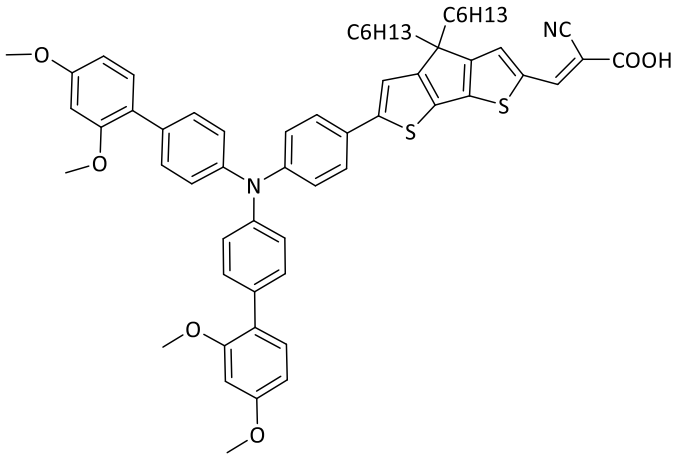

D51

Figure 14: The molecular structures of the organic D45 and D51 dyes.

Furthermore, the performance of the $[Cu(tmabpy)_2]^{2+/1+}$ electrolyte was studied by fabricating 100% aqueous-based DSCs with the CO organic dye, which showed the best performance with the $[Cu(dmdcbpy)_2]^{2+/1+}$ electrolyte. The corresponding I-V curve is shown in Figure 15, and the photovoltaic parameters are summarized in Table 2. A $J_{SC} = 125\ \mu A.cm^{-2}$, a $V_{OC} = 175\ mV$, a $FF = 0.45$, and an overall efficiency η of 0.01%. The poor photovoltaic performance and specifically the low photocurrent obtained by the $[Cu(tmabpy)_2]^{2+/1+}$ electrolyte was explained by the presence of the positively charged trimethyl ammonium groups which are attracted by the negatively charged TiO_2, due to the presence of the injected electrons into its surface, thus increasing the concentration of the electrolyte at the semiconductor surface and causing an increase in the recombination rates and therefore the dark current as shown in Figure 15.

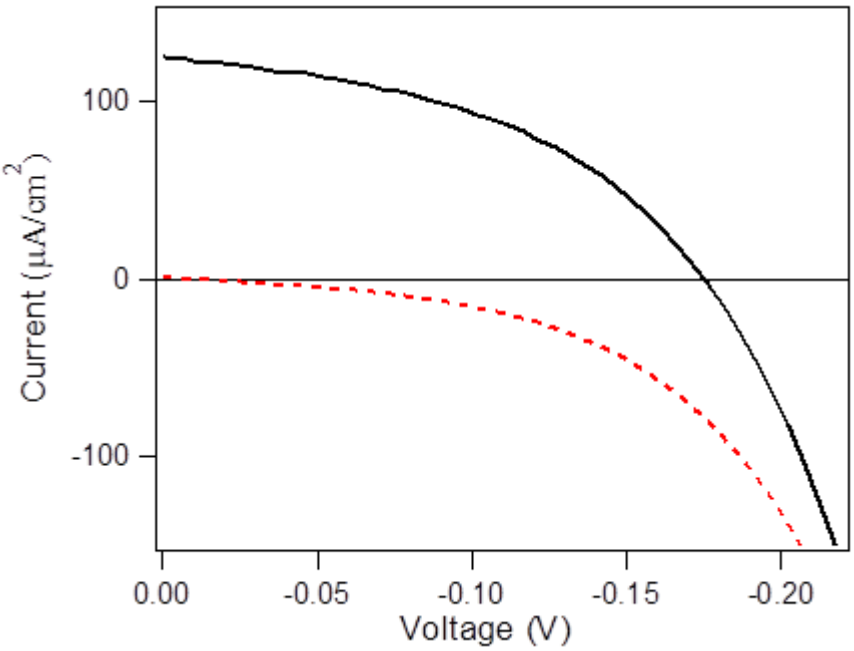

Figure 15: Photocurrent-Voltage characteristic of DSCs sensitized with the CO dye using the $[Cu(tmabpy)_2]^{2+/1+}$ electrolyte and the corresponding dark current.

Table 2: Photovoltaic parameters of CO with the $[Cu(tmabpy)_2]^{2+/1+}$ electrolyte.

Dye	J_{sc} ($\mu A.cm^{-2}$)	V_{oc} (mV)	FF	PCE (%)[a]
CO	125 ± 100	176 ± 2	0.45	0.01

[a]Measured under 100 $mW.cm^{-2}$ simulated AM 1.5 G spectrum with an active area 0.5 x 0.5 cm^2 and a black mask (0.6 x 0.6 cm^2).

Finally, a diffusion limited current was observed due to the sterically hindered substituents at the 6,6' positions of the bipyridyl unit, which causes mass transport limitations.

Following the obtained results, the $Cu(dmdcbpy)_2]^{2+/1+}$ based electrolyte was chosen for further studies with metal complex sensitizers. In general, the metal-organic dyes show desorption from the TiO_2 surface in the presence of water, due to their hydrophilic nature. Therefore, the hydrophobic Ru-based C106 dye was used, which has been previously studied in our lab, having a good performance in aqueous medium. The structure of the C106 sensitizer is shown in Figure 16.

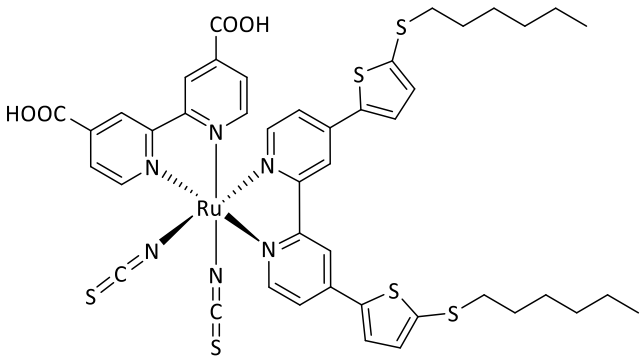

C106

Figure 16: The molecular structure of the Ru-based metal-organic C106 dye.

The preliminary studies of the C106 dye, were done using the same $Cu(dmdcbpy)_2]^{2+/1+}$ electrolyte, that was used for the organic dyes, giving a $J_{SC} = 2.6\ mA.cm^{-2}$, a $V_{OC} = 559\ mV$, a $FF = 0.43$, and an overall efficiency η of 0.63% under standard measurement condition. The corresponding I-V curve is shown in Figure 17, and the photovoltaic parameters are summarized in Table 3.

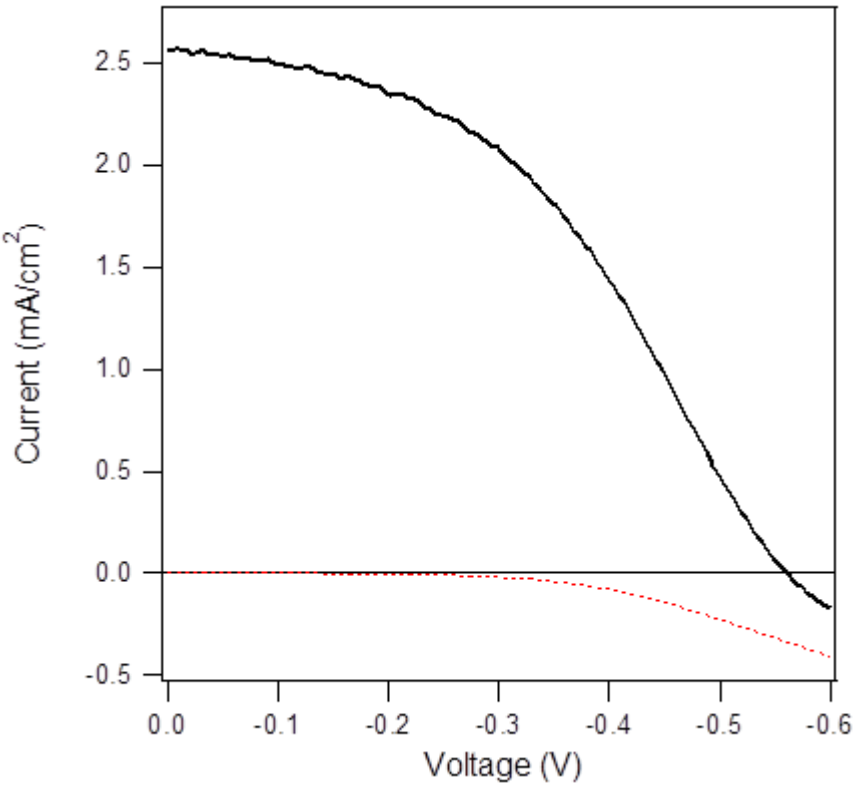

Figure 17: Photocurrent-Voltage characteristic of DSCs sensitized with the C106 dye using the $[Cu(dmdcbpy)_2]^{2+/1+}$ electrolyte and the corresponding dark current.

Table 3: Photovoltaic parameters of C106 with the $[Cu(dmdcbpy)_2]^{2+/1+}$ electrolyte.

Dye	J_{sc} (mA.cm^{-2})	V_{oc} (mV)	FF	PCE (%)[a]
C106	2.6 ± 0.1	559 ± 2	0.43	0.63

[a]Measured under 100 mW.cm^{-2} simulated AM 1.5 G spectrum with an active area 0.5 x 0.5 cm^2 and a black mask (0.6 x 0.6 cm^2).

The IPCE% for DSCs based on the commercial C106 dye and the $Cu(dmdcbpy)_2]^{2+/1+}$ electrolyte is shown in Figure 18. The onset wavelength of the IPCE% spectrum was at 750 nm, whereby an IPCE% value of around 19% was recorded at around 550 nm.

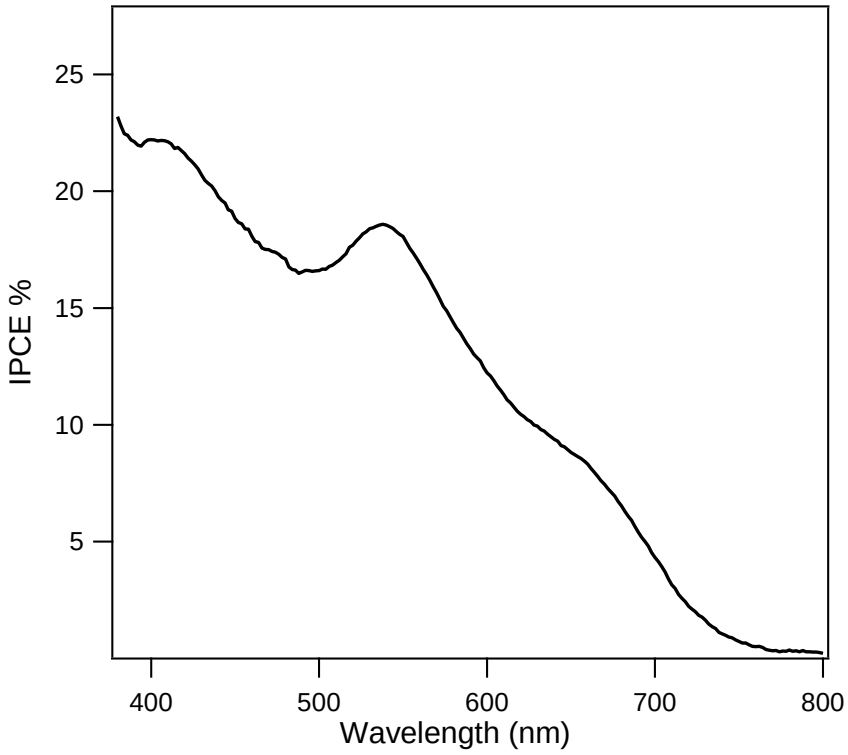

Figure 18: IPCE% spectra of a DSC with the C106 dye and the $[Cu(dmdcbpy)_2]^{2+/1+}$ electrolyte.

3.4 Dye Regeneration:

Among all the used dye sensitizers, the C106 dye showed the highest short circuit photocurrent due to the best wetting conditions along with its appropriate energetics. The regeneration kinetics of the C106 dye with the $Cu(dmdcbpy)_2]^{2+/1+}$ redox mediator was investigated with Photoinduced Absorption Spectroscopy (PIA). The PIA spectrum is given in Figure 19. Without the redox couple in the electrolyte, a bleach was observed at around 500 nm due to the ground-state bleach of the dye upon oxidation and Stark shift i.e., absorption change of the dye as a result of changes in the electrical field across the dye molecules by the photoinjected electrons. We also observed the absorption peak of the oxidized dye sensitizer appearing at around 800 nm in the absence of the copper electrolyte. In the spectrum of C106 in the presence of the electrolyte, the bleach minimized but still appeared at 500 nm, whereas the absorption peak of the oxidized dye disappeared due to somehow efficient regeneration of the oxidized dye molecules with the redox species. The traces of absorption that appear even in the presence of the electrolyte, correspond to absorption of the electrolyte itself, see Figure 20. From the obtained results it can be concluded that the $Cu(dmdcbpy)_2]^{2+/1+}$ electrolyte can effectively regenerate the oxidized C106 species.

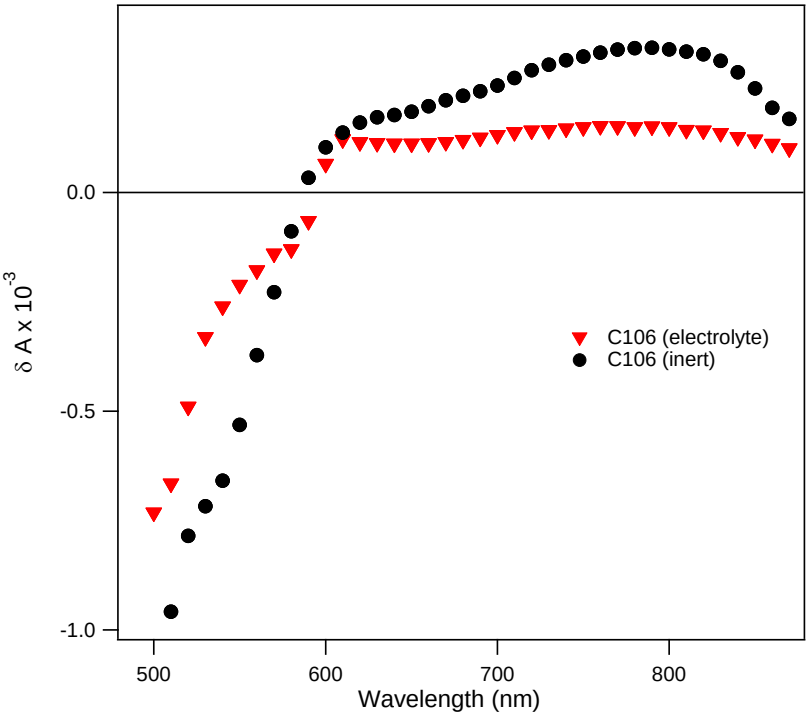

Figure 19: PIA spectra of C106 sensitized TiO_2 with the $[Cu(dmdcbpy)_2]^{2+/1+}$ electrolyte.

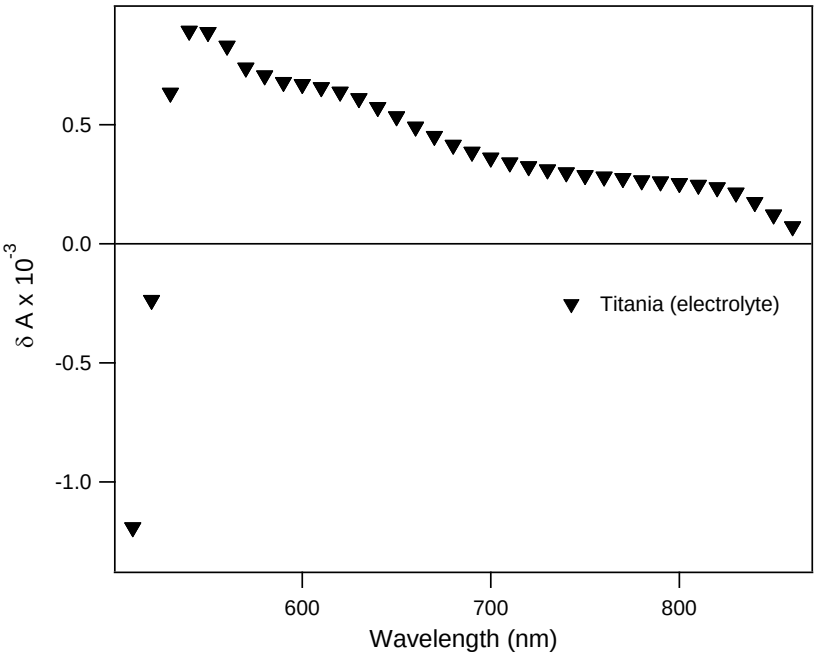

Figure 20: PIA spectra of TiO_2 with the $[Cu(dmdcbpy)2]^{2+/1+}$ electrolyte.

3.5 Electrochemical Impedance Spectroscopy:

To further understand the mentioned photovoltaic results and obtain information about the electron transfer processes inside DSCs sensitized with the C106 dye, electrochemical impedance spectroscopy (EIS) measurements were performed at V_{OC} under different light intensities.

The charge transfer resistance R_{CT}, which represents the resistance for the recombination of the TiO_2 electrons to the oxidized dye in case of low regeneration kinetics, or/and with the oxidized redox species in the electrolyte, the chemical capacitance C_{μ} at the TiO_2/electrolyte interface, and the electron lifetime are shown in Figures 21, 22, and 23, respectively. These three factors were plotted vs the applied voltage.

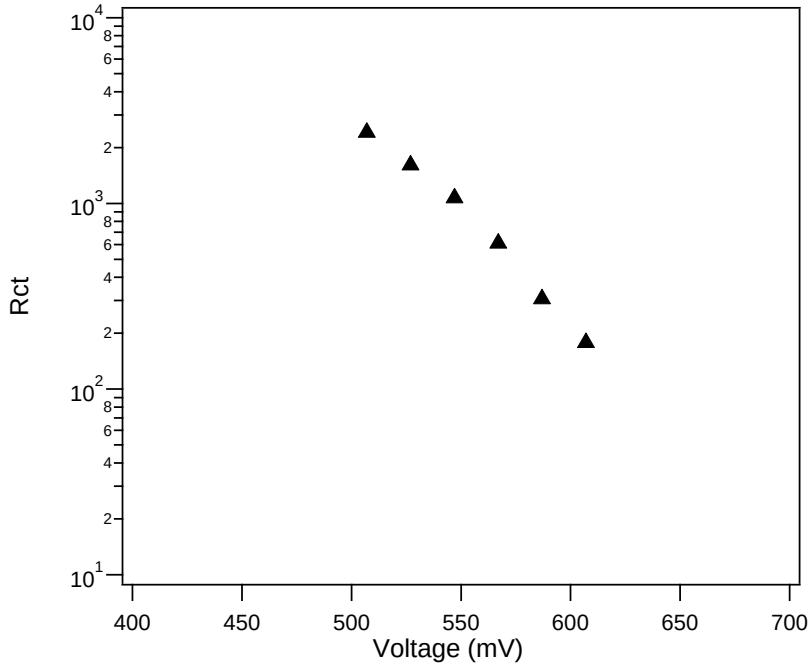

Figure 21: Charge transfer resistance values extracted from EIS measurements of C106 sensitized DSCs.

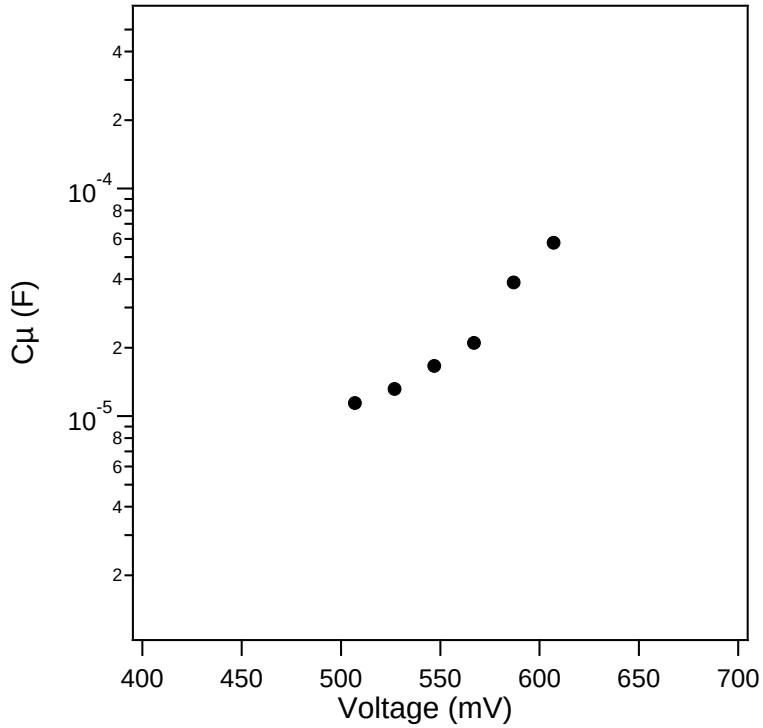

Figure 22: Chemical capacitance values extracted from EIS measurements of C106 sensitized DSCs.

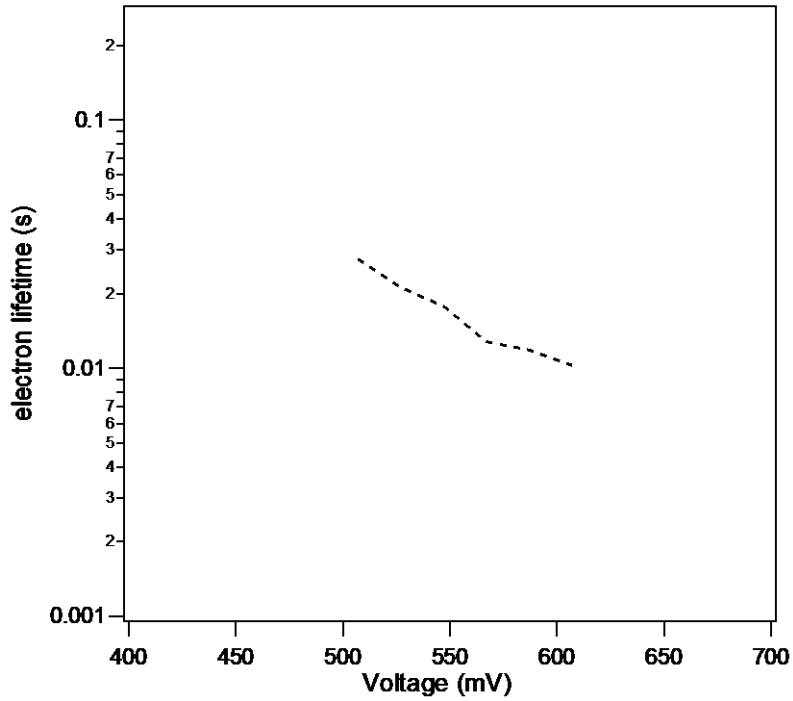

Figure 23: Electron lifetime values extracted from EIS measurements of C106 sensitized DSCs.

According to Figure 21, the R_{CT} of C106 sensitized cells with the $Cu(dmdcbpy)_2]^{2+/1+}$ electrolyte was 2415 at 507 mV. This high resistance is determined by the decrease in electron recombination rates between the injected electrons and the oxidized species of the electrolyte and/or the oxidized dye sensitizer. This is explained by the relatively good dye coverage in the small cells along with sufficient wetting by the aqueous-based electrolyte, leading to the efficient regeneration of the oxidized dye molecules by the redox species as shown in the PIA spectroscopy (Figure 19). The high regeneration rates prevent the recombination of the TiO_2 electrons with the oxidized dye, thus increasing the resistance. Furthermore, in Figure 23, a relatively high electron lifetime is observed compared to standard cobalt complexes that people have used in good efficiency DSCs, and this is consistent with the slow recombination kinetics shown by the R_{CT} values.

3.6 Light Intensity Dependence Measurements:

In order to investigate the reasons behind the still low photocurrents in our C106-based DSCs even with the attained good wetting, low recombination, and good regeneration, we performed a light intensity dependence of the open circuit photovoltage and the short circuit photocurrent density. The attained results are given in Figure 24 and the photovoltaic parameters are summarized in Table 4. The J_{SC} values showed deviation from linearity with increasing light intensities, starting at 20% sun. This effect can be explained with mass transport limitations of the copper complex. Under higher light intensities more internal series resistance arise due to diffusion problems. This is further supported by the data obtained from the Electrochemical Impedance Spectroscopy (EIS). The high resistance which is observed starting at 167.5 Ω (Z') in the Nyquist plot, Figure 25, indicates the resistance associated to the diffusion of the oxidized species in the electrolyte specially at high light intensities, which corresponds to Z_d in the typical plot (Figure 8).

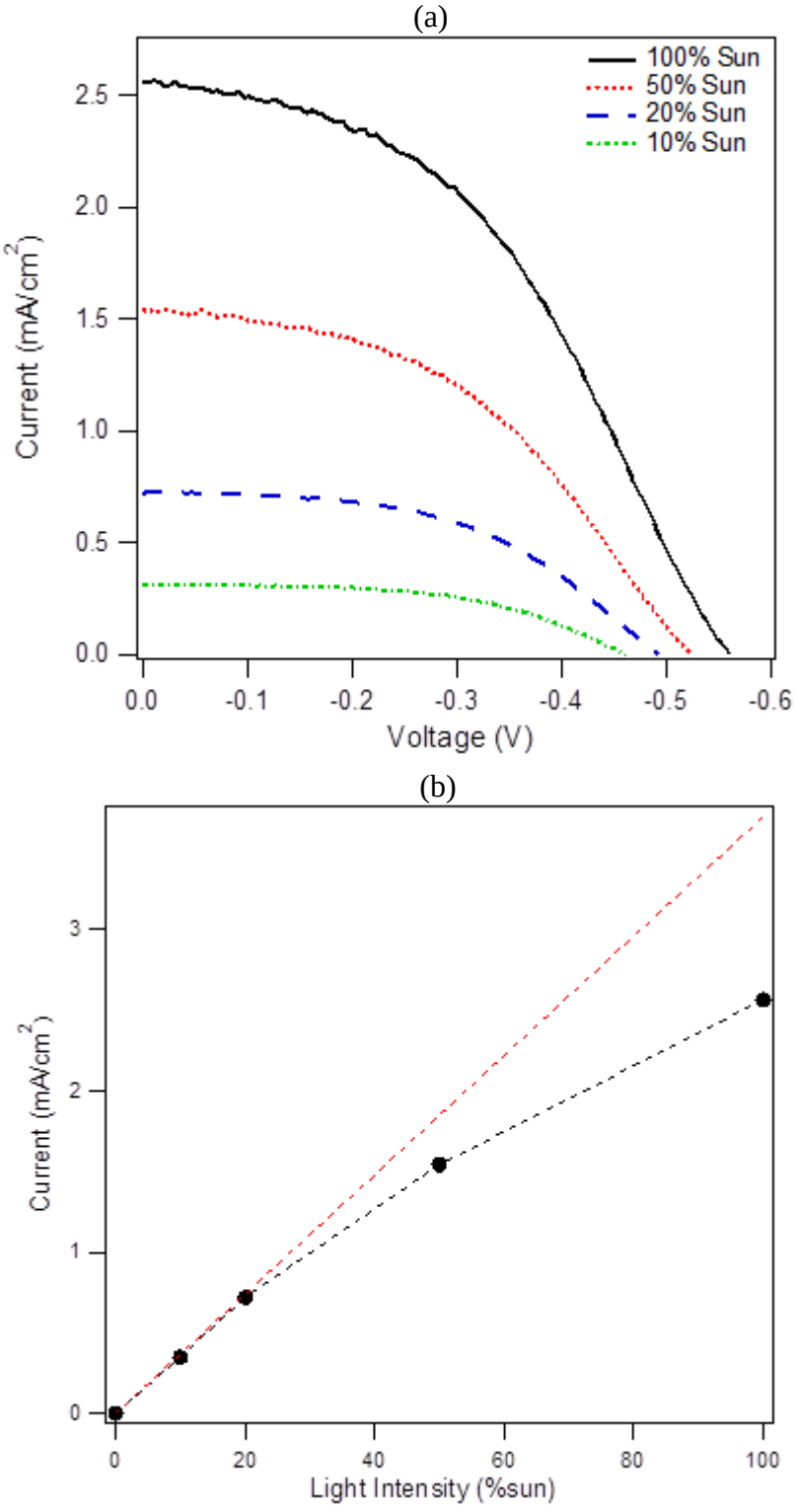

Figure 24: Light intensity dependence of a) I-V characteristic and b) short circuit photocurrent of DSC devices based on the $Cu(dmdcbpy)_2]^{2+/1+}$ electrolyte.

Table 4: Photovoltaic parameters of C106 with the $[Cu(dmdcbpy)_2]^{2+/1+}$ electrolyte at different light intensities (%sun).

Light Intensity (%sun)	J_{sc} (mA.cm^{-2})	V_{oc} (mV)	FF	PCE (%)[a]
10	0.3 ± 0.1	458 ± 2	0.57	0.80
20	0.7 ± 0.1	493 ± 2	0.51	0.90
50	1.6 ± 0.1	524 ± 2	0.43	0.72
100	2.6 ± 0.1	559 ± 2	0.43	0.63

[a]Measured under (100 mW.cm^{-2} for 100% sun) simulated AM 1.5 G spectrum with an active area 0.5 x 0.5 cm^2 and a black mask (0.6 x 0.6 cm^2).

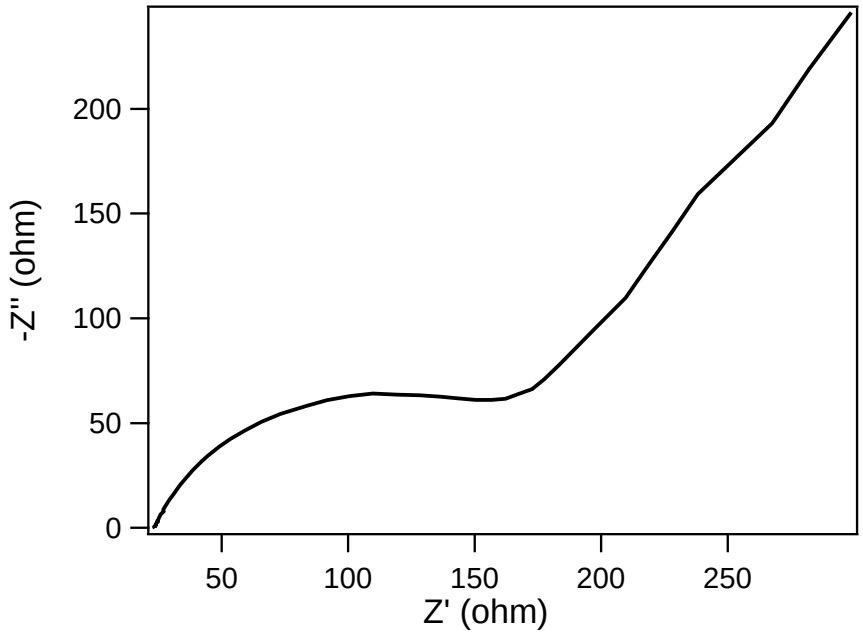

Figure 25: Nyquist plot of a DSC sensitized with C106 dye using the $Cu(dmdcbpy)_2]^{2+/1+}$ electrolyte.

However, the so far obtained data does not give any information whether the limitation by diffusion is in the bulk of the electrolyte, or in the pores of the sensitized semiconductor at the photoanode. Further studies were done concerning the diffusion in the bulk, by applying a reverse-bias and causing the lowering of the TiO_2 conduction band to the same level of the redox potential of the electrolyte and checking the photocurrent response. At very positive voltages the photocurrent increased indicating the direct injection of the electrons from the electrolyte to the conduction band of the TiO_2 without any limitations by diffusion (no diffusion-limited current is present), see Figure 26. Therefore, we speculate that the diffusion of the electrolyte inside the pores of the semiconductor due to phase segregation and not in the bulk of the electrolyte is the reason behind the lower photovoltaic parameters of C106 when compared with those performed usually with organic-base electrolyte systems. This phase segregation can occur inside the pores of the TiO_2 due to pore size heterogeneity and dye coverage, thus resulting in pores with high electrolyte content and others with low electrolyte content. Phase segregation would therefore result in reduced electrolyte diffusion through the pores explaining the saturation in the obtained photocurrent density. This will result in a non-linear behaviour of the photocurrent with light intensity as well as limitations of the fill factor in the DSC device. Additionally, due to uneven dye coverage, dyes which are in contact with pores with low copper complexes cannot regenerate and will capture the injected electrons, thus increasing the recombination rates. This phenomenon was previously observed in the work of O'Regan *et al.*, where a hydrophobic TG6 dye was used with iodine-based electrolyte of varying water

concentration. However, despite the saturation of the short circuit current, the photovoltage stays nearly independent of light intensity, giving the complex a fascinating potential for use in devices for indoor applications, where light intensities are much lower than 0.2 suns and thus the above diffusion limitation is not of an importance.

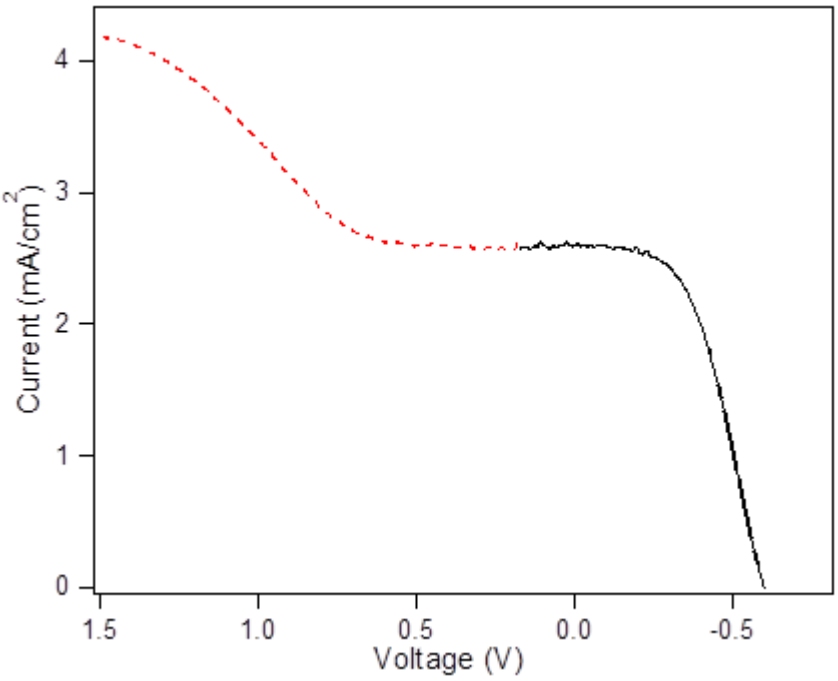

Figure 26: Photocurrent-Voltage characteristics of DSCs sensitized with C106 using the $[Cu(dmdcbpy)_2]^{2+/1+}$ electrolyte as a result of an applied reverse-bias.

3.7 Indoor Applications Under Ambient Light:

Following the obtained results by the light intensity dependence, the performance of the C106 dye with the optimized $Cu(dmdcbpy)_2]^{2+/1+}$ electrolyte was studied under low indoor light intensities of 200 and 1000 lux, using a LED white light source (KONNICE, BL13W). The power of the LED source at 1000 lux was measured to be 238.7 $\mu W.cm^{-2}$. The spectrum and power of the white light was measured with a spectrometer, Figure 27. For 1000 lux, a $J_{SC} = 27\ \mu A.cm^{-2}$, a $V_{OC} = 504\ mV$, a $FF = 0.57$, and an overall efficiency η of 3.45%. An overall PCE% value of 6.29% ($J_{SC} = 9.6\ \mu A.cm^{-2}$, $V_{OC} = 478\ mV$, $FF = 0.65$) was obtained for 200 lux. The obtained I–V curves are shown in Figure 28 and the photovoltaic parameters are summarized in Table 5.

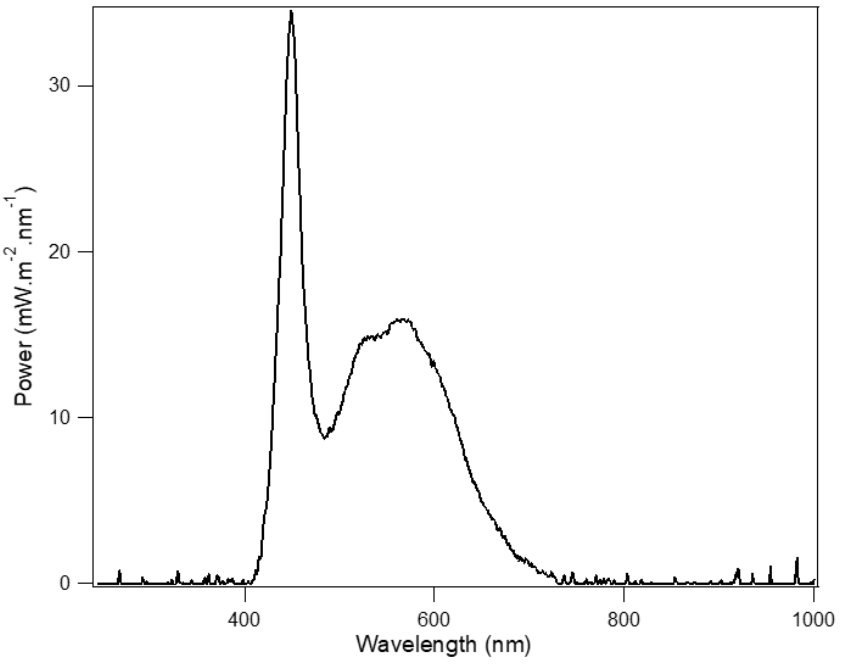

Figure 27: The spectral output from white LED light source.

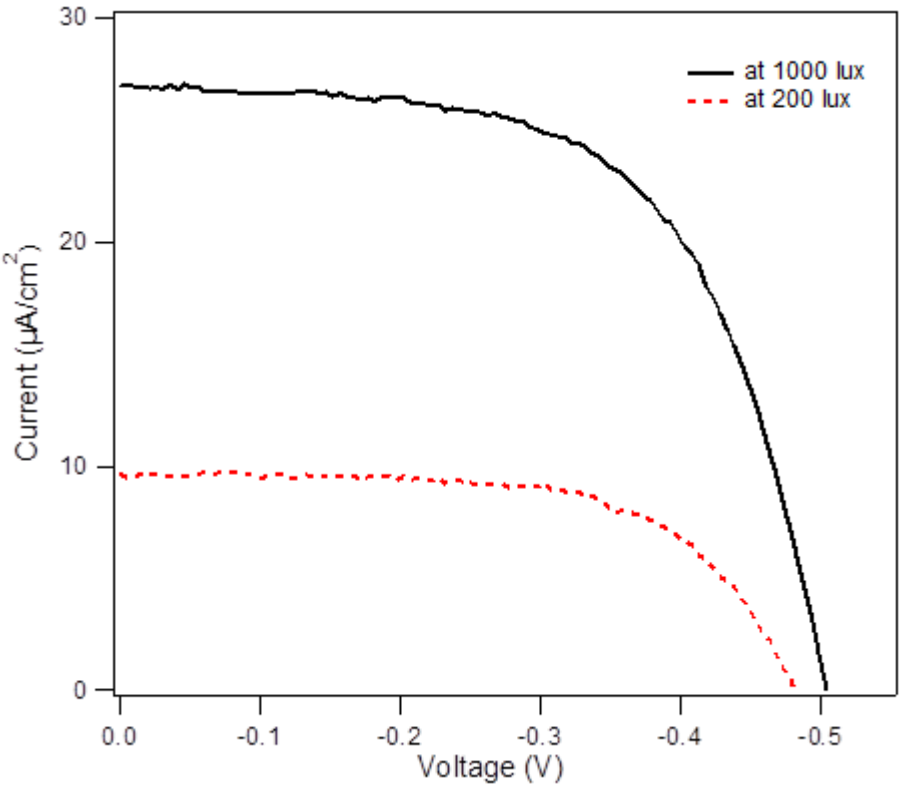

Figure 28: Photocurrent-Voltage characteristics of C106 sensitized small DSCs with the $[Cu(dmdcbpy)_2]^{2+/1+}$ electrolyte under low light intensities of 200 and 1000 lux.

Table 5: Photovoltaic parameters of C106 with the $[Cu(dmdcbpy)_2]^{2+/1+}$ electrolyte at different low light intensities of 200 and 1000 lux.

Light Intensity (lux)	J_{sc} (µA.cm^{-2})	V_{oc} (mV)	FF	Pin (µW.cm-2)	PCE (%)[b]
200	10 ± 1	478 ± 2	0.65	47.7	6.29
1000	27 ± 1	504 ± 2	0.57	238.7	3.45

[b]Measured under white LED light with an active area 0.5 x 0.5 cm^2 and a black mask (0.6 x 0.6 cm^2).

Based on the obtained results under low ambient light conditions, different cells of larger active area (1 x 6 cm^2) were fabricated using the C106 dye sensitizer and the $[Cu(dmdcbpy)_2]^{2+/1+}$ electrolyte, specific for indoor applications. A problem faced in the following DSCs, was the incomplete wetting of the photoanode by the aqueous electrolyte leaving behind a large number of dye molecules not being in contact with the redox species. Therefore, 1% by weight PEG (6000) was added to further minimize the phase separation between the aqueous electrolyte and the hydrophobic dye at the surface of the photoanode, leading to better photovoltaic performances. Hence, the optimized electrolyte solution for the indoor applications contains 0.1 M Cu(I), 0.05 M Cu(II), 0.1 M KCl, 0.02% FS-35, 0.5% Triton X-100, 0.1 M $LiClO_4$ and 1% by weight PEG (6000). Under light intensity of 1000 lux, the C106 sensitized DSCs showed a $J_{SC} = 53\ \mu A.cm^{-2}$, a $V_{OC} = 559\ mV$, a $FF = 0.52$, and an overall efficiency η of 6.54%. The obtained I–V curve is shown in Figure 29 and the photovoltaic parameters are summarized in Table 6.

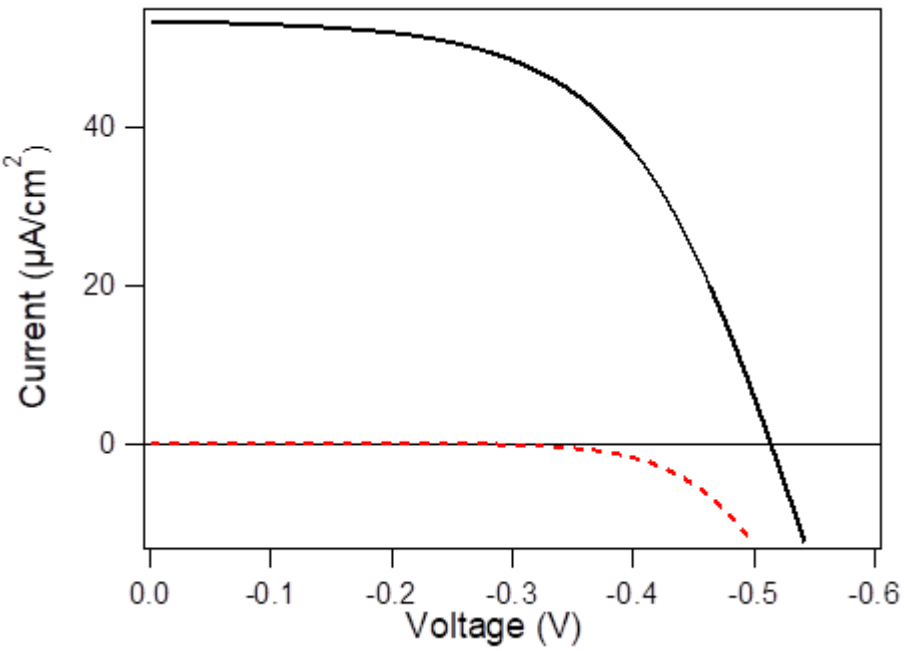

Figure 29: Photocurrent-Voltage characteristic of C106 sensitized DSC with the $[Cu(dmdcbpy)_2]^{2+/1+}$ electrolyte under low ambient light for indoor applications and the corresponding dark current.

Table 6: Photovoltaic parameters of C106 with the $[Cu(dmdcbpy)_2]^{2+/1+}$ electrolyte under low ambient light (1000 lux) for indoor applications.

Dye	J_{sc} (µA.cm^{-2})	V_{oc} (mV)	FF	PCE (%)[c]
C106	53 ± 1	559 ± 2	0.52	6.54

[c]Measured under (238.7 µW.cm^{-2}) white LED light with an active area 1 x 6 cm^2.

CHAPTER 4

CONCLUSION

In conclusion, we were successful in synthesizing three copper complexes $Cu(dmap)_2]^{2+/1+}$, $[Cu(dmdcbpy)_2]^{2+/1+}$, and $[Cu(tmabpy)_2]^{2+/1+}$. The $Cu(dmap)_2]^{2+/1+}$ electrolyte possessed a very slight solubility, while the positively charged $[Cu(tmabpy)_2]^{2+/1+}$ electrolyte gave a very poor photovoltaic performance due to the high recombination rates with the negatively charged semiconductor. The use of $[Cu(dmdcbpy)_2]^{2+/1+}$ in a 100% aqueous electrolyte system gave the best photovoltaic performance with the C106 complex sensitizer. A diffusion limited current was observed for small cells under 1 sun illumination for outdoor applications, resulting in diminished photocurrents. Furthermore, we showed that this loss of photocurrents under high light intensities is mainly due to electrolyte diffusion limitation in the pores of the semiconductor and not at the TiO_2/dye/electrolyte interface. Finally, by the promising results obtained from the light intensity dependence measurements, cells sensitized with the C106 dye were successfully tested under low ambient light of less than 0.2 sun (1000 lux) for indoor applications, where the diffusion limitation is not considered of a great importance, giving a remarkable PCE% of 6.54% for 100% water-based DSCs.

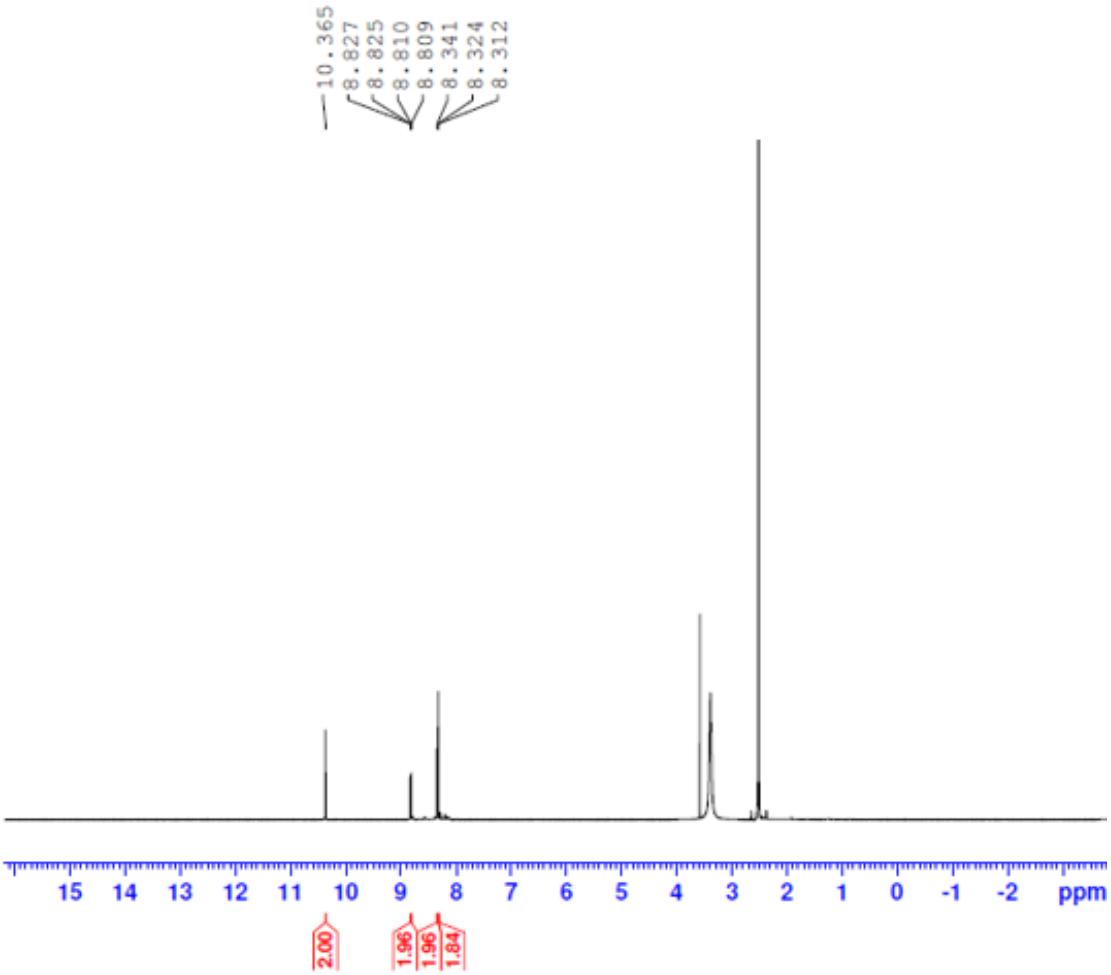

Figure 30S: [1]HNMR of 1,10-phenanthroline-2,9-dicarbaldehyde (**2**) in DMSO at 500 MHz.

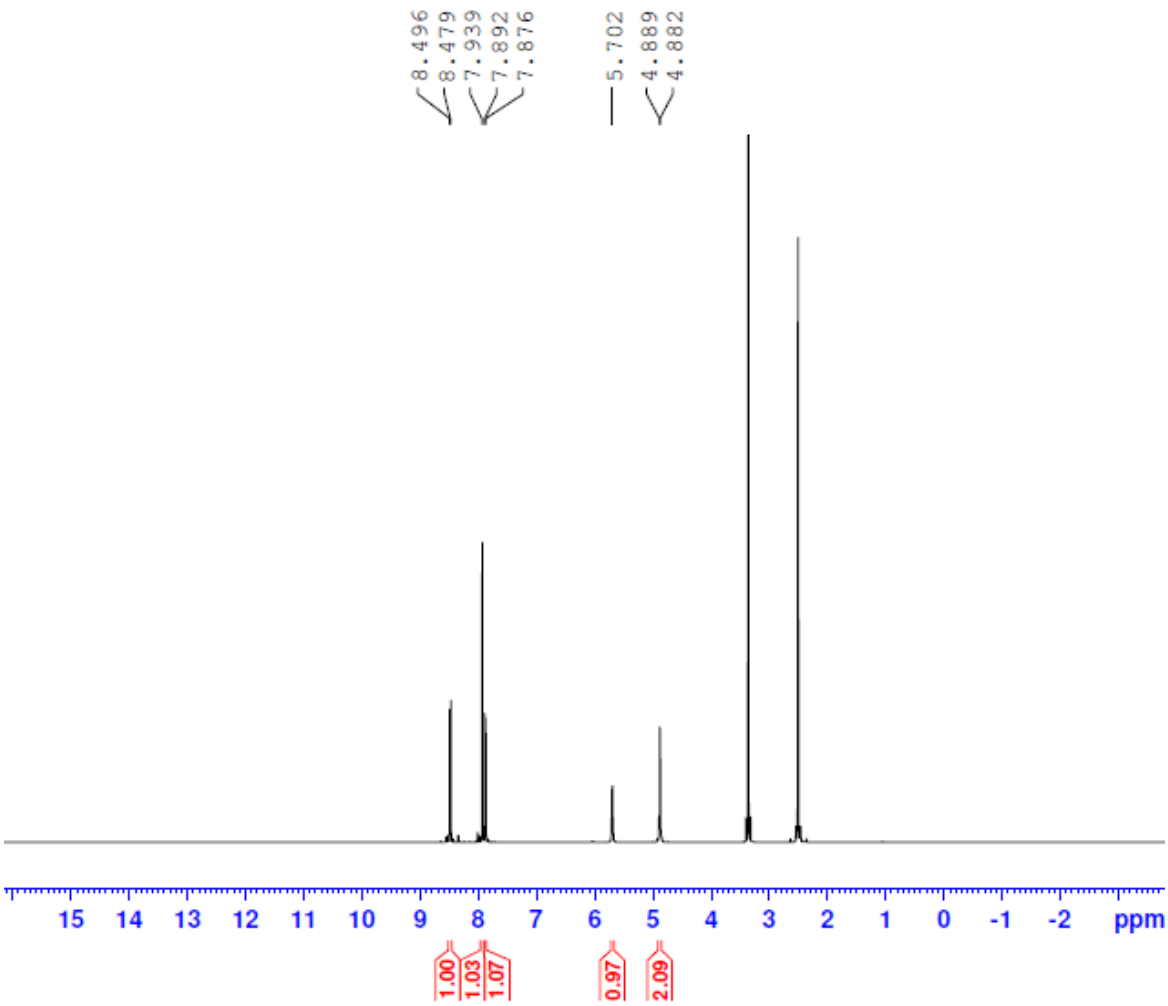

Figure 31S: [1]HNMR of (1,10-phenanthroline-2,9-diyl)dimethanol (dmap) (**3**) in DMSO at 500 MHz.

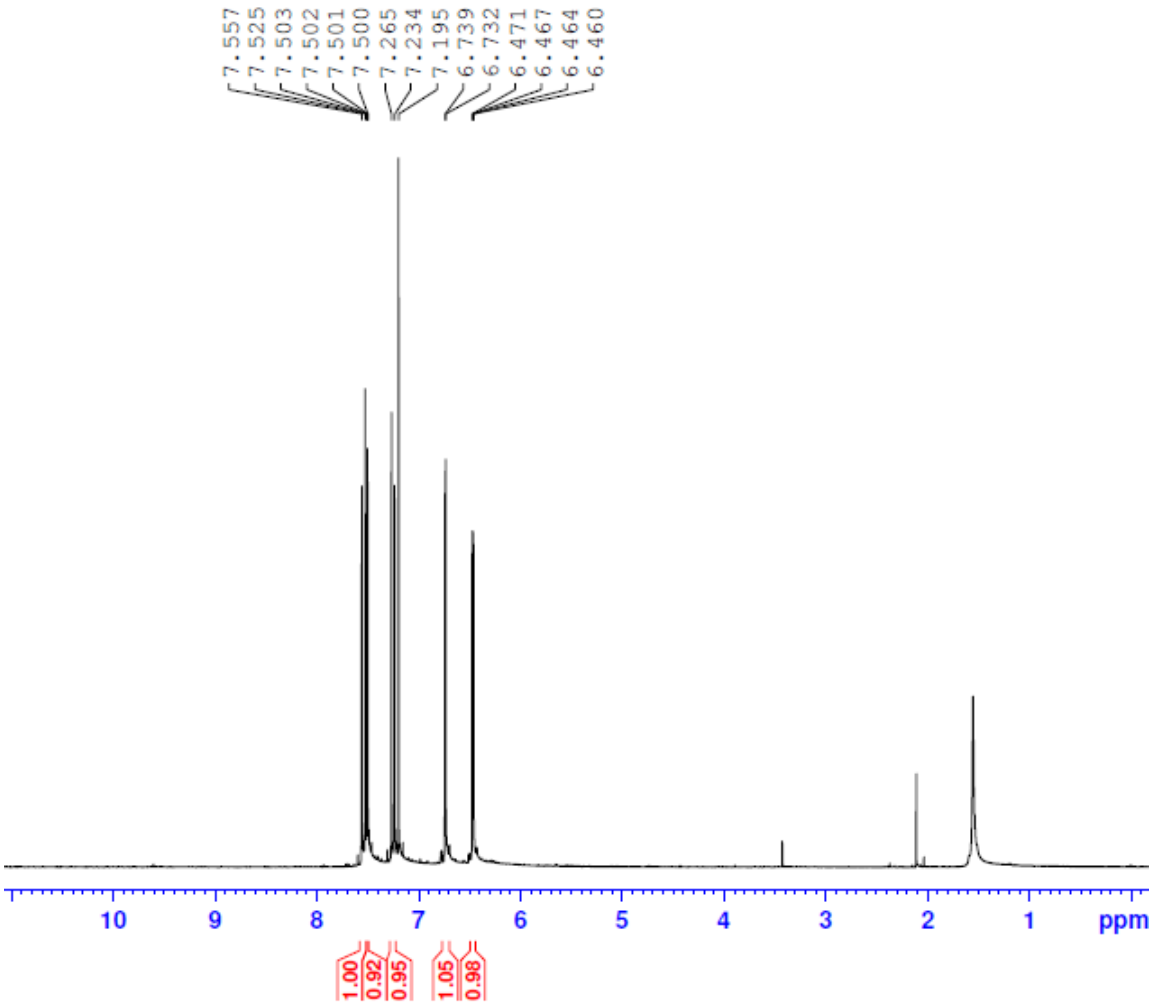

Figure 32S: ^{1}HNMR of (1E,5E)-1,6-di(furan-2-yl)hexa-1,5-diene-3,4-dione (**8**) in $CDCl_3$ at 500 MHz.

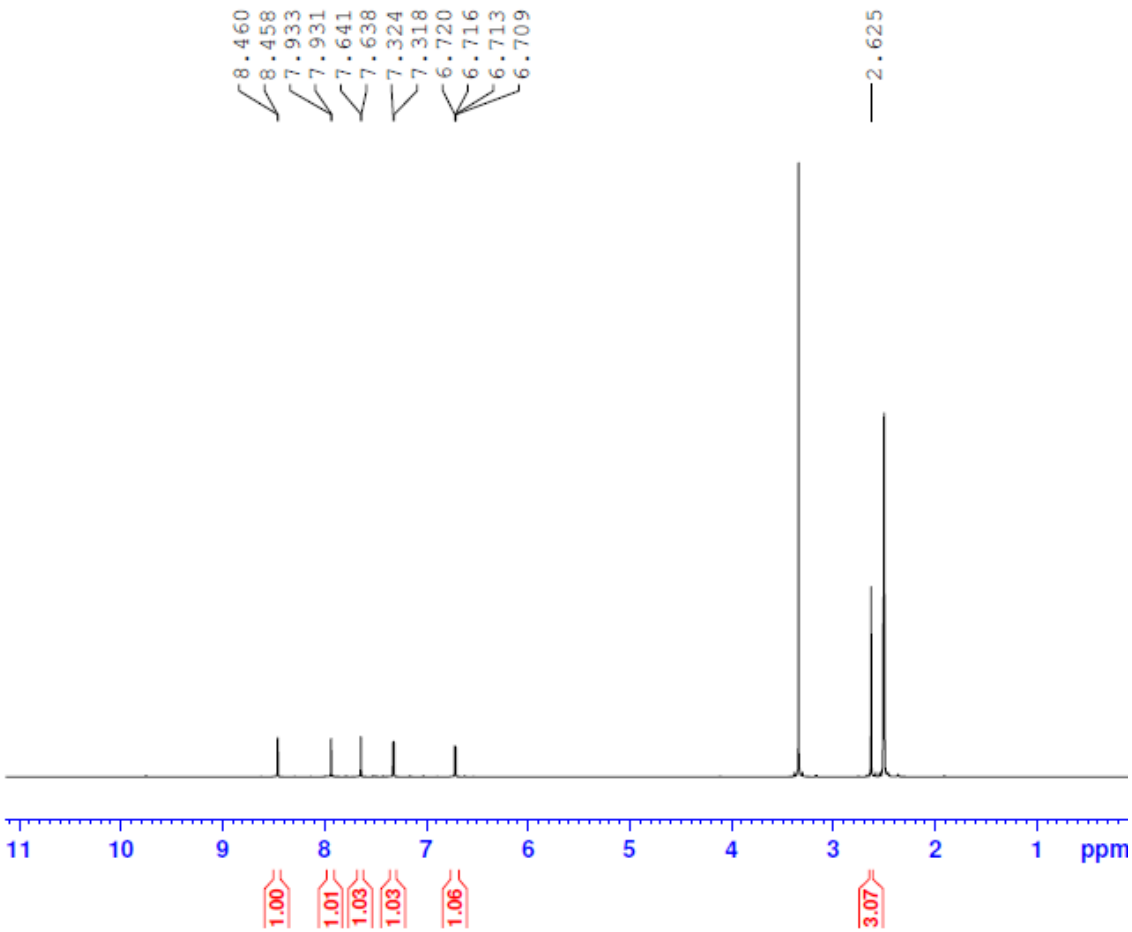

Figure 33S: [1]HNMR of 4,4'-di(furan-2-yl)-6,6'-dimethyl-2,2'-bipyridine (**10**) in DMSO at 500 MHz.

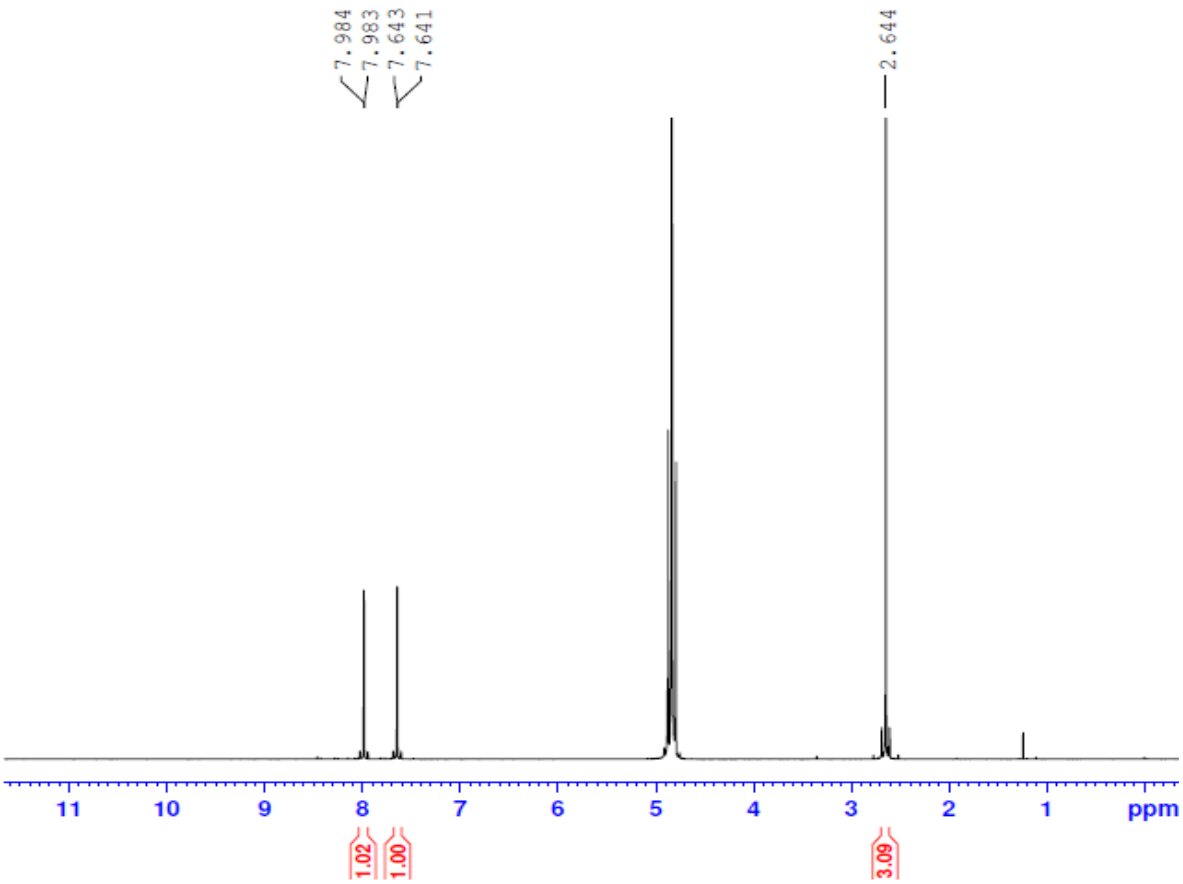

Figure 34S: ^{1}HNMR of 6,6'-dimethyl-[2,2'-bipyridine]-4,4'-dicarboxylic acid (dmdcbpy) (**11**) in D_2O at 500 MHz.

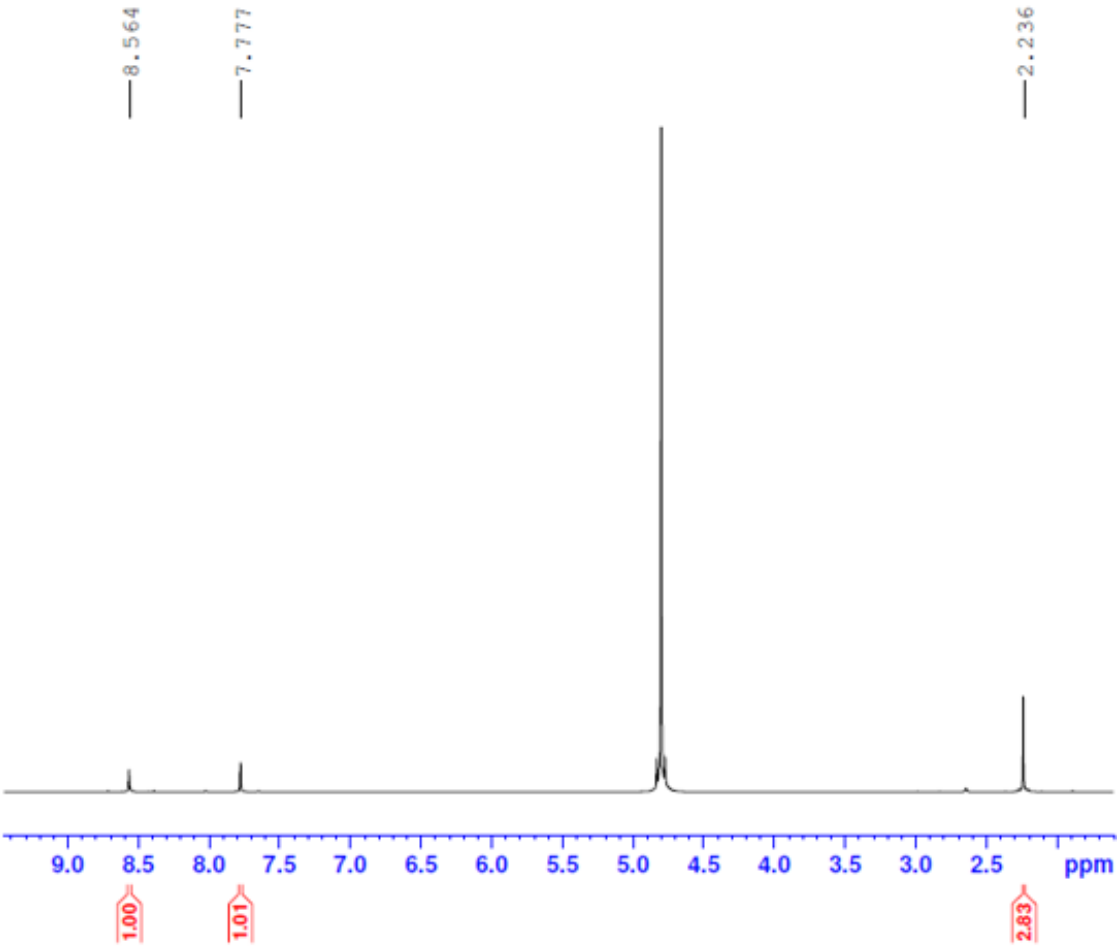

Figure 35S: ^{1}HNMR of Cu(I)(dmdcbpy)$_2$Cl Complex (**12**) in D_2O at 500 MHz.

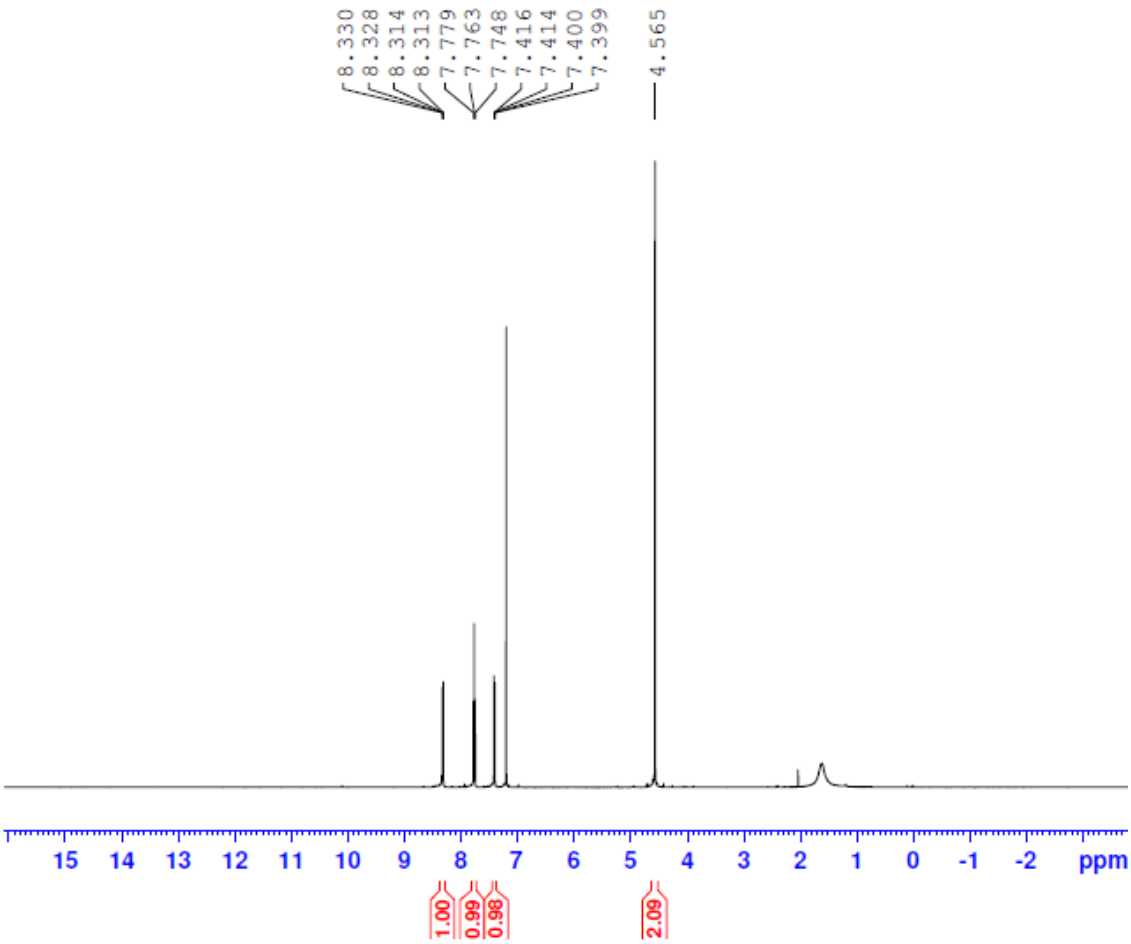

Figure 36S: ^{1}HNMR of 6,6'-bis(bromomethyl)-2,2'-bipyridine (**18**) in $CDCl_3$ at 500 MHz.

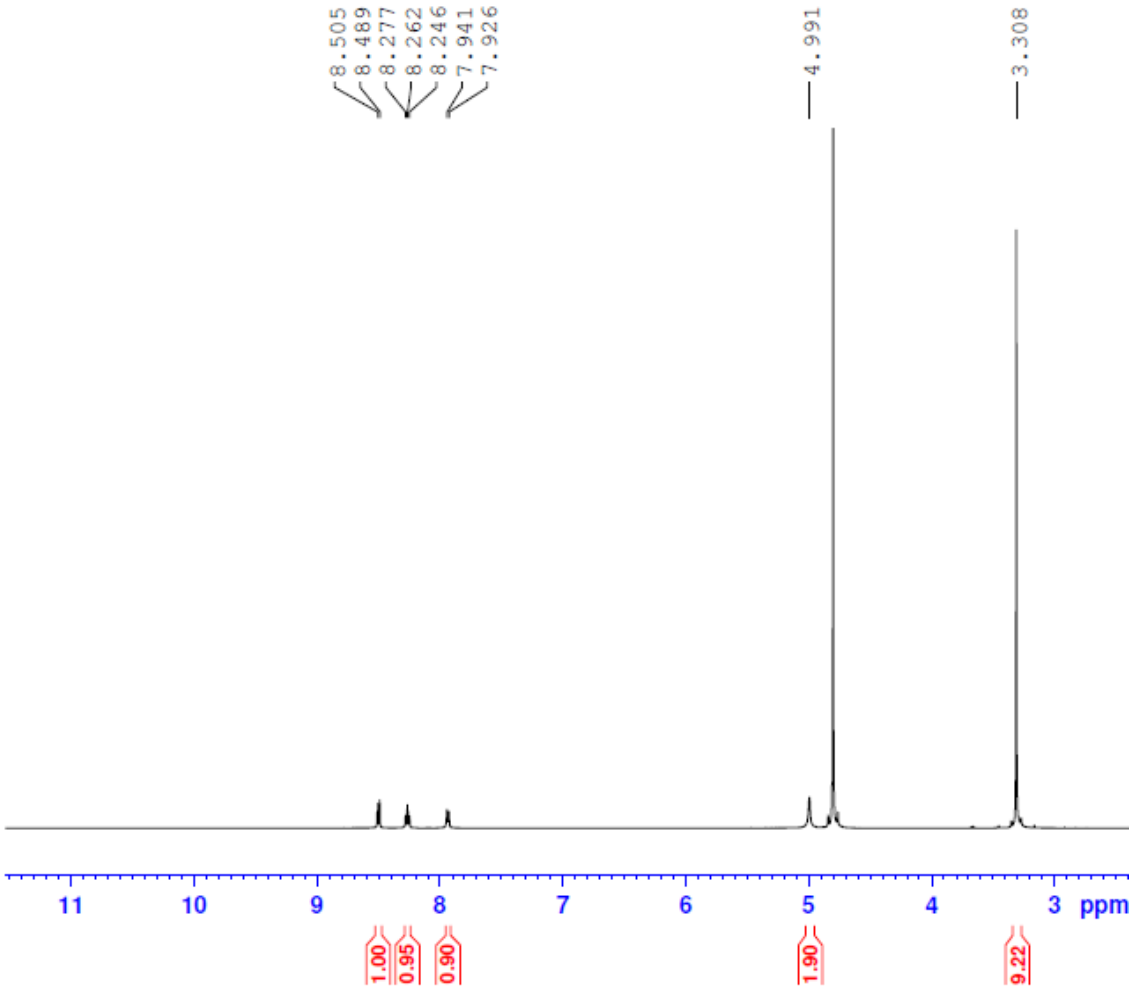

Figure 37S: ^{1}HNMR of 1,1'-([2,2'-bipyridine]-6,6'-diyl)bis(N,N,N-trimethylmethanaminium) (tmabpy) (**19**) in D_2O at 500 MHz.

REFERENCES

1. Lewis, N. S.; Nocera, D. G., Powering the planet: Chemical challenges in solar energy utilization. *Proceedings of the National Academy of Sciences* **2006,** *103* (43), 15729-15735.
2. Asif, M.; Muneer, T., Energy supply, its demand and security issues for developed and emerging economies. *Renewable and Sustainable Energy Reviews* **2007,** *11* (7), 1388-1413.
3. Dresselhaus, M.; Thomas, I., Alternative energy technologies. *Nature* **2001,** *414* (6861), 332-337.
4. Schiermeier, Q.; Tollefson, J.; Scully, T.; Witze, A.; Morton, O., Energy alternatives: Electricity without carbon. *Nature News* **2008,** *454* (7206), 816-823.
5. Nelson, J., *The physics of solar cells*. World Scientific Publishing Company: 2003.
6. Camus, C., Economic benefits of small PV "prosumers" in south European countries. In *EEIC2016 Scientific Session*, 2016.
7. Service, R. F., Solar energy. Is it time to shoot for the sun? *Science (New York, NY)* **2005,** *309* (5734), 548.
8. Green, M., Recent developments in photovoltaics. *Solar energy* **2004,** *76* (1-3), 3-8.
9. Jean, J.; Brown, P. R.; Jaffe, R. L.; Buonassisi, T.; Bulović, V., Pathways for solar photovoltaics. *Energy & Environmental Science* **2015,** *8* (4), 1200-1219.
10. Green, M. A.; Emery, K.; Hishikawa, Y.; Warta, W.; Dunlop, E. D., Solar cell efficiency tables (Version 45). *Progress in photovoltaics: research and applications* **2015,** *23* (1), 1-9.
11. Luque, A.; Hegedus, S., *Handbook of photovoltaic science and engineering*. John Wiley & Sons: 2011.
12. Ibn-Mohammed, T.; Koh, S.; Reaney, I.; Acquaye, A.; Schileo, G.; Mustapha, K.; Greenough, R., Perovskite solar cells: An integrated hybrid lifecycle assessment and review in comparison with other photovoltaic technologies. *Renewable and Sustainable Energy Reviews* **2017,** *80*, 1321-1344.
13. Grätzel, M., Dye-sensitized solar cells. *Journal of photochemistry and photobiology C: Photochemistry Reviews* **2003,** *4* (2), 145-153.
14. Becquerel, A.-E., Recherches sur les effets de la radiation chimique de la lumiere solaire au moyen des courants electriques. *CR Acad. Sci* **1839,** *9* (145), 1.
15. Gurney, R.; Mott, N., The theory of the photolysis of silver bromide and the photographic latent image. *Proceedings of the Royal Society of London. Series A, Mathematical and Physical Sciences* **1938**, 151-167.
16. Herz, A., Aggregation of sensitizing dyes in solution and their adsorption onto silver halides. *Advances in Colloid and Interface Science* **1977,** *8* (4), 237-298.
17. Moser, J., Notiz über Verstärkung photoelektrischer Ströme durch optische Sensibilisirung. *Monatshefte für Chemie und verwandte Teile anderer Wissenschaften* **1887,** *8* (1), 373-373.

18. Namba, S.; Hishiki, Y., Color sensitization of zinc oxide with cyanine dyes1. *The Journal of Physical Chemistry* **1965,** *69* (3), 774-779.
19. Hauffe, K.; Danzmann, H.; Pusch, H.; Range, J.; Volz, H., New experiments on the sensitization of zinc oxide by means of the electrochemical cell technique. *Journal of the Electrochemical Society* **1970,** *117* (8), 993.
20. Gerischer, H.; Tributsch, H., Elektrochemische Untersuchungen zur spektralen Sensibilisierung von ZnO-Einkristallen. *Berichte der Bunsengesellschaft für physikalische Chemie* **1968,** *72* (3), 437-445.
21. Fujishima, A.; Honda, K., Electrochemical photolysis of water at a semiconductor electrode. *nature* **1972,** *238* (5358), 37-38.
22. O'regan, B.; Grätzel, M., A low-cost, high-efficiency solar cell based on dye-sensitized colloidal TiO 2 films. *nature* **1991,** *353* (6346), 737-740.
23. Lee, Y.; Kang, M., The optical properties of nanoporous structured titanium dioxide and the photovoltaic efficiency on DSSC. *Materials Chemistry and Physics* **2010,** *122* (1), 284-289.
24. Wu, J.; Lan, Z.; Hao, S.; Li, P.; Lin, J.; Huang, M.; Fang, L.; Huang, Y., Progress on the electrolytes for dye-sensitized solar cells. *Pure and Applied Chemistry* **2008,** *80* (11), 2241-2258.
25. Listorti, A.; O'Regan, B.; Durrant, J. R., Electron transfer dynamics in dye-sensitized solar cells. *Chemistry of Materials* **2011,** *23* (15), 3381-3399.
26. Asbury, J. B.; Ellingson, R. J.; Ghosh, H. N.; Ferrere, S.; Nozik, A. J.; Lian, T., Femtosecond IR study of excited-state relaxation and electron-injection dynamics of Ru (dcbpy) 2 (NCS) 2 in solution and on nanocrystalline TiO_2 and Al_2O_3 thin films. *The Journal of Physical Chemistry B* **1999,** *103* (16), 3110-3119.
27. Ramakrishna, G.; Jose, D. A.; Kumar, D. K.; Das, A.; Palit, D. K.; Ghosh, H. N., Strongly coupled ruthenium− polypyridyl complexes for efficient electron injection in dye-sensitized semiconductor nanoparticles. *The Journal of Physical Chemistry B* **2005,** *109* (32), 15445-15453.
28. Rothenberger, G.; Fitzmaurice, D.; Graetzel, M., Spectroscopy of conduction band electrons in transparent metal oxide semiconductor films: optical determination of the flatband potential of colloidal titanium dioxide films. *The Journal of physical chemistry* **1992,** *96* (14), 5983-5986.
29. Koops, S. E.; O'Regan, B. C.; Barnes, P. R.; Durrant, J. R., Parameters influencing the efficiency of electron injection in dye-sensitized solar cells. *Journal of the American Chemical Society* **2009,** *131* (13), 4808-4818.
30. Wang, P.; Wenger, B.; Humphry-Baker, R.; Moser, J.-E.; Teuscher, J.; Kantlehner, W.; Mezger, J.; Stoyanov, E. V.; Zakeeruddin, S. M.; Grätzel, M., Charge separation and efficient light energy conversion in sensitized mesoscopic solar cells based on binary ionic liquids. *Journal of the American Chemical Society* **2005,** *127* (18), 6850-6856.
31. Hagfeldt, A.; Boschloo, G.; Sun, L.; Kloo, L.; Pettersson, H., Dye-sensitized solar cells. *Chemical reviews* **2010,** *110* (11), 6595-6663.
32. Wenger, S.; Bouit, P.-A.; Chen, Q.; Teuscher, J.; Censo, D. D.; Humphry-Baker, R.; Moser, J.-E.; Delgado, J. L.; Martín, N.; Zakeeruddin, S. M., Efficient

electron transfer and sensitizer regeneration in stable π-extended tetrathiafulvalene-sensitized solar cells. *Journal of the American Chemical Society* **2010,** *132* (14), 5164-5169.
33. Pelet, S.; Moser, J.-E.; Grätzel, M., Cooperative effect of adsorbed cations and iodide on the interception of back electron transfer in the dye sensitization of nanocrystalline TiO2. *The Journal of Physical Chemistry B* **2000,** *104* (8), 1791-1795.
34. Kroeze, J. E.; Hirata, N.; Koops, S.; Nazeeruddin, M. K.; Schmidt-Mende, L.; Grätzel, M.; Durrant, J. R., Alkyl chain barriers for kinetic optimization in dye-sensitized solar cells. *Journal of the American Chemical Society* **2006,** *128* (50), 16376-16383.
35. Papageorgiou, N.; Maier, W.; Grätzel, M., An iodine/triiodide reduction electrocatalyst for aqueous and organic media. *Journal of the electrochemical Society* **1997,** *144* (3), 876.
36. Lan, J.-L.; Wang, Y.-Y.; Wan, C.-C.; Wei, T.-C.; Feng, H.-P.; Peng, C.; Cheng, H.-P.; Chang, Y.-H.; Hsu, W.-C., The simple and easy way to manufacture counter electrode for dye-sensitized solar cells. *Current Applied Physics* **2010,** *10* (2), S168-S171.
37. Barzykin, A.; Tachiya, M., Mechanism of charge recombination in dye-sensitized nanocrystalline semiconductors: random flight model. *The Journal of Physical Chemistry B* **2002,** *106* (17), 4356-4363.
38. Kopidakis, N.; Schiff, E. A.; Park, N.-G.; Van de Lagemaat, J.; Frank, A., Ambipolar diffusion of photocarriers in electrolyte-filled, nanoporous TiO2. *The Journal of Physical Chemistry B* **2000,** *104* (16), 3930-3936.
39. Haque, S. A.; Tachibana, Y.; Willis, R. L.; Moser, J. E.; Grätzel, M.; Klug, D. R.; Durrant, J. R., Parameters influencing charge recombination kinetics in dye-sensitized nanocrystalline titanium dioxide films. *The Journal of Physical Chemistry B* **2000,** *104* (3), 538-547.
40. O'Regan, B. C.; López-Duarte, I.; Martínez-Díaz, M. V.; Forneli, A.; Albero, J.; Morandeira, A.; Palomares, E.; Torres, T.; Durrant, J. R., Catalysis of recombination and its limitation on open circuit voltage for dye sensitized photovoltaic cells using phthalocyanine dyes. *Journal of the American Chemical Society* **2008,** *130* (10), 2906-2907.
41. Cameron, P. J.; Peter, L. M., Characterization of titanium dioxide blocking layers in dye-sensitized nanocrystalline solar cells. *The Journal of Physical Chemistry B* **2003,** *107* (51), 14394-14400.
42. Boschloo, G.; Häggman, L.; Hagfeldt, A., Quantification of the effect of 4-tert-butylpyridine addition to I-/I3-redox electrolytes in dye-sensitized nanostructured TiO2 solar cells. *The Journal of Physical Chemistry B* **2006,** *110* (26), 13144-13150.
43. Diamant, Y.; Chappel, S.; Chen, S.; Melamed, O.; Zaban, A., Core–shell nanoporous electrode for dye sensitized solar cells: the effect of shell characteristics on the electronic properties of the electrode. *Coordination Chemistry Reviews* **2004,** *248* (13-14), 1271-1276.

44. Liu, Y.; Hagfeldt, A.; Xiao, X.-R.; Lindquist, S.-E., Investigation of influence of redox species on the interfacial energetics of a dye-sensitized nanoporous TiO2 solar cell. *Solar Energy Materials and Solar Cells* **1998,** *55* (3), 267-281.
45. Schlichthörl, G.; Park, N.; Frank, A. J., Evaluation of the charge-collection efficiency of dye-sensitized nanocrystalline TiO2 solar cells. *The Journal of Physical Chemistry B* **1999,** *103* (5), 782-791.
46. Clifford, J. N.; Martínez-Ferrero, E.; Viterisi, A.; Palomares, E., Sensitizer molecular structure-device efficiency relationship in dye sensitized solar cells. *Chemical Society Reviews* **2011,** *40* (3), 1635-1646.
47. Asbury, J. B.; Anderson, N. A.; Hao, E.; Ai, X.; Lian, T., Parameters affecting electron injection dynamics from ruthenium dyes to titanium dioxide nanocrystalline thin film. *The Journal of Physical Chemistry B* **2003,** *107* (30), 7376-7386.
48. Asbury, J. B.; Hao, E.; Wang, Y.; Ghosh, H. N.; Lian, T., Ultrafast electron transfer dynamics from molecular adsorbates to semiconductor nanocrystalline thin films. ACS Publications: 2001.
49. Mann, J. R.; Gannon, M. K.; Fitzgibbons, T. C.; Detty, M. R.; Watson, D. F., Optimizing the photocurrent efficiency of dye-sensitized solar cells through the controlled aggregation of chalcogenoxanthylium dyes on nanocrystalline titania films. *The Journal of Physical Chemistry C* **2008,** *112* (34), 13057-13061.
50. Yen, Y.-S.; Chou, H.-H.; Chen, Y.-C.; Hsu, C.-Y.; Lin, J. T., Recent developments in molecule-based organic materials for dye-sensitized solar cells. *Journal of Materials Chemistry* **2012,** *22* (18), 8734-8747.
51. Ardo, S.; Meyer, G. J., Photodriven heterogeneous charge transfer with transition-metal compounds anchored to TiO 2 semiconductor surfaces. *Chemical Society Reviews* **2009,** *38* (1), 115-164.
52. Nazeeruddin, M. K.; Kay, A.; Rodicio, I.; Humphry-Baker, R.; Müller, E.; Liska, P.; Vlachopoulos, N.; Grätzel, M., Conversion of light to electricity by cis-X2bis (2, 2'-bipyridyl-4, 4'-dicarboxylate) ruthenium (II) charge-transfer sensitizers (X= Cl-, Br-, I-, CN-, and SCN-) on nanocrystalline titanium dioxide electrodes. *Journal of the American Chemical Society* **1993,** *115* (14), 6382-6390.
53. Nazeeruddin, M. K.; Zakeeruddin, S.; Humphry-Baker, R.; Jirousek, M.; Liska, P.; Vlachopoulos, N.; Shklover, V.; Fischer, C.-H.; Grätzel, M., Acid− base equilibria of (2, 2 ‘-bipyridyl-4, 4 ‘-dicarboxylic acid) ruthenium (II) complexes and the effect of protonation on charge-transfer sensitization of nanocrystalline titania. *Inorganic Chemistry* **1999,** *38* (26), 6298-6305.
54. Lammi, R. K.; Wagner, R. W.; Ambroise, A.; Diers, J. R.; Bocian, D. F.; Holten, D.; Lindsey, J. S., Mechanisms of excited-state energy-transfer gating in linear versus branched multiporphyrin arrays. *The Journal of Physical Chemistry B* **2001,** *105* (22), 5341-5352.
55. Tachibana, Y.; Haque, S. A.; Mercer, I. P.; Durrant, J. R.; Klug, D. R., Electron injection and recombination in dye sensitized nanocrystalline titanium dioxide films: a comparison of ruthenium bipyridyl and porphyrin sensitizer dyes. *The Journal of Physical Chemistry B* **2000,** *104* (6), 1198-1205.

56. Macor, L.; Fungo, F.; Tempesti, T.; Durantini, E. N.; Otero, L.; Barea, E. M.; Fabregat-Santiago, F.; Bisquert, J., Near-IR sensitization of wide band gap oxide semiconductor by axially anchored Si-naphthalocyanines. *Energy & Environmental Science* **2009,** *2* (5), 529-534.
57. Nazeeruddin, M. K.; Humphry-Baker, R.; Grätzel, M.; Wöhrle, D.; Schnurpfeil, G.; Schneider, G.; Hirth, A.; Trombach, N., Efficient near-IR sensitization of nanocrystalline TiO 2 films by zinc and aluminum phthalocyanines. *Journal of Porphyrins and Phthalocyanines* **1999,** *3* (03), 230-237.
58. Mishra, A.; Fischer, M. K.; Bäuerle, P., Metal-free organic dyes for dye-sensitized solar cells: From structure: Property relationships to design rules. *Angewandte Chemie International Edition* **2009,** *48* (14), 2474-2499.
59. Wiberg, J.; Marinado, T.; Hagberg, D. P.; Sun, L.; Hagfeldt, A.; Albinsson, B., Effect of anchoring group on electron injection and recombination dynamics in organic dye-sensitized solar cells. *The Journal of Physical Chemistry C* **2009,** *113* (9), 3881-3886.
60. Hagberg, D. P.; Jiang, X.; Gabrielsson, E.; Linder, M.; Marinado, T.; Brinck, T.; Hagfeldt, A.; Sun, L., Symmetric and unsymmetric donor functionalization. comparing structural and spectral benefits of chromophores for dye-sensitized solar cells. *Journal of Materials Chemistry* **2009,** *19* (39), 7232-7238.
61. Hara, K.; Wang, Z.-S.; Sato, T.; Furube, A.; Katoh, R.; Sugihara, H.; Dan-oh, Y.; Kasada, C.; Shinpo, A.; Suga, S., Oligothiophene-containing coumarin dyes for efficient dye-sensitized solar cells. *The Journal of Physical Chemistry B* **2005,** *109* (32), 15476-15482.
62. Hara, K.; Sato, T.; Katoh, R.; Furube, A.; Ohga, Y.; Shinpo, A.; Suga, S.; Sayama, K.; Sugihara, H.; Arakawa, H., Molecular design of coumarin dyes for efficient dye-sensitized solar cells. *The Journal of Physical Chemistry B* **2003,** *107* (2), 597-606.
63. Horiuchi, T.; Miura, H.; Sumioka, K.; Uchida, S., High efficiency of dye-sensitized solar cells based on metal-free indoline dyes. *Journal of the American Chemical Society* **2004,** *126* (39), 12218-12219.
64. Wang, Z.-S.; Koumura, N.; Cui, Y.; Takahashi, M.; Sekiguchi, H.; Mori, A.; Kubo, T.; Furube, A.; Hara, K., Hexylthiophene-functionalized carbazole dyes for efficient molecular photovoltaics: tuning of solar-cell performance by structural modification. *Chemistry of Materials* **2008,** *20* (12), 3993-4003.
65. Ooyama, Y.; Inoue, S.; Nagano, T.; Kushimoto, K.; Ohshita, J.; Imae, I.; Komaguchi, K.; Harima, Y., Dye-sensitized solar cells based on donor–acceptor π-conjugated fluorescent dyes with a pyridine ring as an electron-withdrawing anchoring group. *Angewandte Chemie International Edition* **2011,** *50* (32), 7429-7433.
66. Ooyama, Y.; Nagano, T.; Inoue, S.; Imae, I.; Komaguchi, K.; Ohshita, J.; Harima, Y., Dye-Sensitized Solar Cells Based on Donor-π-Acceptor Fluorescent Dyes with a Pyridine Ring as an Electron-Withdrawing-Injecting Anchoring Group. *Chemistry–A European Journal* **2011,** *17* (52), 14837-14843.
67. Kakiage, K.; Aoyama, Y.; Yano, T.; Oya, K.; Fujisawa, J.-i.; Hanaya, M., Highly-efficient dye-sensitized solar cells with collaborative sensitization by silyl-

anchor and carboxy-anchor dyes. *Chemical Communications* **2015,** *51* (88), 15894-15897.
68. Kuang, D.; Walter, P.; Nüesch, F.; Kim, S.; Ko, J.; Comte, P.; Zakeeruddin, S. M.; Nazeeruddin, M. K.; Grätzel, M., Co-sensitization of organic dyes for efficient ionic liquid electrolyte-based dye-sensitized solar cells. *Langmuir* **2007,** *23* (22), 10906-10909.
69. Hao, Y.; Saygili, Y.; Cong, J.; Eriksson, A.; Yang, W.; Zhang, J.; Polanski, E.; Nonomura, K.; Zakeeruddin, S. M.; Grätzel, M., Novel blue organic dye for dye-sensitized solar cells achieving high efficiency in cobalt-based electrolytes and by co-sensitization. *ACS applied materials & interfaces* **2016,** *8* (48), 32797-32804.
70. Hilal, H. M.; El Bitar Nehme, M. A.; Ghaddar, T. H., Large enhancement of dye sensitized solar cell efficiency by co-sensitizing pyridyl-and carboxylic acid-based dyes. *ACS Applied Energy Materials* **2018,** *1* (6), 2776-2783.
71. Nehme, V. A. E. B.; Nehme, M. A. E. B.; Ghaddar, T. H., New pyridyl-based dyes for co-sensitization in dye sensitized solar cells. *Solar Energy* **2019,** *187*, 108-114.
72. Wang, M.; Grätzel, C.; Zakeeruddin, S. M.; Grätzel, M., Recent developments in redox electrolytes for dye-sensitized solar cells. *Energy & Environmental Science* **2012,** *5* (11), 9394-9405.
73. Ye, M.; Wen, X.; Wang, M.; Iocozzia, J.; Zhang, N.; Lin, C.; Lin, Z., Recent advances in dye-sensitized solar cells: from photoanodes, sensitizers and electrolytes to counter electrodes. *Materials Today* **2015,** *18* (3), 155-162.
74. Grätzel, M., Recent advances in sensitized mesoscopic solar cells. *Accounts of chemical research* **2009,** *42* (11), 1788-1798.
75. Wu, J.; Lan, Z.; Lin, J.; Huang, M.; Huang, Y.; Fan, L.; Luo, G., Electrolytes in dye-sensitized solar cells. *Chemical reviews* **2015,** *115* (5), 2136-2173.
76. Stanley, A.; Matthews, D., The dark current at the TiO2 electrode of a dye-sensitized TiO_2 photovoltaic cell. *Australian journal of chemistry* **1995,** *48* (7), 1293-1300.
77. Grätzel, M., Perspectives for dye-sensitized nanocrystalline solar cells. *Progress in photovoltaics: research and applications* **2000,** *8* (1), 171-185.
78. Boschloo, G.; Lindström, H.; Magnusson, E.; Holmberg, A.; Hagfeldt, A., Optimization of dye-sensitized solar cells prepared by compression method. *Journal of Photochemistry and Photobiology A: Chemistry* **2002,** *148* (1-3), 11-15.
79. Hara, K.; Horiguchi, T.; Kinoshita, T.; Sayama, K.; Arakawa, H., Influence of electrolytes on the photovoltaic performance of organic dye-sensitized nanocrystalline TiO2 solar cells. *Solar Energy Materials and Solar Cells* **2001,** *70* (2), 151-161.
80. Papageorgiou, N.; Athanassov, Y.; Armand, M.; Bonho, P.; Pettersson, H.; Azam, A.; Grätzel, M., The performance and stability of ambient temperature molten salts for solar cell applications. *Journal of the Electrochemical Society* **1996,** *143* (10), 3099.
81. Yu, Q.; Wang, Y.; Yi, Z.; Zu, N.; Zhang, J.; Zhang, M.; Wang, P., High-efficiency dye-sensitized solar cells: the influence of lithium ions on exciton dissociation, charge recombination, and surface states. *ACS nano* **2010,** *4* (10), 6032-6038.

82. Tian, H.; Sun, L., Iodine-free redox couples for dye-sensitized solar cells. *Journal of Materials Chemistry* **2011,** *21* (29), 10592-10601.
83. Rowley, J. G.; Farnum, B. H.; Ardo, S.; Meyer, G. J., Iodide chemistry in dye-sensitized solar cells: making and breaking I− I bonds for solar energy conversion. *The Journal of Physical Chemistry Letters* **2010,** *1* (20), 3132-3140.
84. Sapp, S. A.; Elliott, C. M.; Contado, C.; Caramori, S.; Bignozzi, C. A., Substituted polypyridine complexes of cobalt (II/III) as efficient electron-transfer mediators in dye-sensitized solar cells. *Journal of the American Chemical Society* **2002,** *124* (37), 11215-11222.
85. Stergiopoulos, T.; Falaras, P., Minimizing Energy Losses in Dye-Sensitized Solar Cells Using Coordination Compounds as Alternative Redox Mediators Coupled with Appropriate Organic Dyes. *Advanced Energy Materials* **2012,** *2* (6), 616-627.
86. Feldt, S. M.; Wang, G.; Boschloo, G.; Hagfeldt, A., Effects of driving forces for recombination and regeneration on the photovoltaic performance of dye-sensitized solar cells using cobalt polypyridine redox couples. *The Journal of Physical Chemistry C* **2011,** *115* (43), 21500-21507.
87. Mosconi, E.; Yum, J.-H.; Kessler, F.; Gómez García, C. J.; Zuccaccia, C.; Cinti, A.; Nazeeruddin, M. K.; Grätzel, M.; De Angelis, F., Cobalt electrolyte/dye interactions in dye-sensitized solar cells: a combined computational and experimental study. *Journal of the American Chemical Society* **2012,** *134* (47), 19438-19453.
88. Feldt, S. M.; Cappel, U. B.; Johansson, E. M.; Boschloo, G.; Hagfeldt, A., Characterization of surface passivation by poly (methylsiloxane) for dye-sensitized solar cells employing the ferrocene redox couple. *The Journal of Physical Chemistry C* **2010,** *114* (23), 10551-10558.
89. Klahr, B. M.; Hamann, T. W., Performance enhancement and limitations of cobalt bipyridyl redox shuttles in dye-sensitized solar cells. *The Journal of Physical Chemistry C* **2009,** *113* (31), 14040-14045.
90. Nelson, J. J.; Amick, T. J.; Elliott, C. M., Mass transport of polypyridyl cobalt complexes in dye-sensitized solar cells with mesoporous TiO_2 photoanodes. *The Journal of Physical Chemistry C* **2008,** *112* (46), 18255-18263.
91. Hathaway, B., Annual Report on Copper 1980. *Coord. Chem. Rev.* **1981,** *35*, 211.
92. Hathaway, B.; Billing, D., The electronic properties and stereochemistry of mono-nuclear complexes of the copper (II) ion. *Coordination Chemistry Reviews* **1970,** *5* (2), 143-207.
93. Karlin, K.; Yandell, J., Redox behavior of blue copper model complexes. Redox potentials and electron-transfer kinetics of some copper (II)-copper (I) complexes with nitrogen and thioether donors. *Inorganic Chemistry* **1984,** *23* (9), 1184-1188.
94. Hattori, S.; Wada, Y.; Yanagida, S.; Fukuzumi, S., Blue copper model complexes with distorted tetragonal geometry acting as effective electron-transfer mediators in dye-sensitized solar cells. *Journal of the American Chemical Society* **2005,** *127* (26), 9648-9654.

95. Brugnati, M.; Caramori, S.; Cazzanti, S.; Marchini, L.; Argazzi, R.; Bignozzi, C. A., Electron transfer mediators for photoelectrochemical cells based on Cu (I) metal complexes. *International Journal of Photoenergy* **2007,** *2007*.
96. Bai, Y.; Yu, Q.; Cai, N.; Wang, Y.; Zhang, M.; Wang, P., High-efficiency organic dye-sensitized mesoscopic solar cells with a copper redox shuttle. *Chemical Communications* **2011,** *47* (15), 4376-4378.
97. Zhang, J.; Freitag, M.; Hagfeldt, A.; Boschloo, G., Solid-state dye-sensitized solar cells. In *Molecular Devices for Solar Energy Conversion and Storage*, Springer: 2018; pp 151-185.
98. Hoffeditz, W. L.; Katz, M. J.; Deria, P.; Cutsail III, G. E.; Pellin, M. J.; Farha, O. K.; Hupp, J. T., One electron changes everything. A multispecies copper redox shuttle for dye-sensitized solar cells. *The Journal of Physical Chemistry C* **2016,** *120* (7), 3731-3740.
99. Saygili, Y.; Söderberg, M.; Pellet, N.; Giordano, F.; Cao, Y.; Muñoz-García, A. B.; Zakeeruddin, S. M.; Vlachopoulos, N.; Pavone, M.; Boschloo, G., Copper bipyridyl redox mediators for dye-sensitized solar cells with high photovoltage. *Journal of the American Chemical Society* **2016,** *138* (45), 15087-15096.
100. Huang, S.; Schlichthörl, G.; Nozik, A.; Grätzel, M.; Frank, A., Charge recombination in dye-sensitized nanocrystalline TiO2 solar cells. *The Journal of Physical Chemistry B* **1997,** *101* (14), 2576-2582.
101. Yin, X.; Tan, W.; Zhang, J.; Weng, Y.; Xiao, X.; Zhou, X.; Li, X.; Lin, Y., The effect mechanism of 4-ethoxy-2-methylpyridine as an electrolyte additive on the performance of dye-sensitized solar cell. *Colloids and Surfaces A: Physicochemical and Engineering Aspects* **2008,** *326* (1-2), 42-47.
102. Kusama, H.; Konishi, Y.; Sugihara, H.; Arakawa, H., Influence of alkylpyridine additives in electrolyte solution on the performance of dye-sensitized solar cell. *Solar energy materials and solar cells* **2003,** *80* (2), 167-179.
103. Jennings, J. R.; Wang, Q., Influence of lithium ion concentration on electron injection, transport, and recombination in dye-sensitized solar cells. *The Journal of Physical Chemistry C* **2010,** *114* (3), 1715-1724.
104. Watson, D. F.; Meyer, G. J., Cation effects in nanocrystalline solar cells. *Coordination Chemistry Reviews* **2004,** *248* (13-14), 1391-1406.
105. Kelly, C. A.; Farzad, F.; Thompson, D. W.; Stipkala, J. M.; Meyer, G. J., Cation-controlled interfacial charge injection in sensitized nanocrystalline TiO_2. *Langmuir* **1999,** *15* (20), 7047-7054.
106. Zhang, C.; Huang, Y.; Huo, Z.; Chen, S.; Dai, S., Photoelectrochemical effects of guanidinium thiocyanate on dye-sensitized solar cell performance and stability. *The Journal of Physical Chemistry C* **2009,** *113* (52), 21779-21783.
107. Kopidakis, N.; Benkstein, K. D.; Van De Lagemaat, J.; Frank, A. J., Transport-limited recombination of photocarriers in dye-sensitized nanocrystalline TiO_2 solar cells. *The Journal of Physical Chemistry B* **2003,** *107* (41), 11307-11315.
108. Haque, S. A.; Palomares, E.; Cho, B. M.; Green, A. N.; Hirata, N.; Klug, D. R.; Durrant, J. R., Charge separation versus recombination in dye-sensitized nanocrystalline

solar cells: the minimization of kinetic redundancy. *Journal of the American Chemical Society* **2005,** *127* (10), 3456-3462.
109. Bella, F.; Gerbaldi, C.; Barolo, C.; Grätzel, M., Aqueous dye-sensitized solar cells. *Chemical Society Reviews* **2015,** *44* (11), 3431-3473.
110. Tropsha, Y. G.; Harvey, N. G., Activated rate theory treatment of oxygen and water transport through silicon oxide/poly (ethylene terephthalate) composite barrier structures. *The Journal of Physical Chemistry B* **1997,** *101* (13), 2259-2266.
111. Brown, T.; De Rossi, F.; Di Giacomo, F.; Mincuzzi, G.; Zardetto, V.; Reale, A.; Di Carlo, A., Progress in flexible dye solar cell materials, processes and devices. *Journal of Materials Chemistry A* **2014,** *2* (28), 10788-10817.
112. Bella, F.; Lamberti, A.; Sacco, A.; Bianco, S.; Chiodoni, A.; Bongiovanni, R., Novel electrode and electrolyte membranes: towards flexible dye-sensitized solar cell combining vertically aligned TiO_2 nanotube array and light-cured polymer network. *Journal of membrane science* **2014,** *470*, 125-131.
113. Liska, P.; Vlachopoulos, N.; Graetzel, M., Conversion of light to electricity by cis-X2bis (2, 20-bipyridyl-4, 40-dicarboxylate) ruthenium (II) charge-transfer sensitizers (X= Cl-, Br-, I-, CN-, and SCN-) on nanocrystalline titanium dioxide electrodes. *J Am Chem Soc* **1993,** *115*, 63826390.
114. Lu, H.-L.; Shen, T. F.-R.; Huang, S.-T.; Tung, Y.-L.; Yang, T. C.-K., The degradation of dye sensitized solar cell in the presence of water isotopes. *Solar energy materials and solar cells* **2011,** *95* (7), 1624-1629.
115. Park, S. J.; Yoo, K.; Kim, J.-Y.; Kim, J. Y.; Lee, D.-K.; Kim, B.; Kim, H.; Kim, J. H.; Cho, J.; Ko, M. J., Water-based thixotropic polymer gel electrolyte for dye-sensitized solar cells. *ACS nano* **2013,** *7* (5), 4050-4056.
116. Law, C.; Pathirana, S. C.; Li, X.; Anderson, A. Y.; Barnes, P. R.; Listorti, A.; Ghaddar, T. H.; O′ Regan, B. C., Water-based electrolytes for dye-sensitized solar cells. *Advanced Materials* **2010,** *22* (40), 4505-4509.
117. Juris, A.; Balzani, V.; Barigelletti, F.; Campagna, S.; Belser, P. l.; von Zelewsky, A. v., Ru (II) polypyridine complexes: photophysics, photochemistry, eletrochemistry, and chemiluminescence. *Coordination Chemistry Reviews* **1988,** *84*, 85-277.
118. Hui, Z.; Xiong, Y.; Heng, L.; Yuan, L.; Yu-Xiang, W., Explanation of effect of added water on dye-sensitized nanocrystalline TiO_2 solar cell: correlation between performance and carrier relaxation kinetics. *Chinese Physics Letters* **2007,** *24* (11), 3272.
119. Zhu, K.; Jang, S.-R.; Frank, A. J., Effects of water intrusion on the charge-carrier dynamics, performance, and stability of dye-sensitized solar cells. *Energy & Environmental Science* **2012,** *5* (11), 9492-9495.
120. Heinzel, A.; Teschner, D.; Schumacher, R., Influence of water on the capacitance/potential distribution at the TiO2/CH3CN junction. *Berichte der Bunsengesellschaft für physikalische Chemie* **1981,** *85* (12), 1117-1119.
121. Murakami, T. N.; Saito, H.; Uegusa, S.; Kawashima, N.; Miyasaka, T., Water-based dye-sensitized solar cells: interfacial activation of TiO2 mesopores in contact

with aqueous electrolyte for efficiency development. *Chemistry letters* **2003,** *32* (12), 1154-1155.
122. Avetta, P.; Bella, F.; Bianco Prevot, A.; Laurenti, E.; Montoneri, E.; Arques, A.; Carlos, L., Waste cleaning waste: photodegradation of monochlorophenols in the presence of waste-derived photosensitizer. *ACS Sustainable Chemistry & Engineering* **2013,** *1* (12), 1545-1550.
123. Yu, Z.; Gorlov, M.; Boschloo, G.; Kloo, L., Synergistic effect of N-methylbenzimidazole and guanidinium thiocyanate on the performance of dye-sensitized solar cells based on ionic liquid electrolytes. *The Journal of Physical Chemistry C* **2010,** *114* (50), 22330-22337.
124. Lu, H.-L.; Lee, Y.-H.; Huang, S.-T.; Su, C.; Yang, T. C.-K., Influences of water in bis-benzimidazole-derivative electrolyte additives to the degradation of the dye-sensitized solar cells. *Solar energy materials and solar cells* **2011,** *95* (1), 158-162.
125. Tikariha, D.; Ghosh, K. K.; Quagliotto, P.; Ghosh, S., Mixed micellization properties of cationic monomeric and gemini surfactants. *Journal of Chemical & Engineering Data* **2010,** *55* (10), 4162-4167.
126. Park, N. G.; Chang, S.-H.; van de Lagemaat, J.; Kim, K.-J.; Frank, A. J., Effect of Cations on the Open-Circuit Photovoltage and the Charge-Injection Efficiency of Dye-Sensitized Nanocrystalline Rutile TiO~ 2 Films. *Bulletin-Korean Chemical Society* **2000,** *21* (10), 985-988.
127. Lai, W. H.; Su, Y. H.; Teoh, L. G.; Hon, M. H., Commercial and natural dyes as photosensitizers for a water-based dye-sensitized solar cell loaded with gold nanoparticles. *Journal of Photochemistry and Photobiology A: Chemistry* **2008,** *195* (2-3), 307-313.
128. Daeneke, T.; Uemura, Y.; Duffy, N. W.; Mozer, A. J.; Koumura, N.; Bach, U.; Spiccia, L., Aqueous Dye-Sensitized Solar Cell Electrolytes Based on the Ferricyanide–Ferrocyanide Redox Couple. *Advanced Materials* **2012,** *24* (9), 1222-1225.
129. Tian, H.; Gabrielsson, E.; Lohse, P. W.; Vlachopoulos, N.; Kloo, L.; Hagfeldt, A.; Sun, L., Development of an organic redox couple and organic dyes for aqueous dye-sensitized solar cells. *Energy & Environmental Science* **2012,** *5* (12), 9752-9755.
130. Xiang, W.; Huang, F.; Cheng, Y.-B.; Bach, U.; Spiccia, L., Aqueous dye-sensitized solar cell electrolytes based on the cobalt (II)/(III) tris (bipyridine) redox couple. *Energy & Environmental Science* **2013,** *6* (1), 121-127.
131. Xu, H.; Zhang, C.; Wang, Z.; Pang, S.; Zhou, X.; Zhang, Z.; Cui, G., Nitrogen-doped carbon and iron carbide nanocomposites as cost-effective counter electrodes of dye-sensitized solar cells. *Journal of Materials Chemistry A* **2014,** *2* (13), 4676-4681.
132. Ramasamy, E.; Jo, C.; Anthonysamy, A.; Jeong, I.; Kim, J. K.; Lee, J., Soft-template simple synthesis of ordered mesoporous titanium nitride-carbon nanocomposite for high performance dye-sensitized solar cell counter electrodes. *Chemistry of Materials* **2012,** *24* (9), 1575-1582.
133. Pringle, J. M.; Armel, V.; MacFarlane, D. R., Electrodeposited PEDOT-on-plastic cathodes for dye-sensitized solar cells. *Chemical Communications* **2010,** *46* (29), 5367-5369.

134. Leandri, V.; Ellis, H.; Gabrielsson, E.; Sun, L.; Boschloo, G.; Hagfeldt, A., An organic hydrophilic dye for water-based dye-sensitized solar cells. *Physical Chemistry Chemical Physics* **2014,** *16* (37), 19964-19971.
135. Hora, C.; Santos, F. t.; Sales, M. G. F.; Ivanou, D.; Mendes, A. l., Dye-Sensitized Solar Cells for efficient solar and artificial light conversion. *ACS Sustainable Chemistry & Engineering* **2019,** *7* (15), 13464-13470.
136. De Rossi, F.; Pontecorvo, T.; Brown, T. M., Characterization of photovoltaic devices for indoor light harvesting and customization of flexible dye solar cells to deliver superior efficiency under artificial lighting. *Applied Energy* **2015,** *156*, 413-422.
137. Freitag, M.; Teuscher, J.; Saygili, Y.; Zhang, X.; Giordano, F.; Liska, P.; Hua, J.; Zakeeruddin, S. M.; Moser, J.-E.; Grätzel, M., Dye-sensitized solar cells for efficient power generation under ambient lighting. *Nature Photonics* **2017,** *11* (6), 372.